Master's thesis

NTNU
Norwegian University of Science and Technology
Faculty of Engineering
Department of Marine Technology

Markus Lien

Evaluation of two Commercial Flow Simulation Tools for Modeling of Subsea Carbon Dioxide Injection Systems

Master's thesis in Marine Technology
Supervisor: Bernt Leira
Co-supervisor: Milan Stanko
June 2023

NTNU
Norwegian University of
Science and Technology

Markus Lien

Evaluation of two Commercial Flow Simulation Tools for Modeling of Subsea Carbon Dioxide Injection Systems

Master's thesis in Marine Technology
Supervisor: Bernt Leira
Co-supervisor: Milan Stanko
June 2023

Norwegian University of Science and Technology
Faculty of Engineering
Department of Marine Technology

NTNU
Norwegian University of
Science and Technology

Preface

This thesis represents the culmination of my Master`s degree in Marine Construction and the end of my time at the Subsea Technology program at NTNU. The inspiration for this thesis stems from my internship last summer at SUBPRO, where I first was introduced to LedaFlow and modeling of CO2 flow. This work continued with last semester`s specialization project, and together with my co-supervisor Milan Stanko, a scope for this thesis was defined. Throughout the course of this thesis, I have had the opportunity to investigate the possibilities and limitations of two distinct flow simulators and the many aspects of CO2 injection systems, further building my knowledge in the field of flow assurance.

Trondheim 07.06.2023

Markus Lien

Acknowledgements

I would like to express my utmost gratitude to my supervisors Bernt Leira and Milan Stanko for their invaluable guidance, support, and expertise throughout the completion of this thesis. Especially Milan Stanko for the insightful feedback and encouragement that played a crucial role in shaping the direction and quality of this thesis. I would like to extend my appreciation to the staff and fellow students at IGP at NTNU for providing a stimulating academic work environment and access to resources that guided me on my journey. And at last, I would like to express my gratitude to my family and friends for their understanding and encouragement, a key driving force behind my academic achievements.

To everyone who have contributed to this thesis in any way, thank you.

Abstract

A comparative analysis of two widely used transient multiphase flow simulators, LedaFlow (version 2.8.264.024) and OLGA (version 2020.2.0), in the simulation of CO2 subsea injection systems comprising wells, flowlines and pipelines, were performed with the objective to evaluate the performance of these simulators. This was done with the intention of contributing to the development of more efficient CO2 injection systems.

Carbon Capture, Utilization and Storage consists of vital strategies for mitigating climate change resulting from greenhouse gas emissions. The process of CO2 injection is complex, requiring careful monitoring and planning for safe and effective operations. Simulation software serves as a valuable tool for engineers to assess and design CO2 injection systems. Such tools enables modeling and predictions of CO2 behavior under diverse operating conditions. While OLGA is a commonly used and thoroughly tested software in the industry, LedaFlow is gaining recognition, making a comparative analysis essential.

Multiple steady-state simulation scenarios were conducted to evaluate the simulators` performance. Initial numerical instabilities were observed in both LedaFlow and OLGA during early stages of simulation, with LedaFlow displaying significantly larger fluctuations in mass flow rate. However, both simulators eventually converged towards more consistent values, indicating their suitability for steady state flow simulations.
Mass flow predictions highlighted that OLGA consistently provided higher values compared to LedaFlow, with an average deviation in total mass flow of 9,9 % and 11,7 %, depending on the inlet parameters. These variations may be attributed to differences in modeling assumptions and convergence issues.

Pressure profiles along the pipeline and the wells revealed distinct disparities between LedaFlow and OLGA. LedaFlow exhibited higher a pressure drop in wells, whereas OLGA demonstrated a higher pressure drop in the pipeline and flowlines.
Secondary case simulations, with adjusted pipe geometries, reaffirmed the observed trends in the base case simulations. OLGA consistently predicted higher mass flow rates, while LedaFlow exhibited a higher pressure drop in wells, resulting in deviations in well injection rates and bottom hole pressure.

This study shows that the two commercial software programs tested, provided slightly different results. This is something that should be considered when using the software for designing and operation of CO2 injection systems, as designs and operational decisions will be slightly different due the different input parameters.
However, a more detailed comparison should be performed, for example considering other types of system parameters, as well as the effect of impurities and a wider selection of EOS`s.

Sammendrag

En analyse av to kjente simuleringsverktøy for flerfasestrøm, LedaFlow (versjon 2.8.264.024) og OLGA (versjon 2020.2.0), ble utført for å simulere CO2-injeksjonssystemer og evaluere ytelsen til disse verktøyene. Målet var å bidra til utviklingen av mer effektive CO2-injeksjonssystemer.

Karbonfangst og lagring utgjør et sett med viktige strategier for a redusere klimaendringer som følge av klimagassutslipp. Prosessene for CO2-injeksjon er komplekse og krever nøye overvåking og planlegging for å kunne sikre trygg og effektiv drift. Simuleringsprogramvare er et verdifullt verktøy for ingeniører for å vurdere og utforme CO2-injeksjonssystemer. Disse verktøyene muliggjør modellering og prediksjoner av CO2-atferd under ulike driftsforhold. Mens OLGA er et vanlig brukt og grundig testet programvare i industrien, får LedaFlow også anerkjennelse, noe som gjør en sammenlignende analyse nødvendig.

Flere simuleringsscenarioer ble gjennomført for å evaluere ytelsen til disse simuleringsverktøyene. Innledningsvis ble det observert numeriske ustabiliteter både i LedaFlow og OLGA i de tidlige stadiene av simuleringen, der LedaFlow viste betydelig større variasjoner i massestrømning. Imidlertid konvergerte begge verktøyene etter hvert mot mer konsistente verdier, noe som indikerer deres egnethet for simuleringer av «steady-state» flerfasestrøm.
Prediksjoner av massestrøm viste at OLGA konsekvent ga høyere verdier sammenlignet med LedaFlow, med et gjennomsnittlig avvik i total massestrøm på 9,9% og 11,7%, avhengig av inntaksparametrene. Disse variasjonene kan tilskrives forskjeller i modelleringsantakelser og konvergensproblemer.

Trykkprofiler langs «pipeline» og i «wells» avslørte tydelige forskjeller mellom LedaFlow og OLGA. LedaFlow viste et høyere trykkfall i «wells», mens OLGA demonstrerte et høyere trykkfall i «pipeline» og «flowlines».
Sekundær-simuleringene bekreftet de observerte trendene i base-simuleringene. OLGA predikerte konsekvent høyere massestrømning, mens LedaFlow viste et høyere trykkfall i «wells», noe som resulterte i avvik i injeksjonshastigheter og bunnhullstrykk.

Denne studien viser at de to programmene testet, gir til en grad forskjellige resultat. Dette er noe som må tas i beregning når man bruker disse programmene for design og operasjon av CO2 injeksjonssystemer, ettersom valg kan få varierende utfall basert på inntaksparametrene. En mer detaljert analyse vil være gunstig å gjennomføre. En slik utdypende analyse burde ta for seg flere systemparametere og effekten av urenheter i CO2-strømningen.

Table of Contents

Abbreviations

CCUS – Carbon Capture, Utilization and Storage

PPM – Parts per Million

EOR – Enhanced Oil Recovery

EOS – Equation of State

PVT – Pressure, Volume & Temperature

RKS – Redlich-Soave-Kwong

SW – Span-Wagner

P-T – Pressure-Temperature

P-H – Pressure-Enthalpy

II – Injectivity Index

IPR – Inflow Performance Relationship

Nomenclature

α_k	-	Volume fraction [-]
ρ_k	-	Density [kg/m3]
u_k	-	Velocity [m/s]
p_k	-	Pressure [MPa]
E_k	-	Energy density [J/m3]
Q_k	-	Heat source [J]
M	-	Momentum [kg-m/s]
Γ	-	Mass [kg]
f_x	-	X-component of body force [-]
P	-	Pressure [Pa]
T	-	Temperature [K]
R	-	Ideal gas constant [J/K/mol]
v	-	Volume [m3]
α	-	Dimensionless Helmholtz free energy [-]
r	-	Residual [-]
δ	-	Reduced density [-]
τ	-	Inverse of reduced temperature [-]
n	-	Indices [-]
A	-	Helmholtz free energy [J]
B	-	Second viral coefficient [-]

1. Introduction

Carbon Capture, Utilization and Storage (CCUS) is considered to be one of the most promising factors to mitigate the effect of climate change caused by greenhouse gas emissions. One of the main approaches for CCUS is the injection of CO2 into subsurface formations such as saline aquifers and depleted oil and gas reservoirs. The process of CO2 injection includes the transportation of CO2 from the source to the injection site, and the subsequent injection into the formation. (Global CCS Institute, 2023)

Due to the high complexity of CO2 injection, it is a process that requires careful monitoring and planning, to ensure the safety and effectiveness of the operation. Thus, utilizing simulation software allows for assessment and improved design of the injection system. Such simulations software are crucial tools for today's engineers as it allows for modeling of the behavior of CO2 in injection cases and predictions of the performance of CO2 under various operating conditions.

There are several such software programs used in the industry today, each one with its own advantages and limitations. Two being OLGA and LedaFlow, which are transient multiphase flow simulators, with OLGA being more commonly used in the industry. By comparing these two software programs, an evaluation of the performance of LedaFlow and OLGA in the simulation of network CO2 injection systems can be made. (R. Belt, 2011)

Varying conditions will be simulated, and results compared, with the aim to provide a comprehensive analysis of the simulation of CO2 injection systems and to contribute to the development of more effective and efficient CO2 injection systems for CCUS purposes.

1.1 Objective & tasks

The objective of this thesis is to study the two software programs LedaFlow and OLGA and investigate how they compare in the simulation of a subsea network CO2-injection system. This includes the following tasks:

- Assemble and verify two exact network models in LedaFlow and OLGA.
- Simulation of CO2 injection under a wide variety of conditions and parameters.
- Data gathering and comparison.

1.2 Thesis Outline

This thesis is structured as a scientific report, with Chapter 1 being an introduction of the topic as well as some background information. This is followed by a Chapter 2 Theory. This chapter presents relevant literature and important principles for the study. Chapter 3 presents the method. This includes the assembly of the models and the basic of how the software programs are used. Chapter 4 presents the results in the form of plots and tables. Chapter 5 discusses and compares the results. A conclusion of the work conducted in this thesis and suggested further work is presented in Chapter 6. Additionally, Appendix A presents plots of mass flow vs time.

2. Theory

2.1 Importance of CCUS

CCUS is considered as one of the main strategies in the fight against climate change. This technology is mainly comprised of CO2 capturing from stationary sources, followed by distribution and transportation to various temporary and ultimately, long-term storage sites. With the addition of utilization, the captured CO2 can be used in energy and industrial applications, predominantly. (Tan, 2017)

CO2 levels in the atmosphere are record high, at 400 parts per million (PPM), compared to the pre-industrial revolution of 280 PPM. Thus, reducing the greenhouse gas emissions, is crucial to achieve the goals set by the EU. (Europeen Union, 2023) (Global CCS Institute, 2023) CCUS is generally considered as on the few solutions that efficiently removes emissions from industrial sources in a substantial scale and as well be easily retrofitted to already existing structures, thus being adaptable to a large variety of industrial purposes. One other reason to choose CCUS is the ability to re-inject CO2 in retired reservoirs as a solution for long-term storage. (Global CCS Institute, 2023)

A significant challenge to overcome to reach the emission goals, are the high cost of capturing and transportation of the CO2. (Oil & Gas iQ, 2023) Thus, government-imposed incentives are crucial to promote and deploy CCUS. In 1991, the Norwegian government introduced a CO2-tax on emissions from mineral products and petroleum industry on the Norwegian continental shelf. This tax has increased steadily over the years since and is projected to reach 90 euros per ton by 2030. (Regjeringen, 2023) This, to speed up the transition to sustainable energy sources. An example of a business model for CCUS-projects is shown in Figure 1.

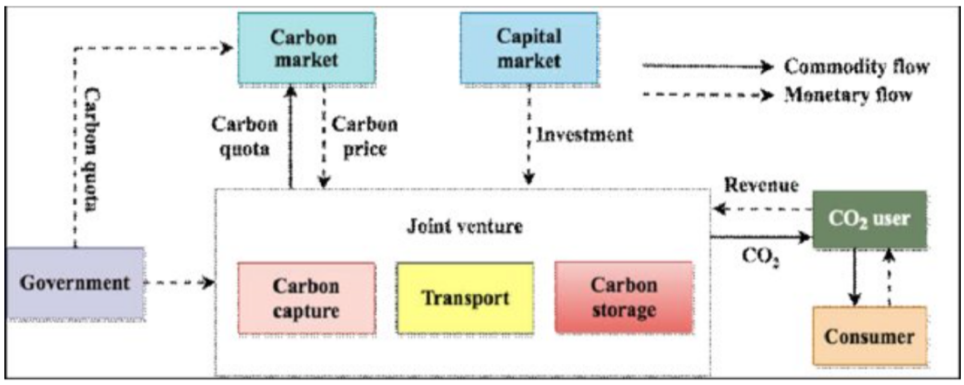

Figure 1: CCUS business model (Hasan Muslemani, 2020)

2.2 Properties & behavior of CO2

CO2 is a naturally occurring colorless and odorless gas. CO2 is a greenhouse gas with an important role in the regulation of the temperature of the Earth, as well as increased photosynthesis and plant growth. However, in excessive amounts, mostly due to human caused emission, the gas has contributed to global warming and climate change. (IPCC, 2005)
The fluid properties of CO2 make it a suitable candidate for aquifer injection and storage. At standard conditions, the CO2 is in gas phase with a density of 1,98 kg/m3, but with higher pressures, the CO2 can become a supercritical fluid. This allows the CO2 to efficiently displace fluids in subsurface reservoirs as well as fill the pore spaces in the rock matrix. (Bachu, 2003)
CO2 is a stable compound under normal conditions and is not particularly likely to react with most substances. However, it can react with some minerals to form carbonates and bicarbonates. (IPCC, 2005)
The solubility of CO2 in water is an important property in its behavior in reservoirs. In the case of water present in the pipeline, high corrosion rates are an issue. The CO2 can dissolve in the water to form carbonic acid. Corrosion rates can become as high as in the order of mm/year. Thus, during transport, it is advantageous to keep the CO2 as dry as possible. (Mohammad Ahmad, 2014) For storage in reservoirs, the dissolved CO2 in formation water is one of the main ways of trapping CO2, called hydrodynamic or solubility trapping. In the early stages of storage, trapping of free CO2 in supercritical phase, called physical or structural trapping, is the most important mechanism. However, in long-term containment of CO2, both hydrodynamic and mineral trapping will make a significant contribution. (C.A. Rochelle, 2002) Figure 2 shows the mechanisms of CO2 trapping over time.

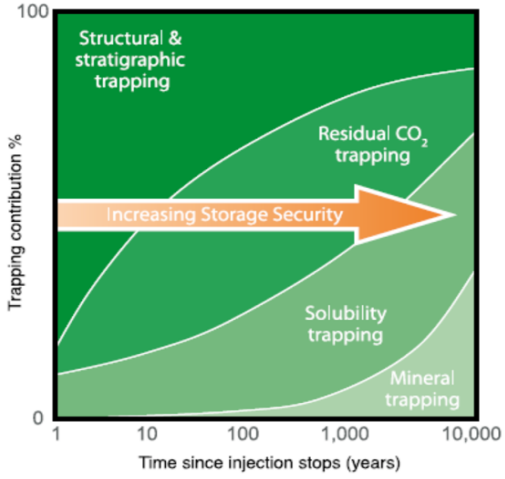

Figure 2: Various mechanisms for CO2 trapping. (Christian Hermanruda, 2009)

2.3 Transport of CO2 in pipelines

The transport of CO2 is a crucial part of CCUS. Often tankers are used, but pipelines have a big advantage as an economical and convenient transport measure. While the initial investment cost of transport pipelines is large, the running costs are low and the transportation volume is large, thus, as a long-term solution, a more reasonable choice compared to tankers. (Hongfang Lu, 2020)

As of today, most CO2 transport pipes are for the purpose of Enhanced Oil Recovery (EOR). These pipelines are made with the intention of providing a direct link between the reservoir and a CO2 source. With demand for CCUS rising, the infrastructure of these installations need a significant scale-up. (National Petroleum Council, 2020)

When transporting CO2 in pipelines, the temperature and pressure govern the state of the fluid. For efficient transport, the fluid should be in a supercritical state. To reach these conditions, the temperature and pressure must be in ranges 12 – 44 °C and 85 – 150 bar respectively. However, during transport, the temperature and pressure are not constant, but rather fluctuating within a given range. At the lower end of the pressure range, concerns regarding the state of the flow are present, while at the upper end, economy and risk is the limiting factor. At the lower end of the temperature range, ambient temperature during seasonal variations will be limiting. For the upper temperature range, the booster's outlet temperature and the limit of the pipe material is the determining factor. Preferably, the transported CO2 should be in supercritical phase as this gives the maximized amount of CO2 transported per volume unit. However, at certain points along the pipeline pressure and temperature may drop below the critical point, thus creating two-phase flow in the pipeline. (V.E. Onyebuchi, 2018)

The phase diagram for CO2 is shown in Figure 3. (Hongfang Lu, 2020)

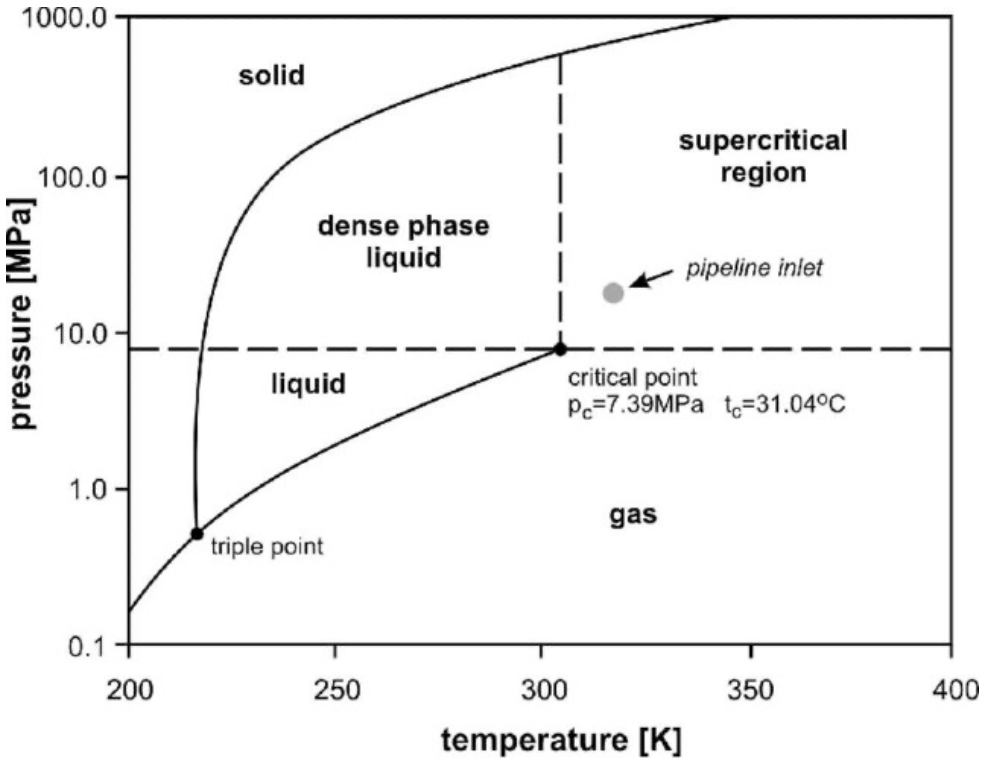

Figure 3: Phase diagram for CO2 (Andrzej Witkowski, 2014)

2.4 Multiphase flow

Multiphase flow refers to the flow of two or more phases occurring simultaneously. For CO2 this occurs when both liquid and gas states are present at the same time. (Yong Bai, 2019) Multiphase flow behavior is significantly more complex than single-phase flow. Due to the different densities of the two phases separate from each other. In addition, varying viscosities between the phases and the expansion of the gas, will cause the phases to flow at different velocities. This phenomenon is called slippage. (James P. Brill, 1999) Modelling of a multiphase problem can be tedious and not easily solved by computational methods. Thus, simplifications are a common solution method. (Pina)
By solving the conservation of mass, momentum and energy balance equations, a multiphase problem can be modelled.

For simplification of the equation set for the sake of reduced computational time, one dimensional flow is assumed. This 1D model is referred to as the two-fluid model. The conservation of mass is given by:

Equation 1

$$\frac{\partial}{\partial t}(\rho_g \alpha_g) + \frac{\partial}{\partial x}(\rho_g \alpha_g u_g) = \Gamma$$

$$\frac{\partial}{\partial t}(\rho_l \alpha_l) + \frac{\partial}{\partial x}(\rho_l \alpha_l u_l) = -\Gamma$$

Conservation of momentum is given by:

Equation 2

$$\frac{\partial}{\partial t}(\rho_g \alpha_g u_g) + \frac{\partial}{\partial x}(\rho_g \alpha_g u_g^2 + \alpha_g p_g) - p^i \frac{\partial \alpha_g}{\partial x} = \rho_g \alpha_g f_x - M_{w,g} - M^i + u_\Gamma^i \Gamma$$

$$\frac{\partial}{\partial t}(\rho_l \alpha_l u_l) + \frac{\partial}{\partial x}(\rho_l \alpha_l u_l^2 + \alpha_l p_l) - p^i \frac{\partial \alpha_l}{\partial x} = \rho_l \alpha_l f_x - M_{w,l} + M^i - u_\Gamma^i \Gamma$$

Conservation of energy is given by:

Equation 3

$$\frac{\partial}{\partial t}(\rho_g \alpha_g E_g) + \frac{\partial}{\partial x}\left(\rho_g \alpha_g u_g \left(E_g + \frac{p_g}{\rho_g}\right)\right) + p^i u_\tau^i \frac{\partial \alpha_g}{\partial x} = \rho_g \alpha_g u_g f_x + Q_{w,g} - Q^i - u_M^i M^i + E^i \Gamma$$

$$\frac{\partial}{\partial t}(\rho_l \alpha_l E_l) + \frac{\partial}{\partial x}\left(\rho_l \alpha_l u_l \left(E_l + \frac{p_l}{\rho_l}\right)\right) + p^i u_\tau^i \frac{\partial \alpha_l}{\partial x} = \rho_l \alpha_l u_l f_x + Q_{w,l} + Q^i + u_M^i M^i - E^i \Gamma$$

In this description, information about the internal moving interfaces is not present. Additionally, information regarding the local gradients along the cross section of the pipe, will not be accurately modelled due to the averaging of the two-fluid model.

By implementing a slip relation in the form $u_1 - u_2 = \phi(\alpha_1, p, T, u_1)$ a reduction of the complexity of the two-fluid model can be achieved, especially if the pressures of the two fluids are equal. Then, the momentum equations can be joined into one combined momentum

equation. This also applies for equal temperatures, allowing for a combined energy equation. This new modified model is called the drift-flux model, with the conservation of mass given as:

Equation 4

$$\frac{\partial}{\partial t}(\rho_g \alpha_g) + \frac{\partial}{\partial x}(\rho_g \alpha_g u_g) = \Gamma$$

Equation 5

$$\frac{\partial}{\partial t}(\rho_l \alpha_l) + \frac{\partial}{\partial x}(\rho_l \alpha_l u_l) = -\Gamma$$

Conservation of momentum:

Equation 6

$$\frac{\partial}{\partial t}(\rho_g \alpha_g u_g + \rho_l \alpha_l u_l) + \frac{\partial}{\partial x}(\rho_g \alpha_g u_g^2 + \rho_l \alpha_l u_l^2 + p) = (\rho_g \alpha_g + \rho_l \alpha_l) f_x - M_w$$

Conservation of energy:

Equation 7

$$\frac{\partial}{\partial t}(\rho_g \alpha_g E_g + \rho_l \alpha_l E_l) + \frac{\partial}{\partial x}\left(\rho_g \alpha_g u_g \left(E_g + \frac{p}{\rho_g}\right)\right) + \left(\rho_l \alpha_l u_l \left(E_l + \frac{p}{\rho_l}\right)\right) = (\rho_g \alpha_g u_g + \rho_l \alpha_l u_l) f_x + Q_w$$

In addition to being a simpler model, the drift-flux model has some advantages in stability compared to the two-fluid model. However, depending on the flow regime, this model may not always be the preferred way. (P.Aursand, 2013)

2.4.1 Pressure drop

Pressure drop is a crucial parameter regarding multiphase flow. The pressure drop determines the required energy to transfer a fluid through a pipe. Pressure drop for a multiphase system is generally higher than for a single phase due to the interaction between the phases, but are dependent on several factors, such as flow regime, pipe geometry and fluid properties. (R.W. Lockhart, 1949)

Multiple models have been developed to predict pressure drop in multiphase flow systems with experimental studies to validate the accuracy of these models. Due to the complex nature and physics behind multiphase flow, no one single model or empirical calculation will be optimal for every scenario. (J.P. Brill, 1999)

2.4.2 Holdup

Holdup refers to the fraction of each phase present in the multiphase flow by the volume occupied in the pipe. Holdup is an important parameter in the prediction of pressure drop and flow regime in a multiphase flow system. Several correlations have been made, called "void fraction correlations" to predict the holdup. These correlations are based on parameters such as flow rate, pipe diameter, fluid density, viscosity, and pipe inclination.
Holdup may have significant impact on the flow regime, for example, a high gas holdup can cause the flow regime in a horizontal pipe to transition from stratified flow to slug, which can have a significant impact on flow behavior. (Cheng, 2006) Figure 4 show a representation of liquid holdup.

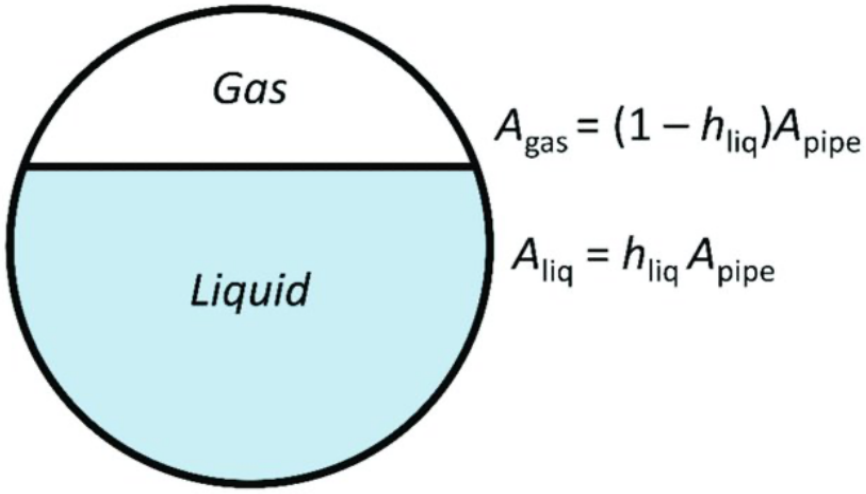

Figure 4: Representation of the definition of liquid holdup. (Rutger Tromp, 2021)

2.4.3 Flow assurance considerations

The feasibility of the CO2 flow is dependent on several factors, including operational conditions, impurities present and the potential of hydrate formation. To achieve a thorough assessment of the flow assurance, it is important to consider the dynamic and the non-steady state. This is due to the difficulty of predicting the frequency of the different operating states. This includes shutdown and start-up. Previous studies have described these occurrences in addition to planned and un-planned shutdown and start-up. It is observed that pressure, density, temperature, viscosity, and interfacial tension affect the flow assurance of the CO2 flow. (V.E. Onyebuchi, 2018)

2.5 Equation of state

An Equation of State (EOS) is an important tool to accurately express the thermodynamic properties of a fluid. This is to describe the state of a fluid at any given condition related to pressure, temperature, and volume. The use of EOS for Pressure, Volume & Temperature (PVT) modeling has shown to be crucial for several reasons:

- Separation process optimization
- Black-oil property generation
- Miscibility calculations
- Estimating hydrocarbon reserves
- Lab report quality check (Bhattacharyya, 2020)

2.5.1 Redlich-Soave-Kwong

The Redlich-Soave-Kwong (RKS) EOS is a modification of the original EOS by Redlich and Kwong from 1949. (Kwong, 1949) This EOS is commonly used in the petroleum industry. Characteristics of the model is high complexity, accounting for intermolecular forces, giving accurate predictions of thermodynamic properties. (Soave, 1972) The structure of the RKS is defined by:

Equation 8

$$P = \frac{RT}{v - b} - \frac{a}{v(v + b)}$$

Where a and b are the model parameters. These parameters can be obtained by:

Equation 9

$$a = \Omega_a \frac{R^2 T_c^2}{p_c} \alpha(T)$$

$$b = \Omega_b \frac{RT_c}{p_c}$$

$$\alpha(T) = \left(1 - m(\omega)\left(1 - \sqrt{\frac{T}{T_c}}\right)\right)\text{^2}$$

To obtain the coefficients Ω_a and Ω_b and $\alpha(T)$, the following can be applied:

Equation 10

$$\Omega_a = 0{,}42748$$

$$\Omega_b = 0{,}08664$$

$$m(\omega) = 0{,}480 + 1{,}574\omega - 0{,}176\omega^2$$

2.5.2 Span-Wagner

In 1996 Span and Wagner presented an EOS for CO2. This EOS is generally considered as the most accurate thermodynamic model for CO2, but comes at the cost of being highly complex, containing as many as 42 terms. Some of these terms are complex exponentials that has been known to cause computational problems.

The Span-Wagner (SW) EOS is valid for pressures up to 30 MPa and for temperatures up to 523 K. The EOS is especially accurate in gas and liquid regions, but other models may be preferable for critical region.

The fundamental equation used to describe all thermodynamic properties is the Helmholtz free energy. The formulation for the residual part of the Helmholtz function is:

Equation 11

$$\alpha r(\delta,\tau) = \sum_{i=1}^{7} n_i\, \delta^{d_i}\tau^{t_i} + \sum_{i=8}^{34} n_i\, \delta^{d_i}\tau^{t_i} e^{-\delta^{c_i}} + \sum_{i=35}^{39} n_i\, \delta^{d_i}\tau^{t_i} e^{-\alpha_i(\delta-\varepsilon_i)^2-\beta_i(\tau-\gamma_i)^2} + \sum_{i=40}^{42} n_i \Delta^{b_i}\, \delta\tau^{t_i} e^{-C_i(\delta-1)^2-D_i(r-1)^2}$$

Where $\Delta = ((1-\tau) + A_i((\delta-1)^2)^{\frac{1}{2\beta_i}})^2 + B_i(\delta-1)^2)^{a_i}$.

The argument shown in the exponential terms is a function of density and temperature, and this the reason for the complexity of the computation. (Kim, 2007)

2.6 Flow regimes

The ability to predict the flow pattern or flow regime at any given location along a pipeline is crucial. The models or correlation equations used to predict the behavior of the flow, such as pressure drop and liquid holdup, is directly dependent on the flow pattern. Flow regimes in horizontal pipelines show similar behavior compared to those of vertical pipelines. However, asymmetry in the annulus, most obvious for lower flow rates, caused by gravity, will be a differencing factor. (Holland, 1995) Flow patterns for upward-vertical flow is shown in Figure 5.

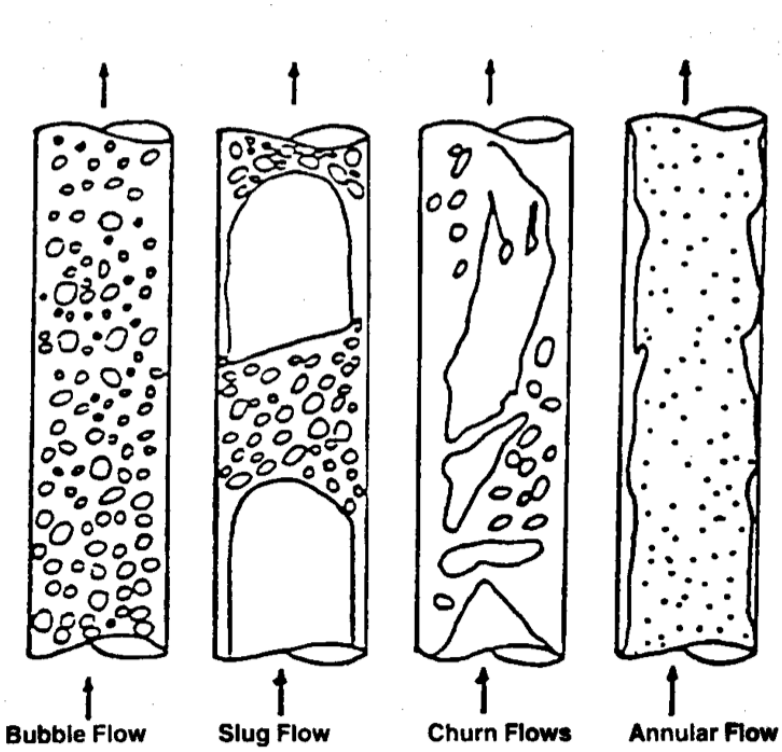

Figure 5: Upward-vertical flow regimes. (James P. Brill, 1999)

2.6.1 Bubble flow

Bubble flow displays a uniformly distributed gas phase in the continuous liquid phase. This flow regime can be distinguished further dependent on any slippage present between the two phases. This classification is bubbly and dispersed bubbly flow. Bubbly flow is characterized by larger but fewer bubbles, that due to slippage, have a higher velocity than the liquid phase. No relative velocity is present in dispersed bubbly flow, and the gas bubbles are moving along the liquid phase. This flow pattern is characterized by smaller bubbles, but at a larger amount. (James P. Brill, 1999)

2.6.2 Slug flow

This flow pattern is characterized by several slugs traveling in the direction of the flow. This slug is composed of liquid, traveling inside a gas bubble called the Taylor bubble. The slug travels in a wave like pattern, periodically picked up by rapidly moving gas, passing along the pipe in a higher velocity than the average velocity. This type of flow can in some cases create dangerous vibrations in the pipe due to impact on bends and other fittings. (Dey, 2023)

2.6.3 Churn flow

This flow pattern is a generally chaotic flow of liquid and gas with no symmetrical bubbles present of either of the phases present. Additionally, either the gas or liquid phase appears to be continuous. Typical for churn flow is an alternating direction of motion in the liquid phase. (James P. Brill, 1999)

2.6.4 Annular flow

Annular flow regime displays axial continuity of gas phase in the central core with a liquid film along the wall of the pipe, and dispersed droplets in the gas core. The amount of dispersed droplets is increased with higher flow rates, resulting in a thin film of liquid at the pipe wall. Interfacial shear stress between the phases is an important parameter for this flow regime. (James P. Brill, 1999)

2.7 CO2 injection

Since the 1950s, CO2 injection has been used for EOR purposes and research on this topic is still ongoing. However, relatively recent, the research into CO2 injection for environmental purposes has become interesting. This includes not only the technical aspects, but also safety, feasibility, and the economics of long-term storage of CO2 in reservoirs. (O. Izgec, 2005)
Due to the economic constraints of CO2 injection into aquifers, it is advantageous to inject with the highest possible flow rate, and with as few wells as possible. The true injection rates tend to fall lower than expected and over time, injection rates will decrease further. (Mohamed, 2022)
CO2 injection has been studied extensively and researchers has proven the feasibility and safety of long-term storage in large quantities. Some potential risks are associated with CO2 injection, such as the potential for CO2 leak to the surface and seismic factors. Thus, careful monitoring is necessary to ensure safety and effectiveness of CO2 injectivity and storage. (Bachu, 2003)

An important parameter in the field of CO2 injection is the injectivity index (II). Injectivity index is the measure of the ability a formation has to accept injection fluid. It is defined as the volume of fluid injected into the formation per time per unit pressure differential. The injectivity index is dependent on the formation rock and fluids, as well as the injection pressure and the configuration of the injection well. A higher II is an indication of a high permeability formation and a good ability to accept fluids at a fast rate. For CCUS projects, the II is a parameter affecting the effectiveness of the injection process. Due to the low economic tolerances for CCUS projects, high effectiveness is advantageous. (Bachu, 2003)

2.7.1 Advantages & challenges with storage in depleted reservoirs

One of the most compelling arguments for using depleted oil and gas reservoirs for long-term storage of CO2 is the low pore pressure. After production of a reservoir has halted, the pressure is significantly lower than the original reservoir pressure before production started. This allows for refilling of the reservoir until the original reservoir pressure is reached. Another advantage of using depleted reservoirs is the already attained geological data, aiding in the assessment of total capacity. Due to the already present infrastructure, such as pipelines and wells, considerations into the use of these for injection can be made, drastically lowering

the upfront cost of the injection project. And at last, the production history confirms the reservoir's ability to contain large amounts of fluid without leakage. (M. Loizzo, 2010)

Using depleted oil and gas reservoirs as long-term storage of CO2 may seem to be an obvious choice, but some disadvantages must be accounted for. First, accessibility is a key factor. the CO2 to be injected must be transported to the site, either by ship or by subsea pipelines. This is costly either way, and therefore some distant reservoirs may be unreachable due to the high cost of pipeline installation or enduring ship transport. Another potential issue is the fact that many depleted reservoirs may have a large number of wells, drilled several decades ago, with outdated technology and poor maintenance, thus being a potential pathway for leakage. When CO2 is injected into the reservoir, re-pressurization occurs, and some unforeseen weakening may impact the integrity of the seal. (M. Loizzo, 2010)

2.8 Simulation of CO2 flow

Throughout the last couple of decades, the development of multiple flow simulation tools has been made. (P.Aursand, 2013)These tools are mostly used for oil and gas, so investigation into the programs accuracy in predicting flow simulations regarding CCUS is an interesting topic. (P.Aursand, 2013)

2.8.1 LedaFlow

LedaFlow is a transient multiphase flow simulation software developed by SINTEF, ConocoPhillips and TotalEnergies. Proof of concept was initialized in 2001, with a set of full-scale experiments performed at the SINTEF Multiphase Flow Laboratory in Tiller. By 2011 a commercial version of LedaFlow was released, but further improvements have still been made. This includes hydrodynamic slug prediction, hydrate transport, wax deposition and CO2 transport. (LedaFlow, 2023)

LedaFlow is based around a model developed on three-phase oil-water-gas mixes, with a few equations of states to choose from, including RKS and Peng-Robinson. (P.Aursand, 2013)

2.8.2 OLGA

OLGA is a tool for dynamic multiphase flow simulation with more than 30 years of research and development. The development was started by Statoil in the early 80s and is continuously being updated. The model solves for three-phase mixes and contains 9 conservation equations. A recent update to OLGA allows for accurate CO2 transport simulation. This model uses six conservation equations and for pure CO2, the Span-Wagner equation of state is used. Currently OLGA cannot consider impurities and the formation of dry ice. (P.Aursand, 2013)

OLGA uses pressure and temperature (P-T), as well as fluid composition as independent variables when performing phase and flash calculations. For a typical oil and gas multicomponent case, this is often an accurate solution since the phase fraction and physical properties change gradually with pressure and temperature. However, along the saturation line, the gas/liquid fraction is dependent on the energy input. For a system with a dominant main component such as for CO2 flow, a close to 100% CO2 concentration, will cause the phase envelope to approach a single line. Thus, causing a small change in pressure or temperature to result in a large change in the equilibrium gas/liquid fraction, in the region of the phase change. This can lead to instability and convergence issues for the simulation.
To solve this issue, a solution is to implement pressure and enthalpy (P-H) as the two independent variables. Causing the gas/liquid fraction to be dependent on the input energy. Plots showing the change from pressure and temperature to pressure and enthalpy is shown in Figure 6. (Morten Langsholt, 2014)

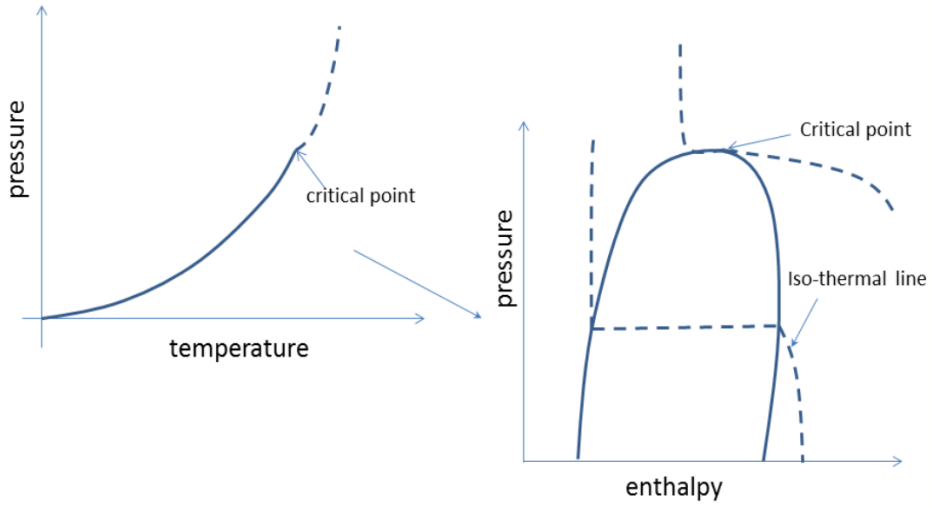

Figure 6: Change of formulation to pressure and enthalpy (Morten Langsholt, 2014).

3. Method

For the purpose of running simulations and obtaining data, the two programs OLGA and LedaFlow has been used. Licenses to LedaFlow version 2.8.264.024 and OLGA 2020.2.0 have been provided by NTNU.

For comparison purposes, two exact cases were created in both LedaFlow and OLGA, with the intent of investigating the accuracy compared to each other and to existing fields. The base case is based on the Snøhvit field in the Barents Sea.

3.1 Snøhvit field

Snøhvit is a field in the Barents Sea outside of Hammerfest. The field was sanctioned in 2002 and was on stream by 2007. Geological storage was evaluated as early as 1991 and by 2005 the injection well 7121/4-F-2H was drilled. A 153 km long pipeline was installed from Melkøya LNG plant to the template and CO2 injection started in 2008. Until 2040 it is expected to be injected 0,7 million tonnes/year. The storage site at Snøhvit is called Tubåen formation and is expected to store 22 million tonnes by the end of the gas production period.

The Snøhvit CO2 injection project was a significant achievement in the research and testing of CCS. The project demonstrated the feasibility and gave valuable insight into the challenges associated with CO2 injection. (Statoil, 2010) Illustration of the Snøhvit field is shown in Figure 7.

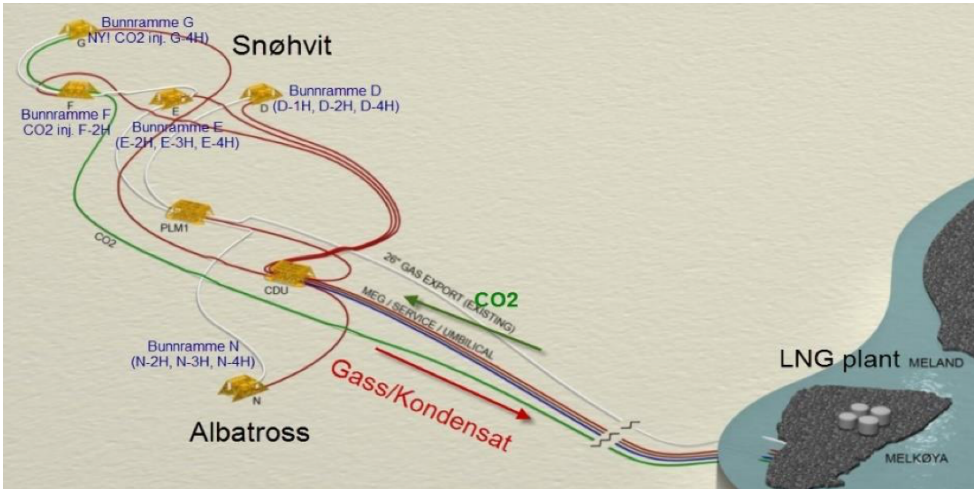

Figure 7: Illustration of Snøhvit field and Melkøya with surrounding fields. (Equinor, 2020)

The CO2 is transported through an 8-inch pipe from Melkøya to the field located at 320 meters belove the sea surface. The inlet pressure at shore is approximately 100 bar and an increase of 10 bar is observed at the end of the transport pipeline. The flow velocity is about 0,55 m/s and the mass flow rate in the range 60 – 85 tons/hour. Continuing from the template, a 7-inch tubing carries the CO2 from the seabed to the perforation, located 2400 m below the seabed. The well is angled at 27 degrees from vertical. (Statoil, 2010)
From exploration wells in the Snøhvit area, pressure recordings from the reservoir were taken. In Figure 8, a plot of pressure vs depth is shown.

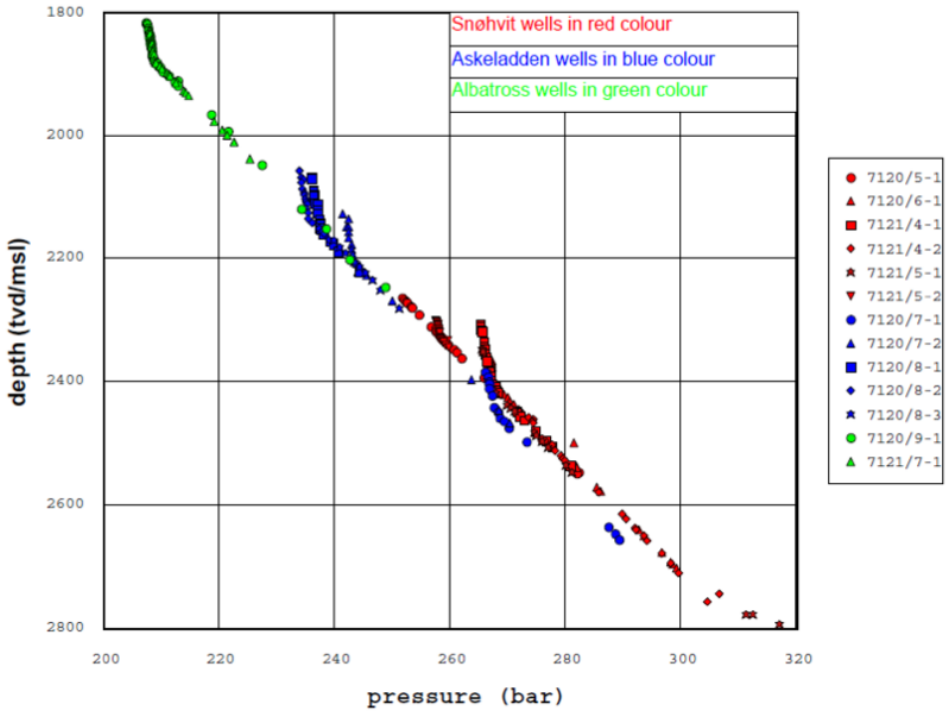

Figure 8: Pressure vs depth at Snøhvit. (Statoil, 2010)

From multiple well tests and measurements during logging, the temperature profile was obtained. Figure 9 show the well temperatures vs depth.

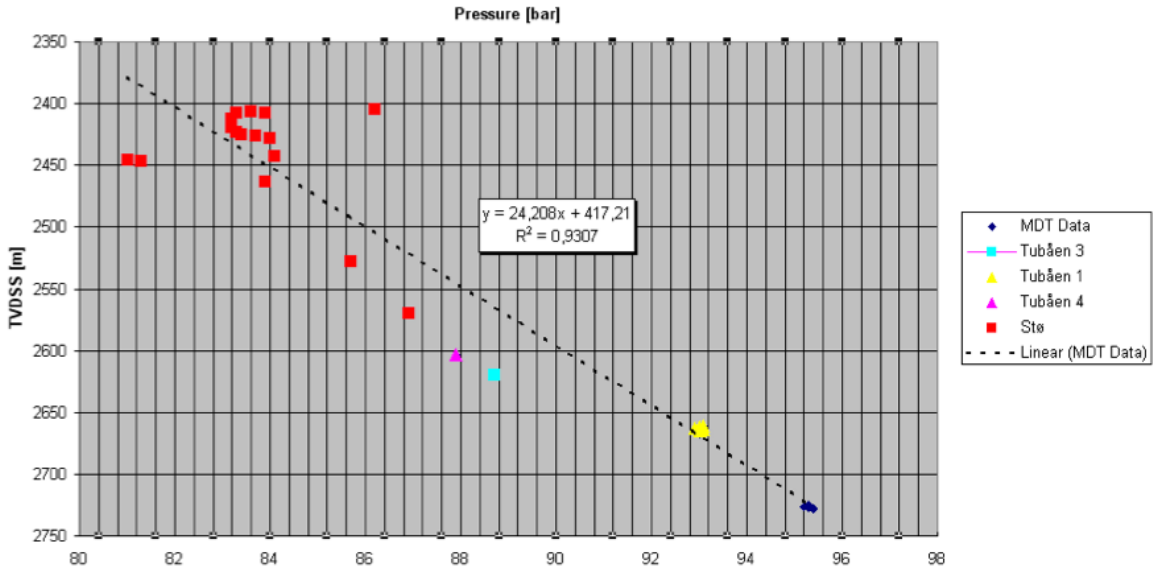

Figure 9: Temperature vs depth at Snøhvit. (Statoil, 2010)

The pipeline transporting the CO2 reaches from the LNG plant, along the seabed to the template above the Tubåen formation. The profile of this pipeline is shown in Figure 10.

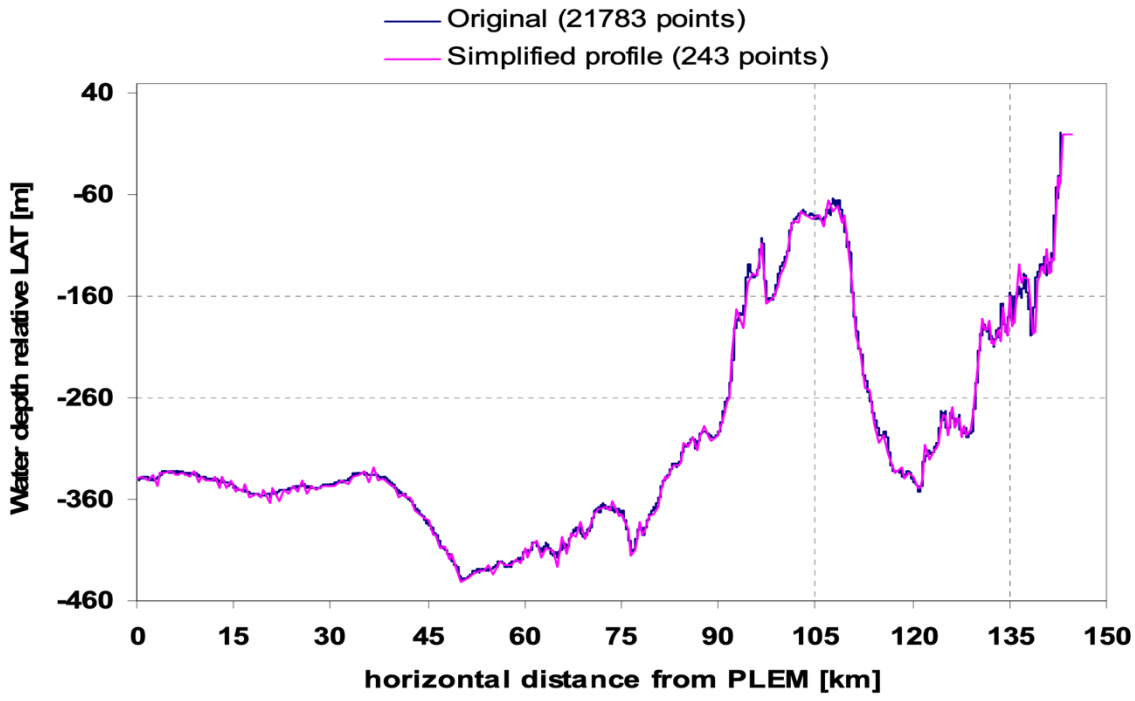

Figure 10: Original and simplified pipeline profile. (Jostein Pettersen, 2011)

3.2 Case assembly

By using the available data for Snøhvit, a simulation case was created in LedaFlow and OLGA. To allow for more investigation into the models' prediction of injectivity and performance, the case was expanded. The number of injection wells was increased from 1 to 3 clusters of 3 wells each, a total of 9 wells. A sketch of the simulation layout is shown in Figure 11.

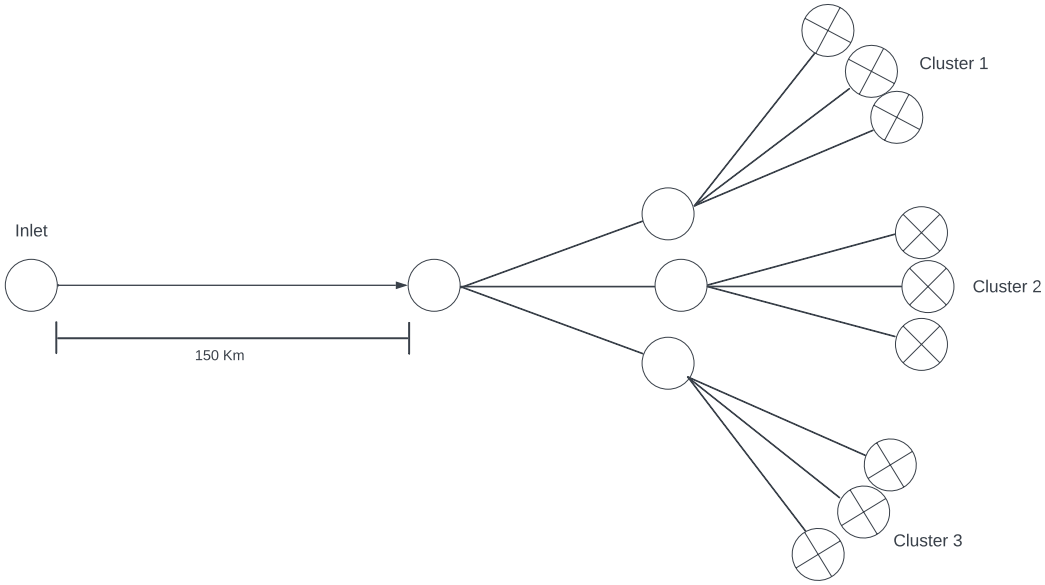

Figure 11: Simulation case layout

When creating the simulation case in LedaFlow and OLGA, creating the exact transport pipeline profile as for Snøhvit was considered both impractical and unnecessary. Due to the complexity and high number of points, a choice was made to simplify the pipeline profile. A rough outline of the profile was made in both LedaFlow and OLGA. The simplified pipeline profile is shown in Figure 12.

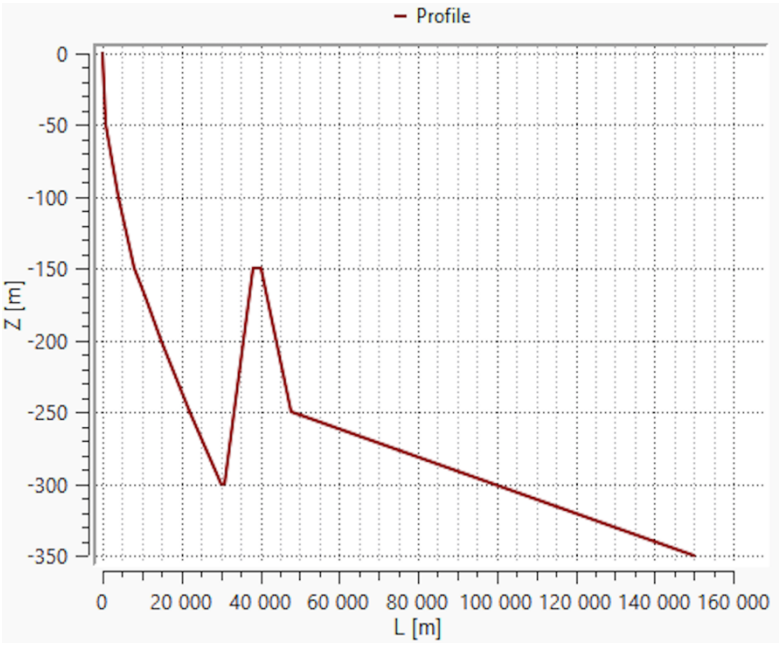

Figure 12: Pipeline profile for the simulation case

Other parameters for the simulations were either taken from Snøhvit data or adjusted to fit the scaling of the number of wells. To handle a significantly higher mass flow of CO2, the original 8-inch pipe used at Snøhvit, was scaled to 860 mm in diameter. Additionally, the flowlines connecting the transport pipeline to the clusters were scaled to 360 mm and the CO2 injection wells were close to original size, at 180 mm.

For both the LedaFlow and OLGA simulations, an Inflow Performance Relationship (IPR) was used to simulate a CO2 injection well. An IPR is the relation between the production rate and flowing bottom hole pressure. Commonly for oil wells, the fluid inflow rate is assumed to be proportional to the difference between reservoir pressure and wellbore pressure. (A. Jahanbani, 2009) By adjusting the injectivity index of the well, the performance of the of the injection well can be adjusted.

3.2.1 OLGA user interface

When opening OLGA, the user is presented with a file menu where the choice is given to either open a blank case, import a case, or choose between a selection of preset sample cases. When creating a blank case, specifying the name and location of storage is possible. A project is created by OLGA when a new case is defined. This case is stored in this project.

When a case is opened, the main page of OLGA is presented. The main components, and most used features on this page is the components view, diagram view and the model browser. Additionally, the page consists of case tabs, case tool bar and check/run bar. Main user interface is shown in Figure 13.

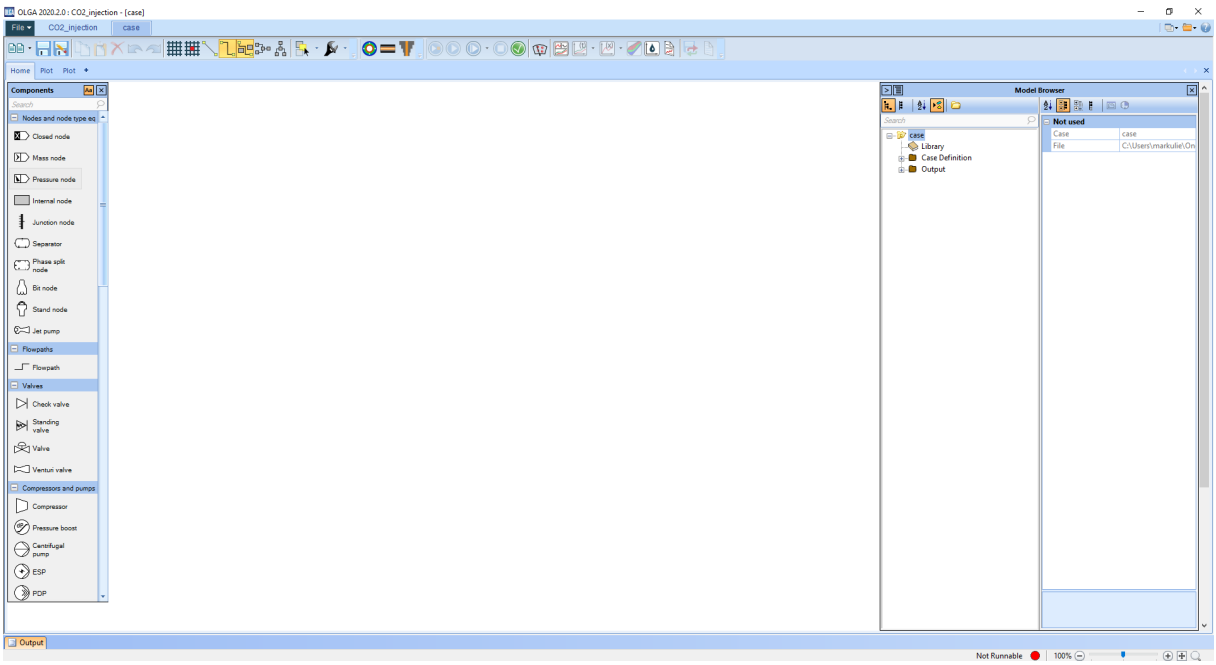

Figure 13: Main user interface

The components view, shown in Figure 14, contains the available components that can be used to build the case. The categories of the components are:

- Flow components
- Controllers
- Process components
- FA-models
- Boundary and initial conditions
- Results

These components are click-and-dragged onto the diagram view and assembled as wanted to obtain the required model.

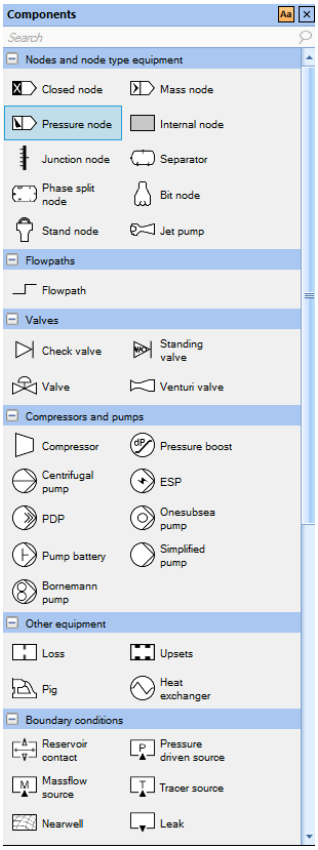

Figure 14: List of components in OLGA

The diagram view is a plain canvas where all components for the case are assembled. The main layout of any model is with a boundary or initial component at inlet and outlet. From here, multiple flow components and process components, as well as controllers can be used to create very complex models.

The model browser is where the user adjusts most of the parameters of the case. The model browser contains the base parameters for the case such as the PVT file info, wall, ambient temperature, and the duration of the simulation runtime. Also found in the model browser, are all the components used to build the model and settings for the component's geometry, position, inlet and outlet conditions and all additional connected parts can be specified here. The model browser is shown in Figure 15.

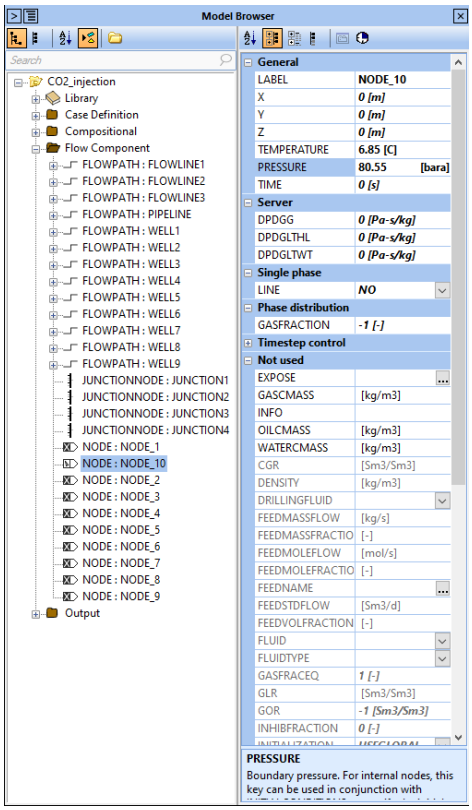

Figure 15: Model browser in OLGA

After assembly of the model, found in the top bar, is the check symbol. This notifies of any critical flaws in the model with notes in the output tab. This lets the user know the location of this flaw and the steps to resolve it. When the check is complete, the case is ready to be run.

The OLGA user interface incudes options for various plots after the run of the simulation. This feature is found in the main tab and allows for plotting either trend or profile variables. Trend plots have time along the x-axis, where profile plots have pipeline length. There is a plethora of variables to plot, such as pressure, temperature, holdup, pressure drop, mass flow and many more.

3.2.2 LedaFlow user interface

When launching the LedaFlow software, the user is taken directly to the main user interface. By pressing the file tab in the top left corner, the user is given the choice to create a new case. This can either be a blank case or one of the sample cases already created by LedaFlow. When opening a blank case, a section of pipeline with two nodes is automatically created, as shown in Figure 16. In LedaFlow, the inlet and outlet node can either be a pressure boundary or a flow boundary, using either fixed pressure or fixed mass flow as the determining parameter, respectively.

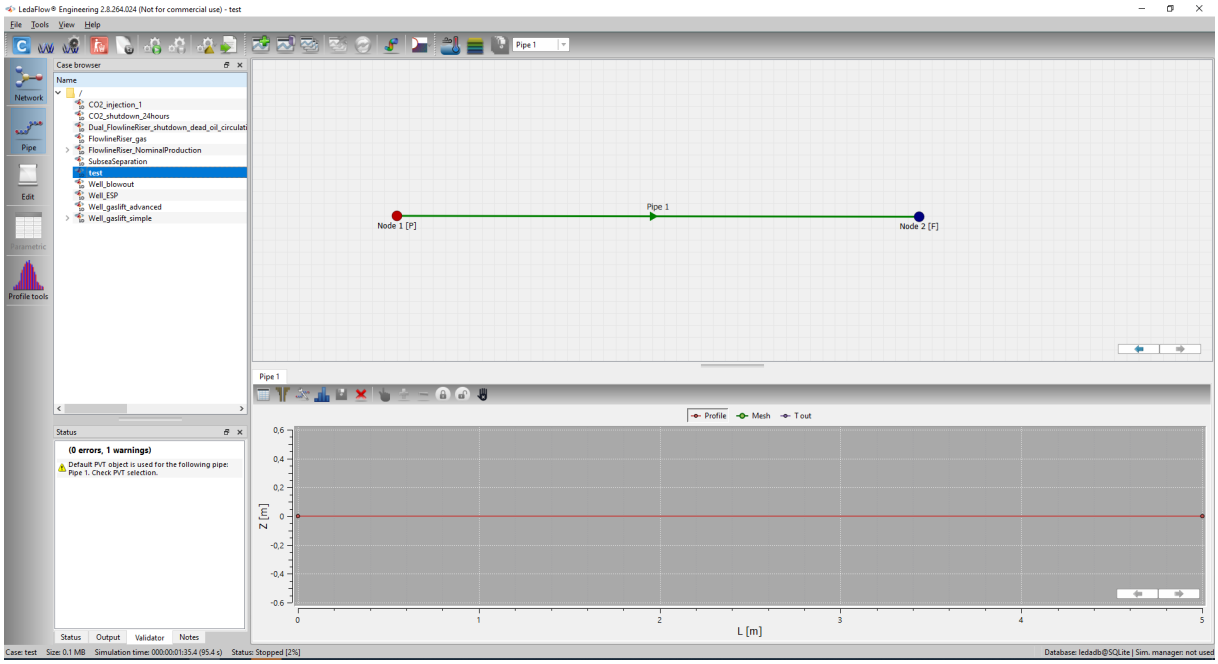

Figure 16: Main user interface of LedaFlow

Along the left side of the main user interface tabs named network, pipe, edit, parametric and profile tools are shown. By only having the network-tab up, the user can see and edit the pipes, connections, and components of the case. The pipe-tab gives a profile of the pipe, including length and inclination. From this tab it is further possible to set the pipe diameter, wall thickness, ambient temperature, and wall parameters. These two tabs are the most used among the five left side tabs.

Top left on the tool bar on the main user interface, a “case” tab is shown. This allows for PVT and fluid settings for the case. The default is LedaFlow’s built in black oil PVT model, but for further customization, the Multiflash add-in is available. This takes the user to the window shown in Figure 17.

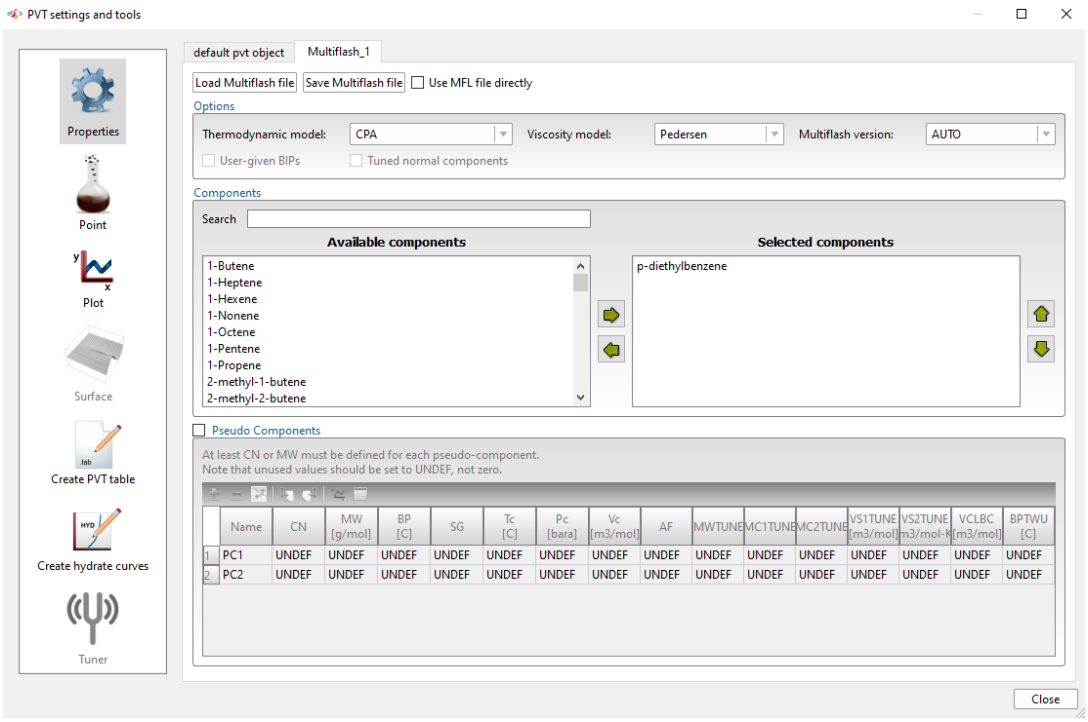

Figure 17: Multiflash PVT table

In this window allows for changes in thermodynamic models, such as, CPA, RKS and SW. The fluid can be created by choosing between a large table of components and adjusting the fractions of the different components.

When assembling the network of the case, right clicking on one the of the nodes allows for additional pipes starting or ending from the given node. This pop up is shown in Figure 18.

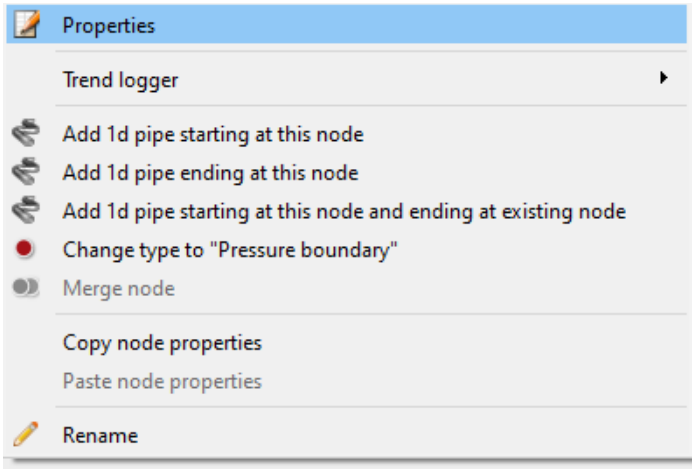

Figure 18: Alternatives for expanding the pipelines.

For further options, right clicking the pipeline section, the user can add different components or features to the pipe section, such as valves, controllers, leaks and other inflow and outflow options. This pop up is shown in Figure 19.

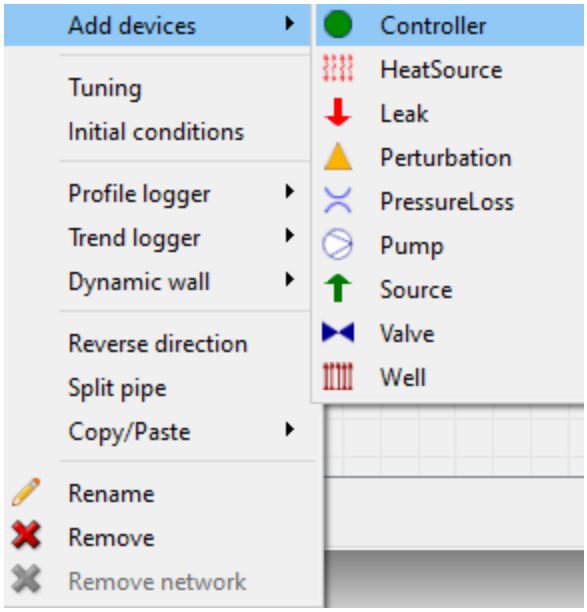

Figure 19: List of features to add to the pipeline.

When the case is assembled, the initialize button can be pressed in the top tool bar. After adjusting the runtime, the case can be run. When finished, plotting options, as well as a 3D model is available in the top tool bar for visual representation of the results.

4. Results

After assembly and verification of the network model in both LedaFlow and OLGA, comparison simulations were run. The intention of these tests was to assess the similarities and differences of the two simulation tools at a wide variety of conditions and parameters. This includes varying inlet pressures, mass flow rates, and injectivity index. From the attained runs using these parameters, plots were made to investigate the simulations time to stabilize, temperature and pressure profiles along the pipelines, flow regimes and mass flow rates at different points along the model and the injection rate into the reservoirs. Investigation into the two model`s ability to simulate mass flow rates with different injectivity indexes of the wells will also be conducted.

The data is presented in the form of plots. This is either trendline plots or profile plots. Trendline plots show the data at one given point along the model versus simulation runtime. Thus, allowing for investigation into the time to stabilize for the given conditions and simulation software. Profile plots show the data versus the length of the pipeline. For this format, data is only shown at a point in time after stabilization. When referencing a location along the model, Figure 20 show the location in question.

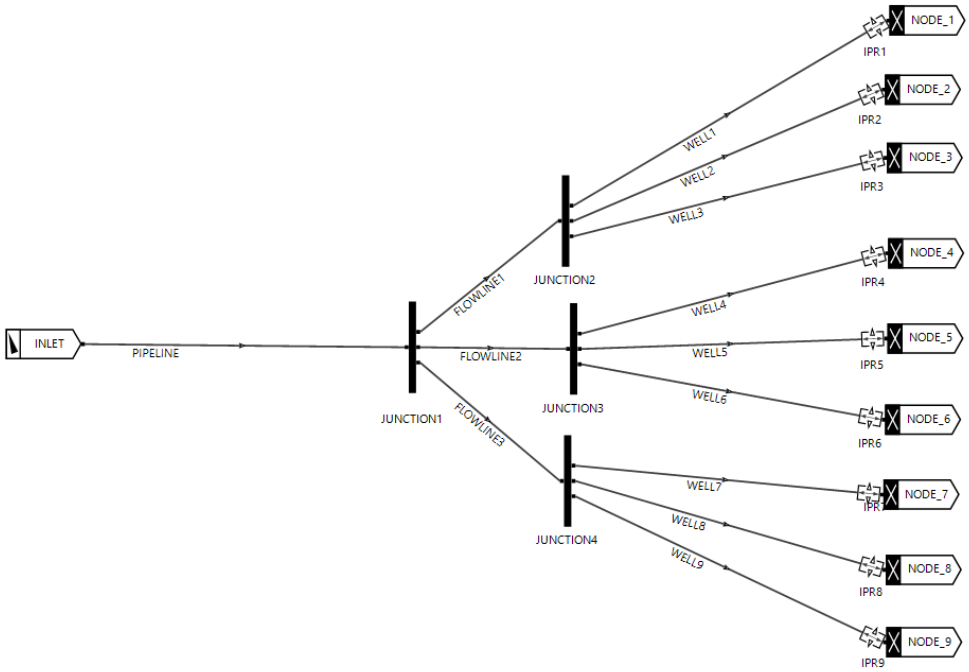

Figure 20: Schematic representation of the model, displaying the pipe and component names.

4.1 Base case, 10 II

For this scenario, the model was based on the Snøhvit field, scaled up to 3 clusters of 3 wells each. For this case, the injectivity index was identical for the 3 clusters, at 10 kg/s-bar. The runtime of the tests was set to 6000 seconds. In LedaFlow, the steady-state processor was used and pure CO2 from the built-in Multiflash add-in with RKS as the chosen EOS. In OLGA, due to the use of the pressure and enthalpy formulation, user defined initial conditions must be given. The fluid is defined by the single component CO2 feature in OLGA, using the SW EOS.

The reservoir pressure for this case was set to 250 bar and reservoir temperature to 95 °C, as well as the inlet fluid temperature to 6,85 °C. Parameters for the pipe system for this case is shown in Table 1.

Table 1: Parameters for pipe system

	Length	**Diameter**	**Ambient temperature**	**Roughness**
Pipeline	150 km	860 mm	4°C	0,045 mm
Flowline	1 km	360 mm	4°C	0,045 mm
Well	3 km (depth)	180 mm	7-95°C (gradient)	0,045 mm

4.1.1 80 bar inlet, mass flow vs time

Tests were run with 80 bar inlet in both LedaFlow and OLGA. Simulations were run and data extracted as trendline data at start of inlet, flowline 1 and well 1. In Table 2, mass flow after stabilization is shown.

Table 2: Mass flow for 80 bar inlet after stabilization

80 bar		**LedaFlow**	**OLGA**	
Inlet		920	1100	kg/s
Flowline 1		315	340	kg/s
Well 1		105	113	kg/s

Additional plots this run is shown in Appendix A. For these plots, the orange line represents LedaFlow data and the blue OLGA. Figure A1, at inlet display some instabilities for the first half of the LedaFlow simulation, but eventually stabilizes at around 920 kg/s. The mass flow from OLGA is significantly higher at around 1100 kg/s at the point of stabilization.
In Figure A2, at flowline 1, a smaller deviation between LedaFlow and OLGA is observed, with 315 kg/s and 340 kg/s respectively at the point of stabilization.
A similar deviation is observed in Figure A3, with a mass flow at the inlet of well 1 to be 105 kg/s from LedaFlow and 113 kg/s from OLGA.
Due to the symmetry of the model, and equal injectivity index for all wells, every flowline and well will show similar results, respectively.
The deviation between LedaFlow and OLGA is shown in Figure 21 for inlet, flowline and well, respectively.

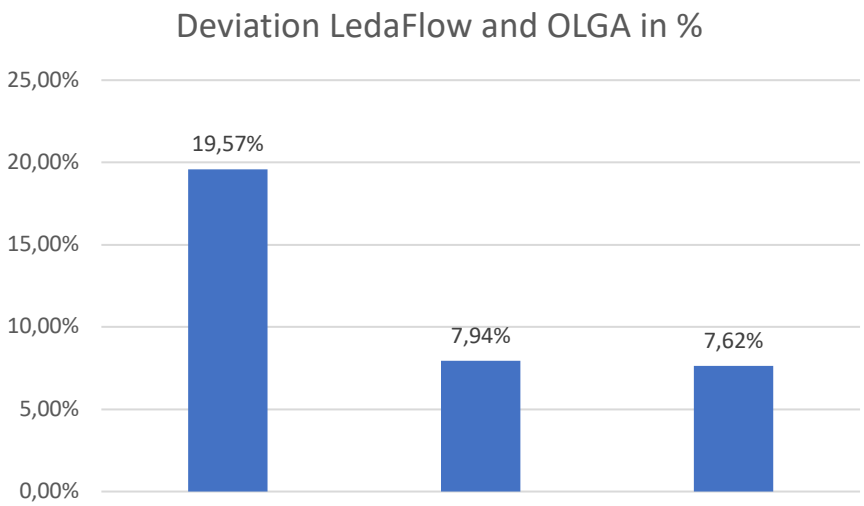

Figure 21: Deviation in mass flow between LedaFlow and OLGA

4.1.2 80 bar inlet, pressure profile

From the same simulation run, data for pressure profile was extracted from LedaFlow and OLGA. These plots display data after stabilization had occurred and were plotted as pressure vs the length of the pipeline. Figure 22 and 23 show pressure profile of the pipeline and well 1, respectively.

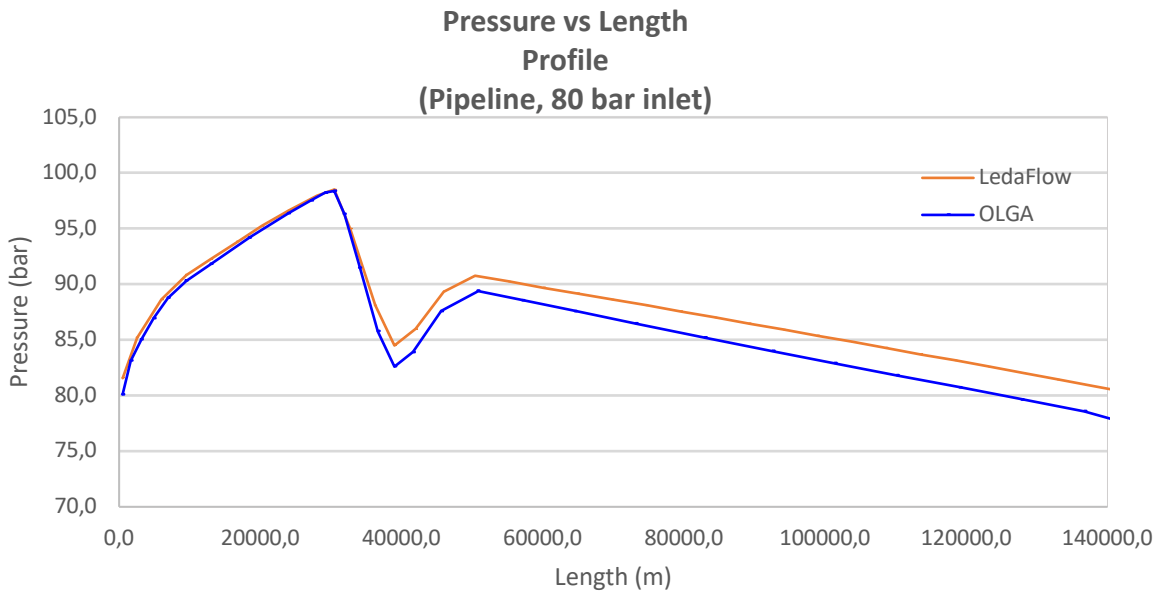

Figure 22: Pressure vs length for 80 bar inlet at pipeline

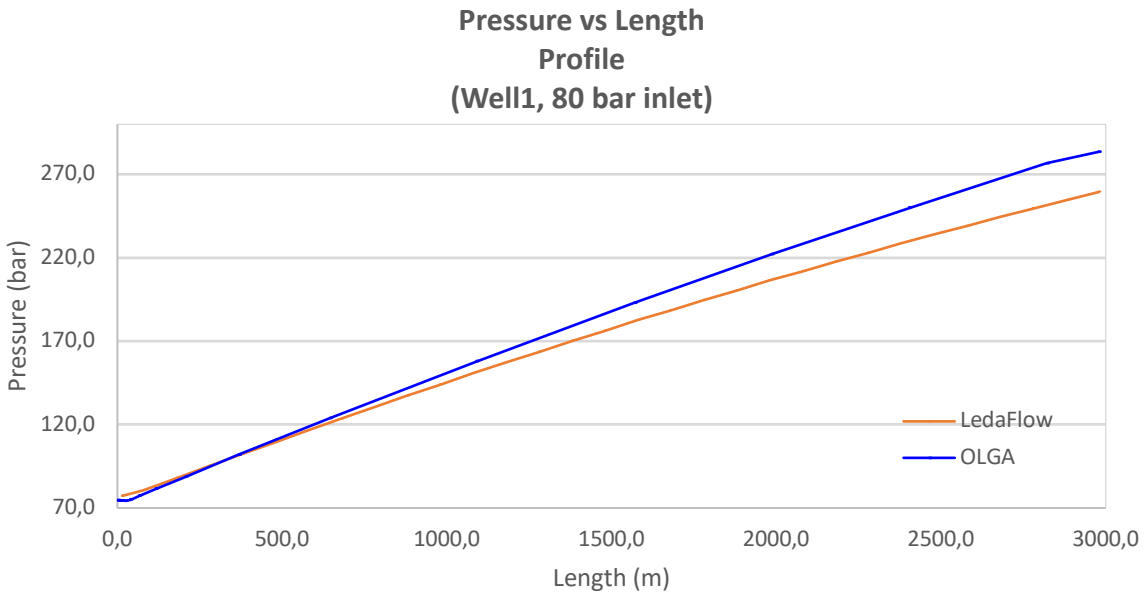

Figure 23: Pressure vs length for 80 bar inlet at well 1

In Figure 22, the pressure profiles for the pipeline for OLGA and LedaFlow follow a similar path up until approximately 40000 meters. Some deviation is present and the pressure at the outlet of the pipeline is approximately 80 bar and 77 bar for LedaFlow and OLGA, respectively.

In Figure 23, both LedaFlow and OLGA show a pressure of approximately 70 bar, and some deviation along the well, with pressures at the IPR being at 260 bar and 283 bar for LedaFlow and OLGA, respectively. The deviation between LedaFlow and OLGA is shown in Figure 24 for pipeline and well, respectively.

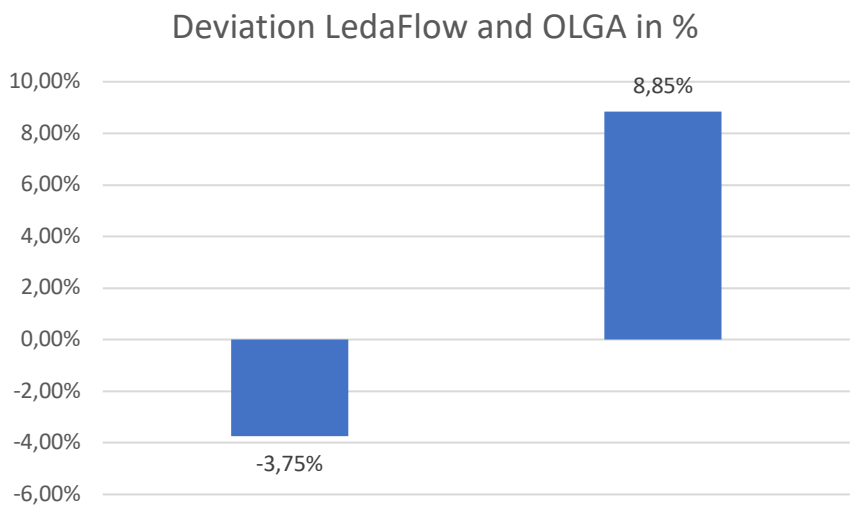

Figure 24: Deviation in pressure profiles for LedaFlow and OLGA

4.1.3 100 bar inlet, mass flow vs time

A new simulation was run, with a higher inlet pressure at 100 bar to gather more data for the purpose of comparing LedaFlow and OLGA. The remaining parameters for the simulation was identical to the 80 bar inlet, with a 6000 s runtime. Table 3 show mass flow after stabilization.

Table 3: Mass flow for 100 bar inlet after stabilization

100 bar		LedaFlow	OLGA	
Inlet		1100	1270	kg/s
Flowline 1		370	400	kg/s
Well 1		125	133	kg/s

Plots for this simulation is shown in Appendix A. In Figure A4, some instability is observed at the first half of the LedaFlow simulation, and eventually stabilizes at around 1100 kg/s, were as the OLGA simulation is slightly higher with a mass flow of 1270 kg/s. A more coherent result is observed at flowline 1 in Figure A5. With approximately 370 kg/s and 400 kg/s at stabilization for LedaFlow and OLGA, respectively. At the inlet of well 1, in Figure A6, LedaFlow show a mass flow of approximately 125 kg/s, while OLGA is at 133 kg/s. The deviation between LedaFlow and OLGA is shown in Figure 25 for inlet, flowline and well, respectively.

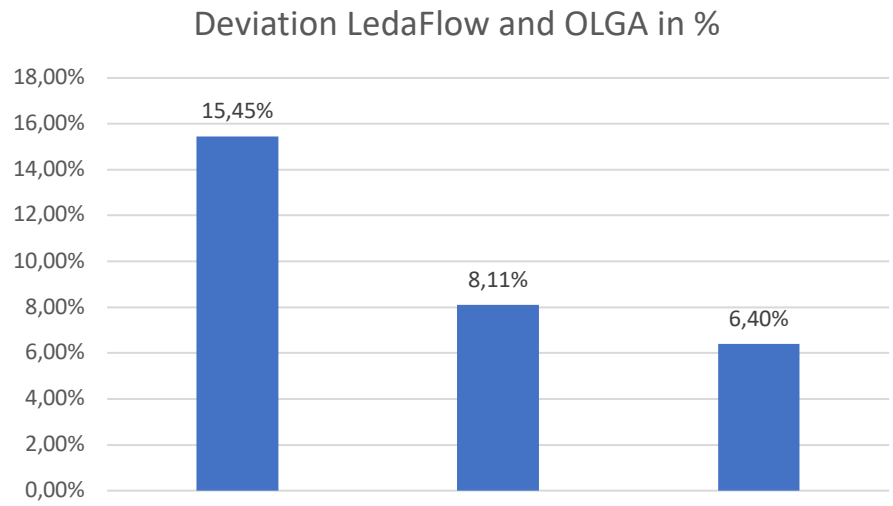

Figure 25: Deviation in mass flow for LedaFlow and OLGA

4.1.4 100 bar inlet, pressure profile

Pressure profile data was also extracted for this simulation run. This data was plotted after stabilization and Figures 26 and 27 show the pressure profile for the pipeline and well 1 at 100 bar, for LedaFlow and OLGA, respectively.

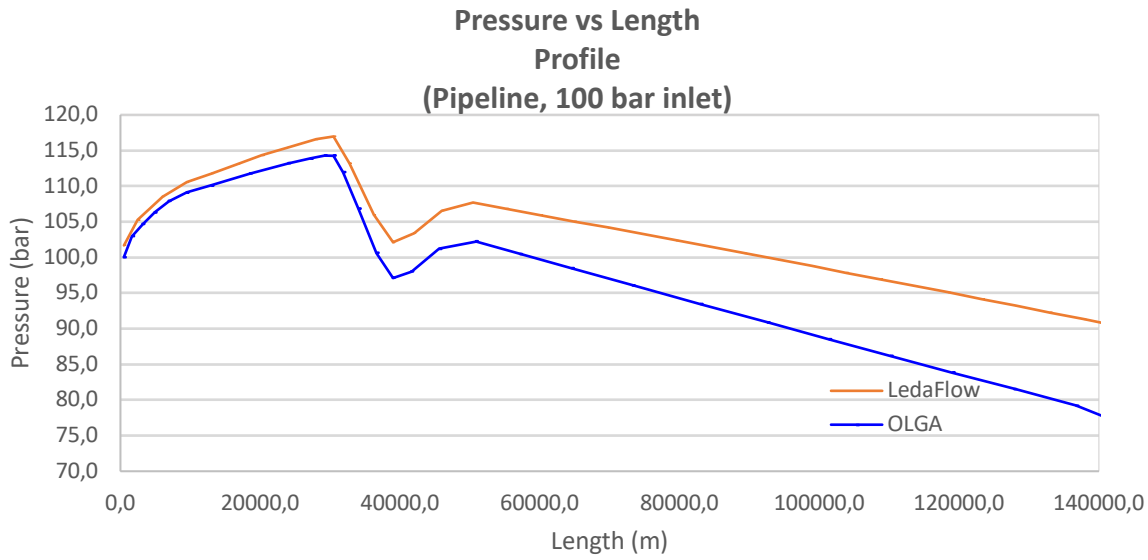

Figure 26: Pressure vs length for 100 bar inlet at inlet

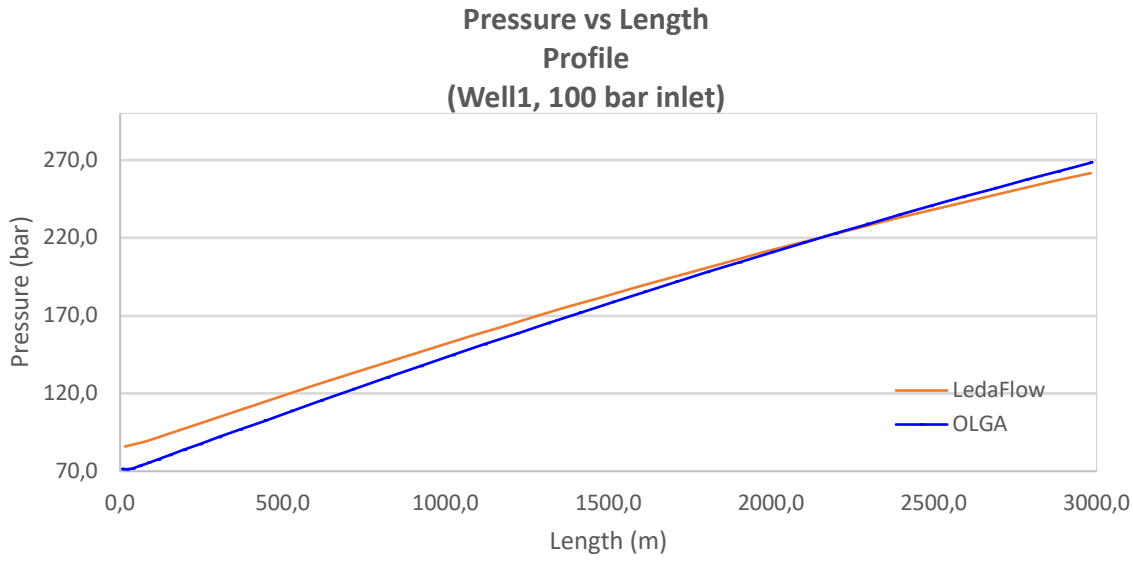

Figure 27: Pressure vs length for 100 bar inlet at well 1

Figure 26 show some deviation between LedaFlow and OLGA increasing gradually along the length of the pipeline. At the outlet LedaFlow and OLGA show a pressure of 90 and 75 bar, respectively. In Figure 27, the two simulations show a dissimilarity in the inlet pressure, with LedaFlow showing a higher inlet pressure, but eventually a lower pressure at the IPR of 261 bar, compared to OLGA at 268 bar. Deviation for LedaFlow and OLGA is shown in Figure 28 for pipeline and well, respectively.

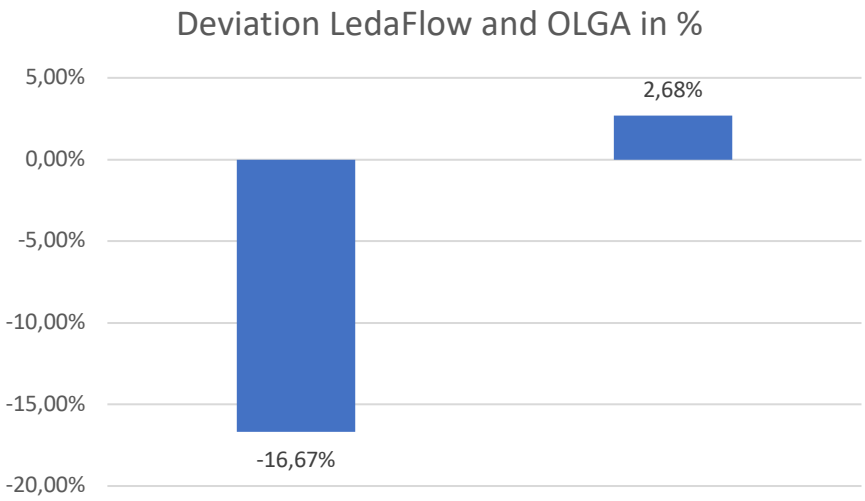

Figure 28: Deviation in pressure profiles for LedaFlow and OLGA

4.1.5 100 bar inlet, temperature profile

Additionally for this simulation run, data for the temperature profile was extracted. These plots, in Figures 29 and 30 show the fluid temperature after stabilization along the length of the pipe for the pipeline and well 1, respectively.

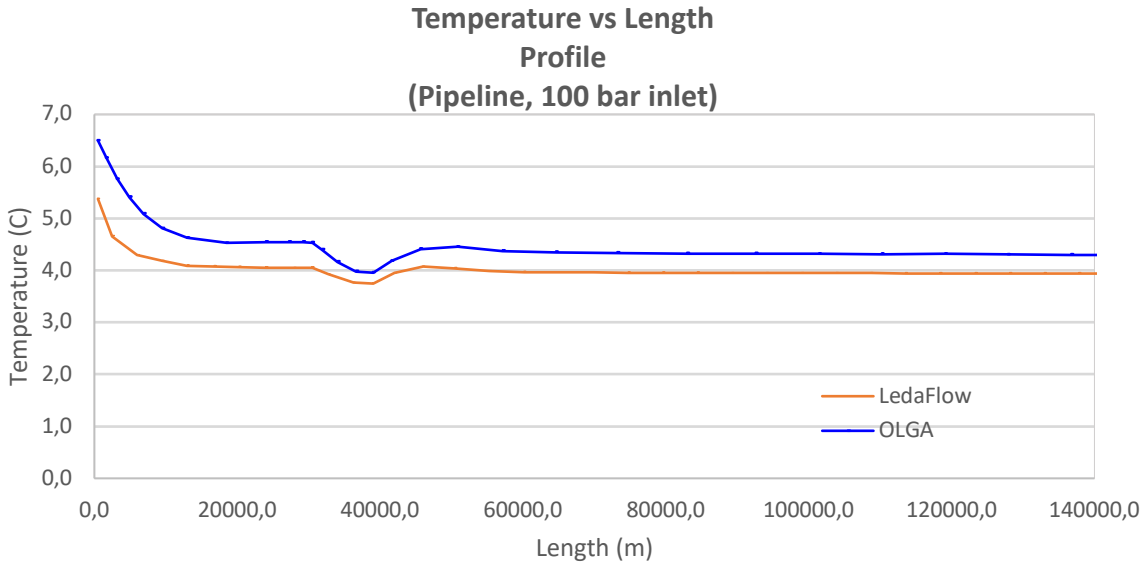

Figure 29: Temperature vs length for 100 bar inlet at pipeline

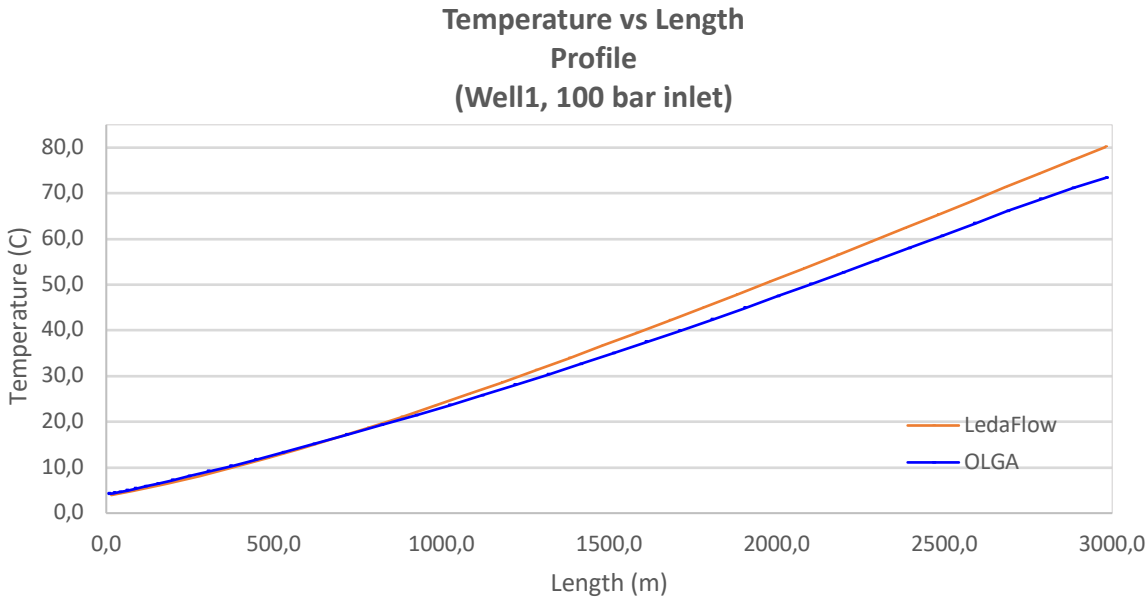

Figure 30: Temperature vs length for 100 bar inlet at well 1

Figure 29 show the fluid rapidly adjusting to the ambient temperature and hold a steady temperature the length of the pipeline, with LedaFlow and OLGA showing a fluid temperature at outlet of 3,94 and 4,3°C, respectively. Figure 30 show the temperature of both simulations increasing as the ambient temperature increases with depth. The fluid temperature at the IPR is 80,1 and 73,4°C for LedaFlow and OLGA, respectively.

Deviation for LedaFlow and OLGA is shown in Figure 31 for pipeline and well, respectively.

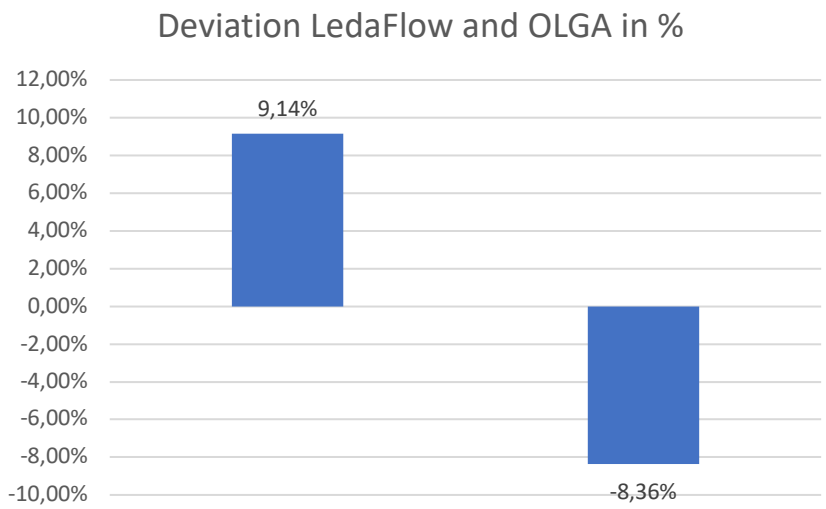

Figure 31: Deviation in temperature profile for LedaFlow and OLGA

4.2 Base case, 10-5-1 II

For these simulation runs, the scaled Snøhvit based model was applied, with a runtime of 6000 s and RKS and SW EOS used for LedaFlow and OLGA, respectively. The injectivity indexes for well 1-3 was set to 10 kg/s-bar, well 4-6 at 5 kg/s-bar and well 7-9 at 1 kg/s-bar. Additionally, the reservoir pressure was at 250 bar, reservoir temperature at 95°C and inlet fluid temperature at 6,85°C. The parameters for the pipe system are shown in Table 1.

4.2.1 100 bar inlet, mass flow vs time

Simulations were run, and the data extracted in both LedaFlow and OLGA. Due to the differencing injectivity indexes for the 3 clusters, the results may vary for the different wells and flowlines. Table 4 show the mass flow after stabilization given by LedaFlow and OLGA

Table 4: Mass flow for 100 bar inlet after stabilization

100 bar		LedaFlow	OLGA	
Inlet		955	1230	kg/s
Flowline 1		425	503	kg/s
Flowline 2		380	447	kg/s
Flowline 3		168	188	kg/s
Well 1		142	167	kg/s
Well 4		127	149	kg/s
Well 7		56	63	kg/s

Plots are in shown in Appendix A. In Figure A7, at the inlet of the pipeline, some instability in the LedaFlow simulation is observed for the first 2000 s of runtime. After stabilization the mass flow given by LedaFlow and OLGA is 955 kg/s and 1230 kg/s, respectively. In Figure A8, at the inlet of flowline 1, the mass flow after stabilization for LedaFlow is 425 kg/s and 503 kg/s for OLGA. In Figure A9, in flowline 2, the mass flow is somewhat lower at 380 kg/s and 447 kg/s, respectively. The same is to be said for flowline 3, in Figure A10, with 168 kg/s and 188 kg/s, respectively. Figure A11 – A13 for well 1, 4 and 7, the mass flow given by LedaFlow and OLGA is 142 kg/s, 167 kg/s, and 127 kg/s, 149 kg/s, and 56 kg/s, 63 kg/s, respectively.

Deviation for LedaFlow and OLGA is shown in Figure 32 for inlet, flowline 1, 2, 3 and well 1, 4 and 7, respectively.

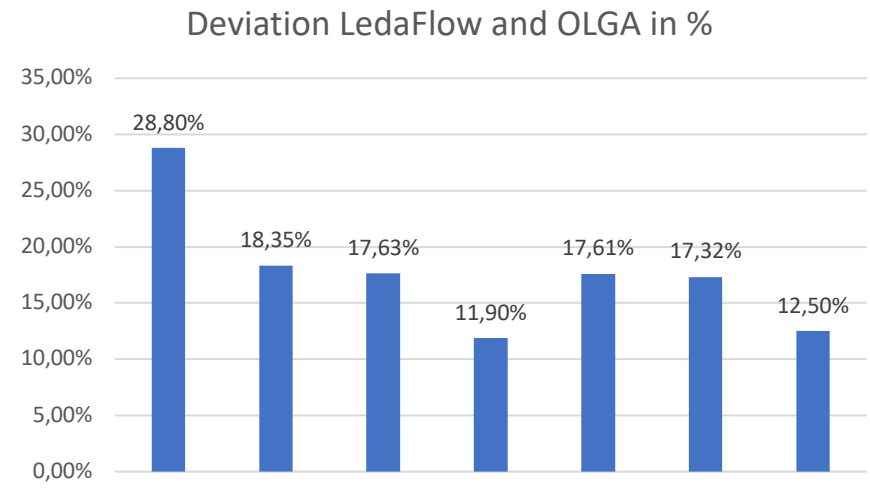

Figure 32: Deviation in mass flow for LedaFlow and OLGA

4.2.2 100 bar inlet, pressure profile

Pressure profile data from the same run was extracted from both LedaFlow and OLGA after stabilization and plotted. Shown in Figure 33 - 36 is the pressure profile for the pipeline and well 1, 4 and 7.

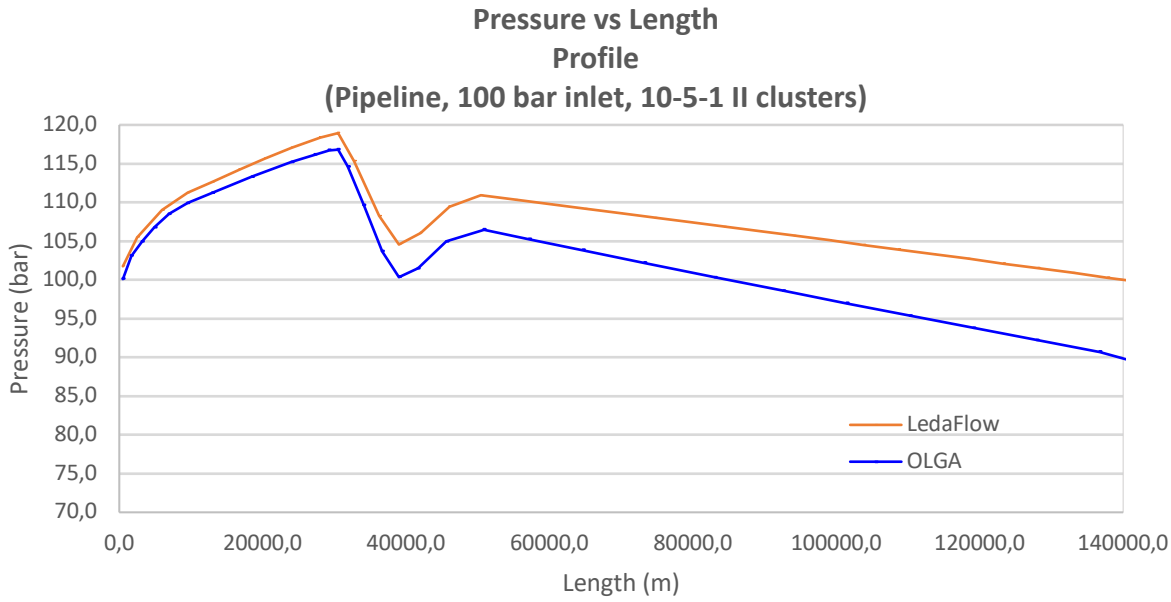

Figure 33: Pressure vs length for 100 bar inlet at inlet

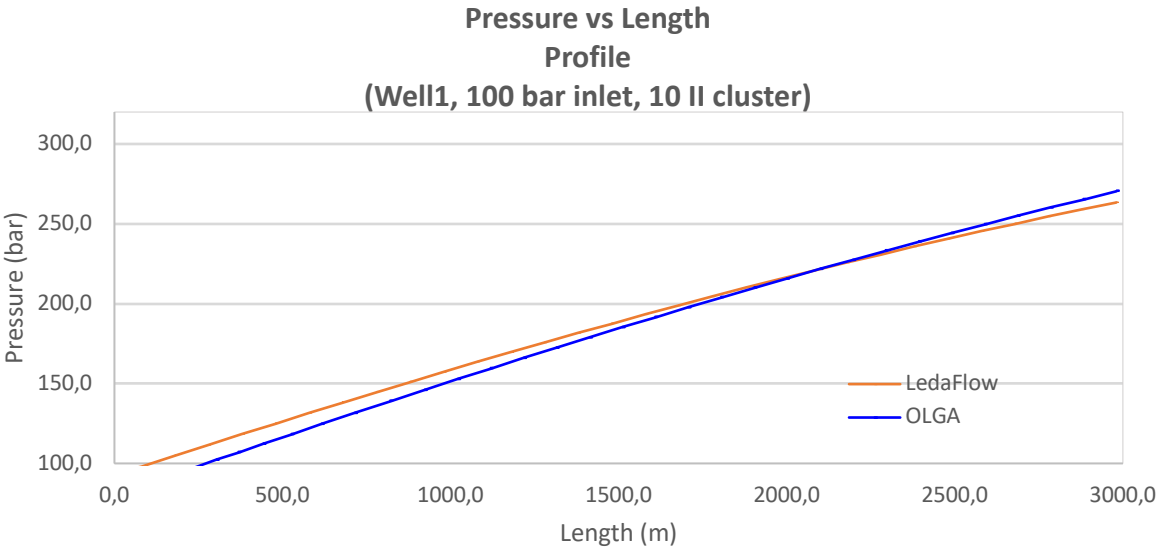

Figure 34: Pressure vs length for 100 bar inlet at well 1

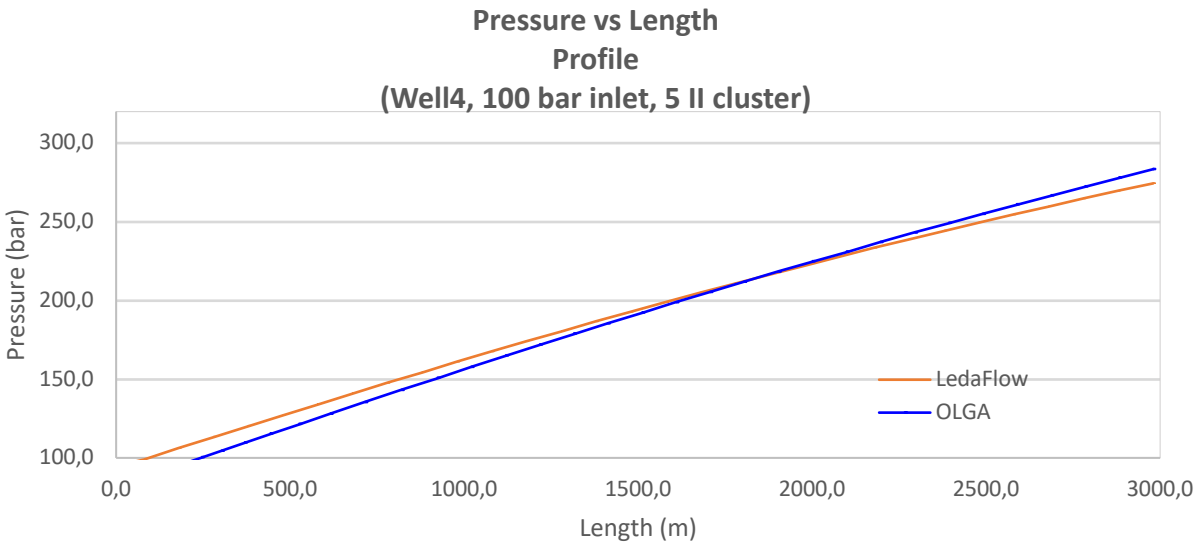

Figure 35: Pressure vs length for 100 bar inlet at well 4

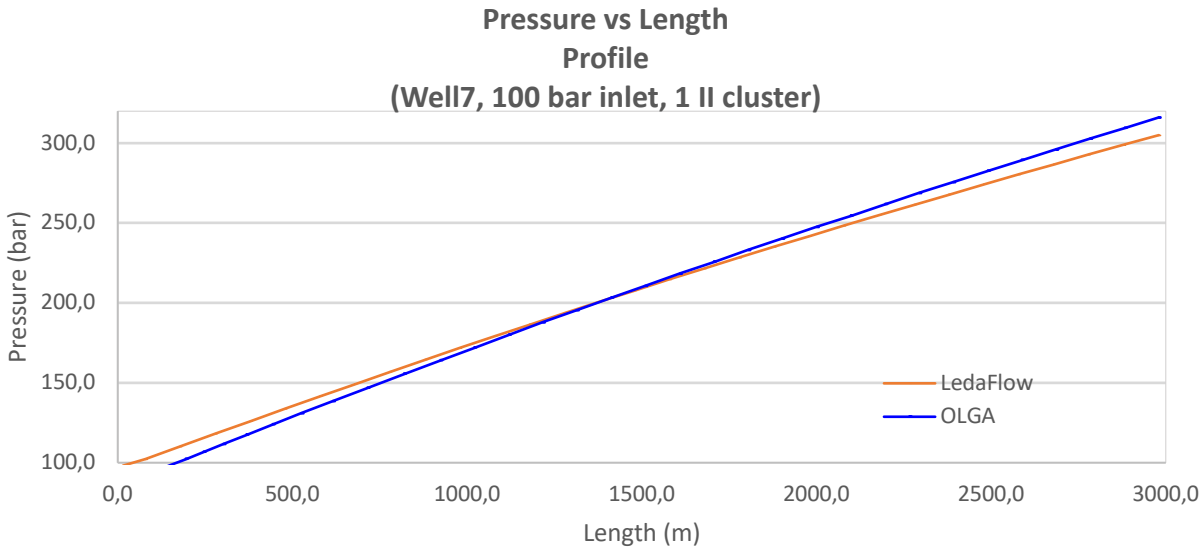

Figure 36: Pressure vs length for 100 bar inlet at well 7

In Figure 33, a gradual deviation between LedaFlow and OLGA is observed along the length of the pipeline. At outlet the pressure given by LedaFlow and OLGA is 99 bar and 88 bar, respectively. In Figure 34, 35 and 36, a similar trend is observed for the three wells. LedaFlow tend to give a higher inlet pressure but experience a lower pressure at the IPR compared to OLGA. Pressures at the IPR for well 1, 4 and 7 is 263 bar, 270 bar and 274 bar, 283 bar and 305 bar, 316 bar for LedaFlow and OLGA, respectively. Deviation for LedaFlow and OLGA is shown in Figure 37 for pipeline, well 1, 4 and 7, respectively.

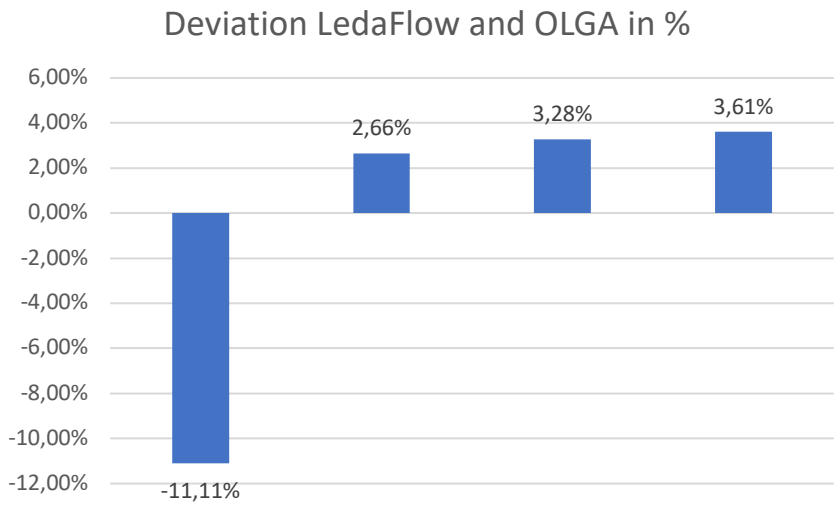

Figure 37: Deviation in pressure profile for LedaFlow and OLGA

4.2.3 100 bar inlet, temperature profile

Fluid temperature data was extracted and plotted for LedaFlow and OLGA for well 1, 4 and 7 at a point after stabilization. These plots are shown in Figure 38 - 40.

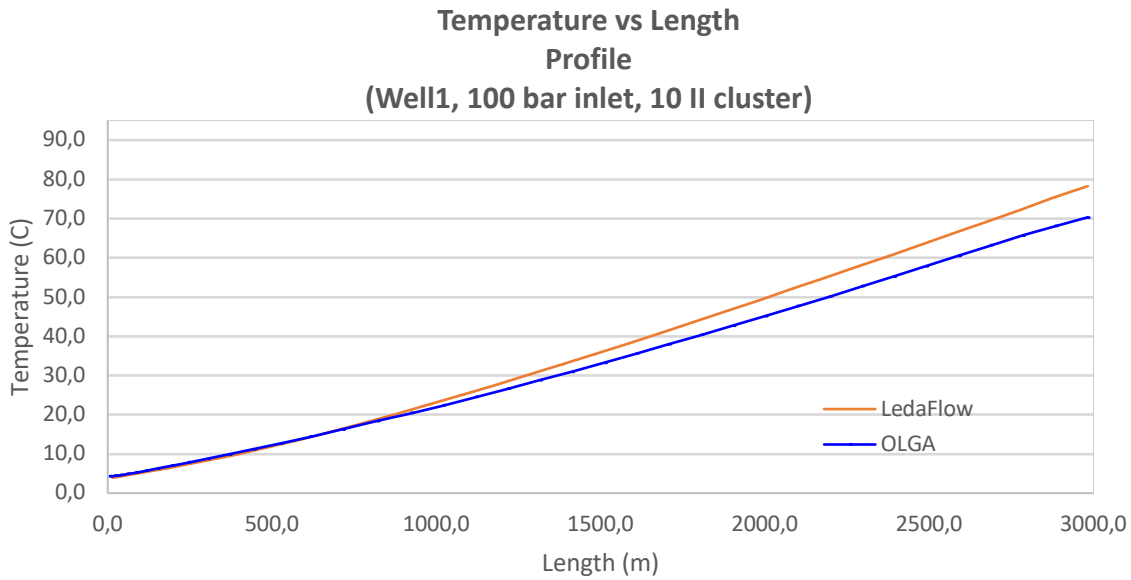

Figure 38: Temperature vs length for 100 bar inlet at well 1

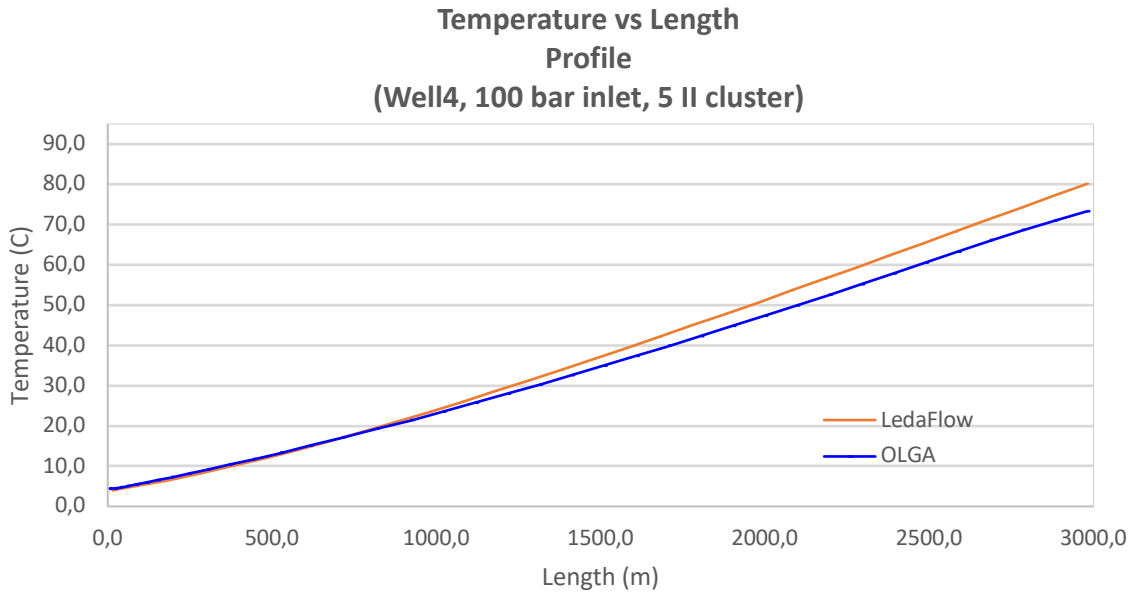

Figure 39: Temperature vs length for 100 bar inlet at well 4

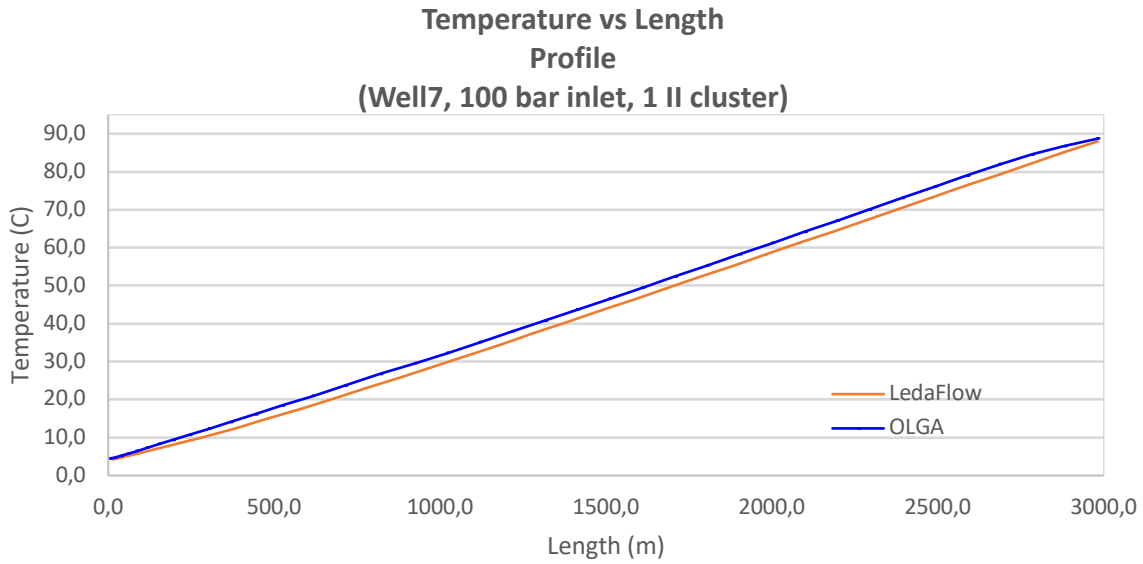

Figure 40: Temperature vs length for 100 bar inlet at well 7

In Figure 38, some deviation between LedaFlow and OLGA is observed, with fluid temperature at the IPR at 78°C and 70°C, respectively. The results shown in Figure 39, are quite similar with LedaFlow and OLGA at 80°C and 73°C. A more coherent result is shown in Figure 40 with LedaFlow giving a fluid temperature at the IPR of 87,9°C and OLGA, 88,7°C. Deviation for LedaFlow and OLGA is shown in Figure 41 for well 1, 4 and 7, respectively.

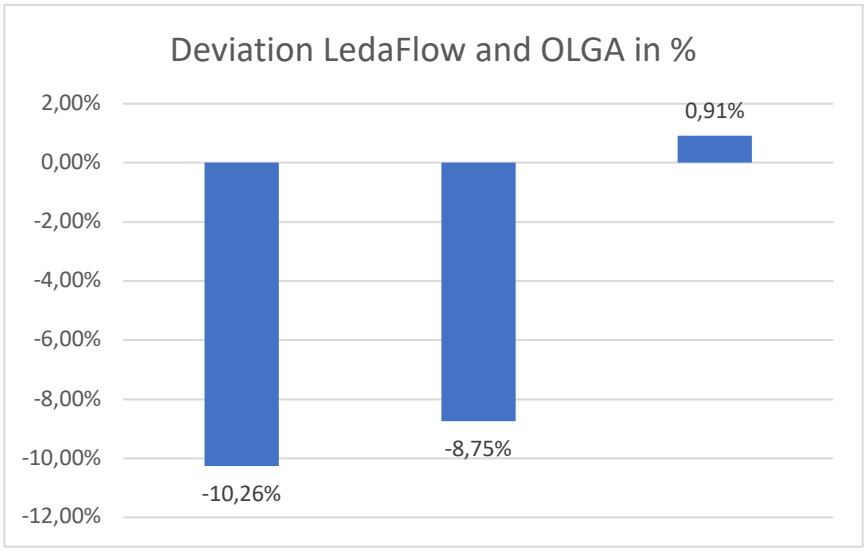

Figure 41: Deviation in temperature profiles for LedaFlow and OLGA

4.2.4 100 bar inlet, flow regime

Additionally for this simulation run, data for flow regime was extracted. This data is presented as a profile plot taken after stabilization. The flow regime is given as an integer between 1 and 5. Each number represent a flow regime pattern. These patterns are given as: 1 = stratified smooth, 2 = stratified wavy, 3 = annular, 4 = slug and 5 = bubbly. Plots for flow regime vs length for the pipeline and well 1 is shown in Figure 42 and 43.

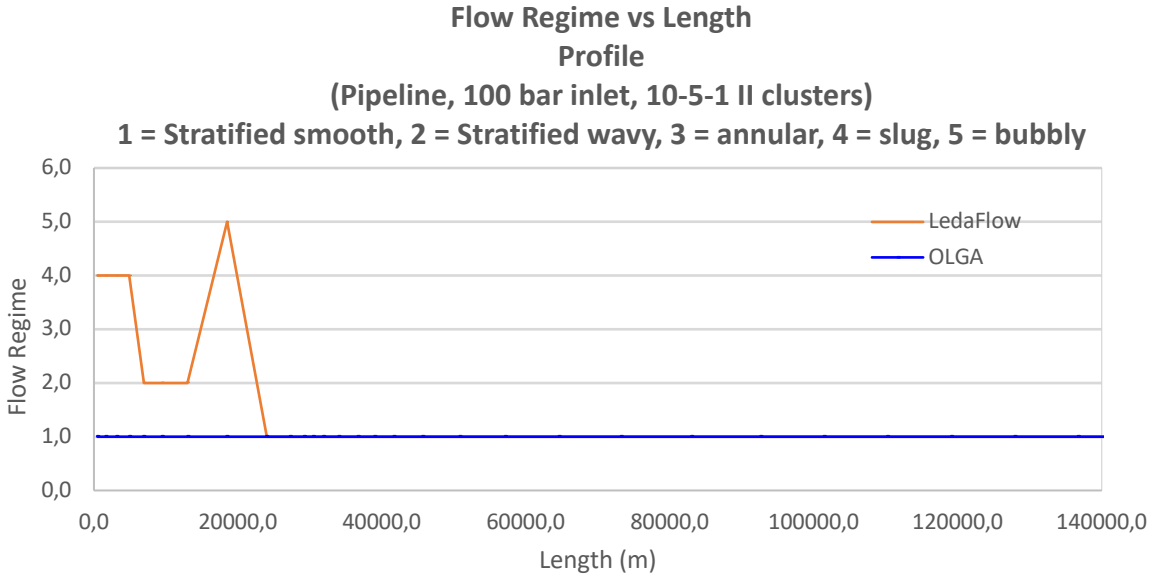

Figure 42: Flow regime vs length for 100 bar inlet at inlet

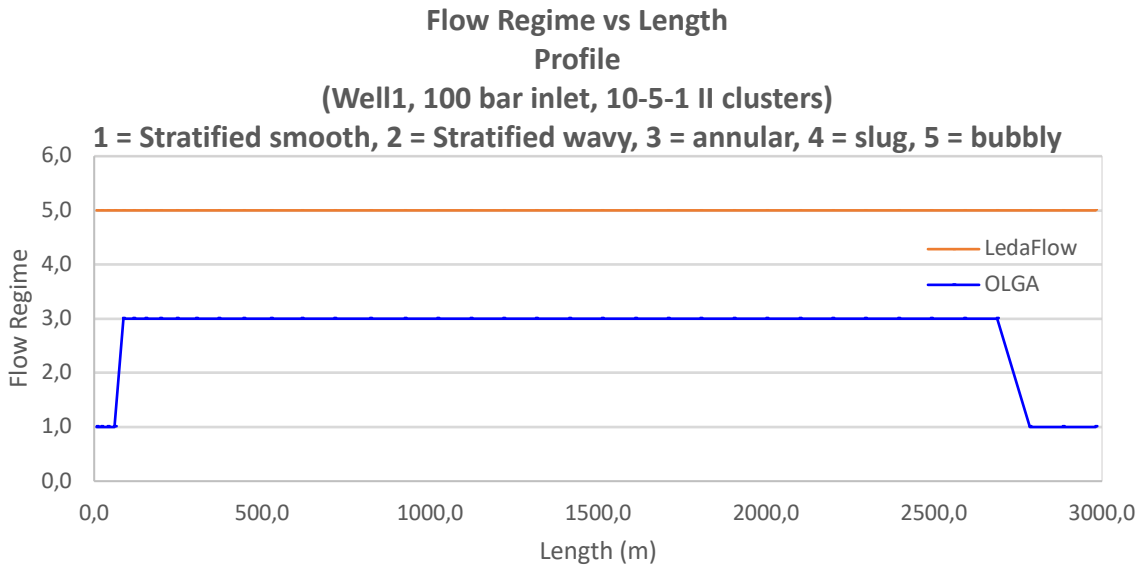

Figure 43: Flow regime vs length for 100 bar inlet at well 1

In Figure 42, some variation in the flow regime is detected by LedaFlow in the first part of the pipeline, before settling in the stratified smooth flow pattern as detected by OLGA the whole length of the pipeline. In Figure 43, LedaFlow gave bubbly flow pattern for the full length of the well, while OLGA show annular for most part, with stratified smooth at the very start and end of the well.

4.3 Base case, 10 II, 280-210-180 bar reservoir pressure

For these simulation runs, the scaled Snøhvit based model was applied, with a runtime of 9000 s and RKS and SW EOS used for LedaFlow and OLGA, respectively. A longer runtime was choses due to some stability issues in the LedaFlow simulation. The injectivity index for all wells were set to 10 kg/s-bar. For this simulation well 1-3 had a reservoir pressure of 280 bar, well 4-6 at 210 bar and well 7-9 a reservoir pressure of 180 bar. Additionally, reservoir temperature at 95°C and inlet fluid temperature at 6,85°C. The parameters for the pipe system are shown in Table 1.

4.3.1 100 bar inlet, mass flow vs time

Simulations were run and data extracted from both LedaFlow and OLGA. Due to the varying reservoir pressure of the 3 cluster, data from each flowline, and one well from each cluster was collected and plotted. Data for mass flow for this simulation is shown in Table 5.

Table 5: Mass flow for 100 bar inlet after stabilization

100 bar		LedaFlow	OLGA	
Inlet		1173	1451	kg/s
Flowline 1		152	216	kg/s
Flowline 2		476	553	kg/s
Flowline 3		554	635	kg/s
Well 1		51	72	kg/s
Well 4		159	184	kg/s
Well 7		185	212	kg/s

Plots for the simulation is shown in Appendix A. In Figure A14 some instability in the simulation is observed at the beginning of the simulation and at a section by the end. At some point after stabilization the mass flow from LedaFlow and OLGA is 1173 kg/s and 1451 kg/s, respectively. Figure A15, for flowline 1 show a mass flow after stabilization given by LedaFlow of 152 kg/s, and by OLGA of 216 kg/s. For flowline 2, the mass flow is 476 kg/s and 553 kg/s by LedaFlow and OLGA, respectively. For the wells a similar deviation to the flowlines is observed, with the mass flow given by LedaFlow and OLGA for well 1, 4 and 7 to be 51 kg/s, 72 kg/s, and 159 kg/s, 184 kg/s, and 185 kg/s, 212 kg/s, respectively.

Deviation for LedaFlow and OLGA is shown in Figure 44 for the pipeline, flowlines 1, 2 and 3, and well 1, 4 and 7, respectively.

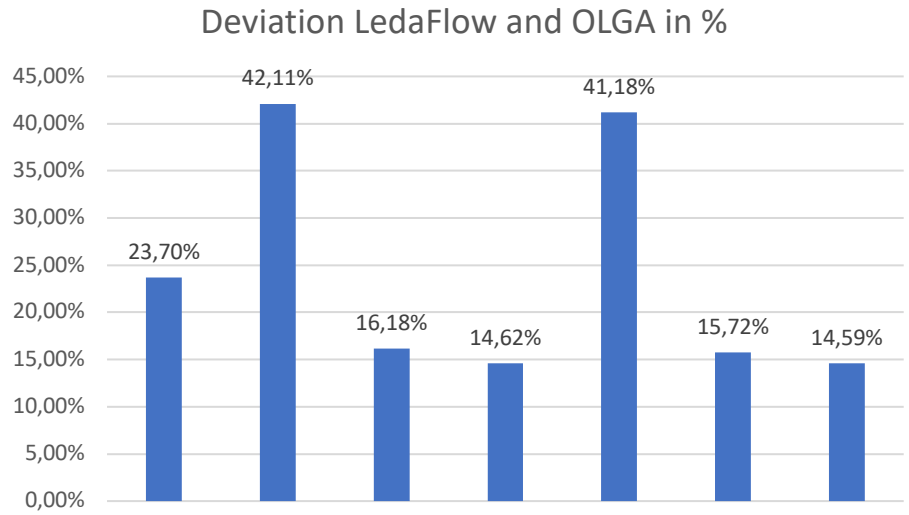

Figure 44: Deviation in mass flow vs time for LedaFlow and OLGA

4.3.2 100 bar inlet, pressure profile

Data for pressure profile was extracted for the same simulation run and plotted as pressure vs length. These plots are shown in Figure 45 - 48 for pipeline, well 1, 4 and 7, respectively.

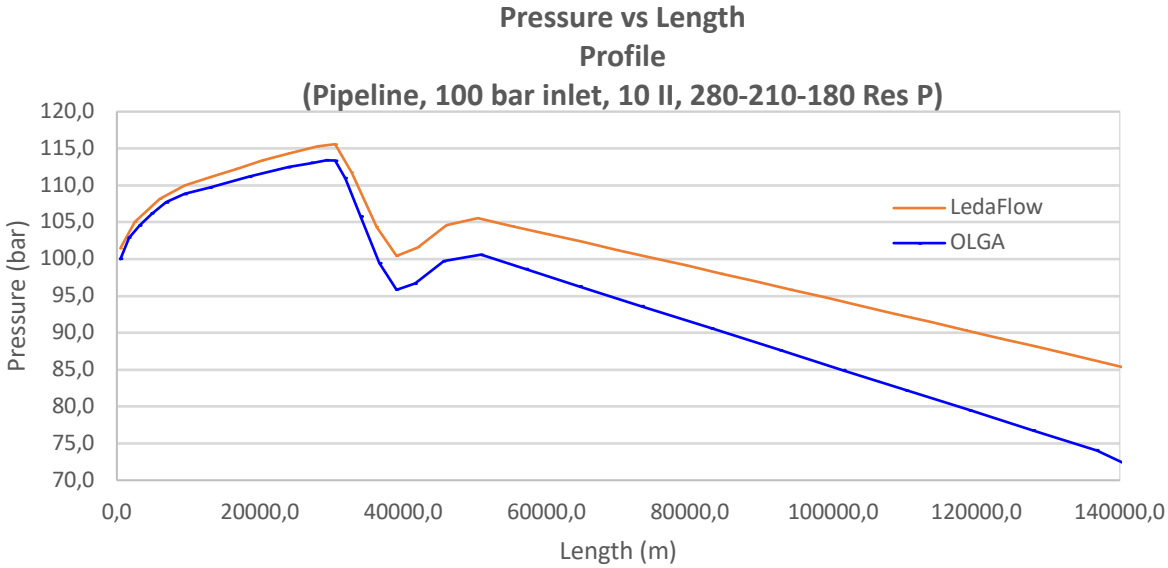

Figure 45: Pressure vs length for 100 bar inlet at inlet

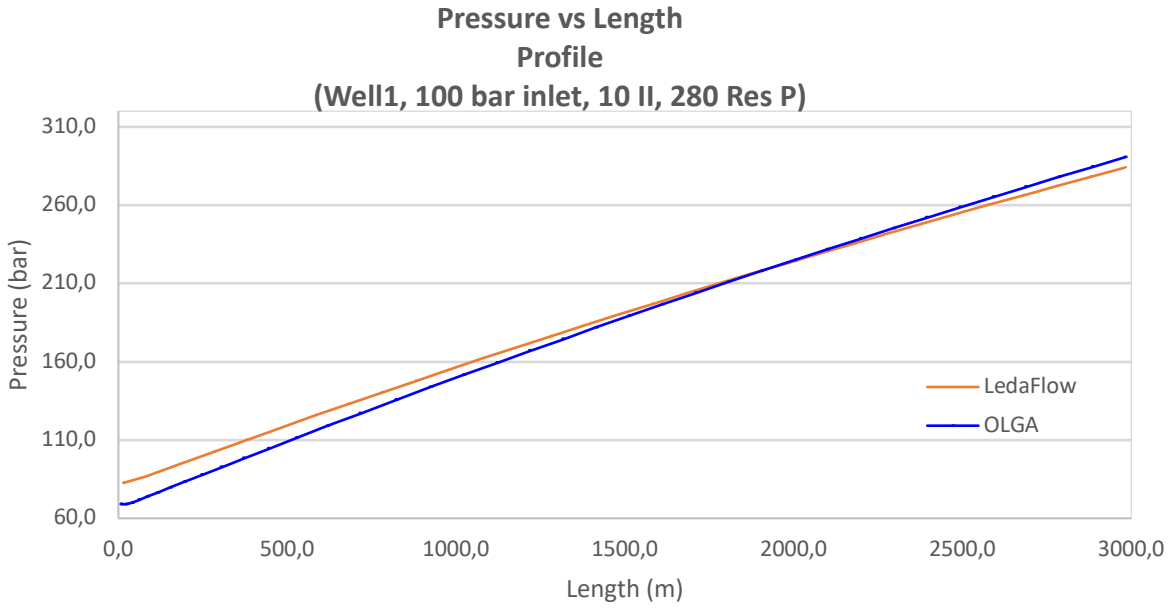

Figure 46: Pressure vs length for 100 bar inlet at well 1

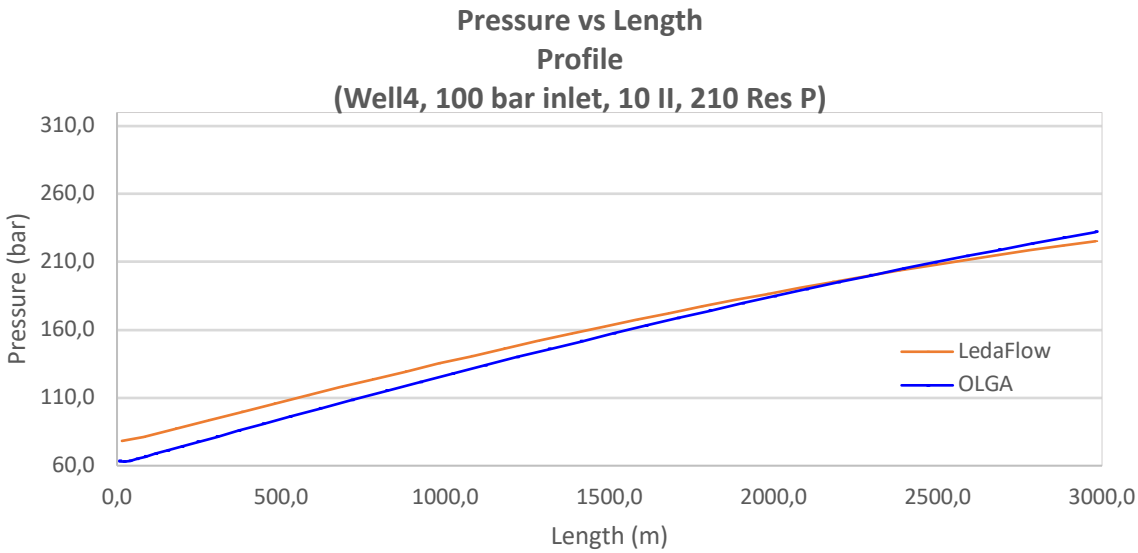

Figure 47: Pressure vs length for 100 bar inlet at well 4

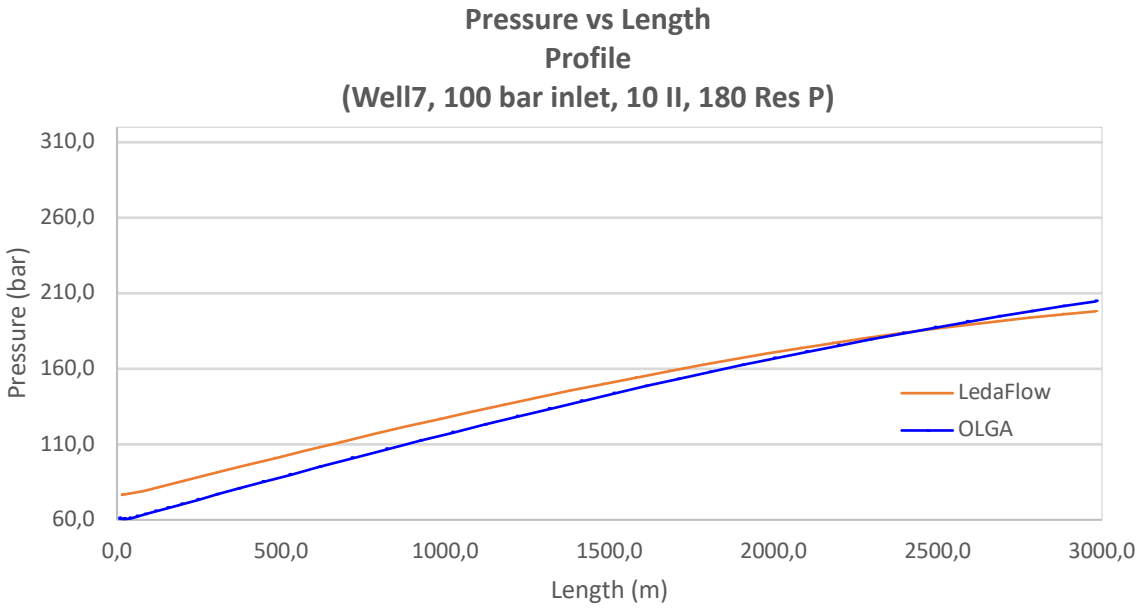

Figure 48: Pressure vs length for 100 bar inlet at well 7

In Figure 45 it is observed a gradual deviation in the pressure given by LedaFlow and OLGA along the length of the pipeline. At the outlet of the pipeline the pressure is 84 bar and 70 bar given by LedaFlow and OLGA, respectively. A more coherent result is shown in the plots for the wells, in Figure 46 - 48. In well 1, the pressure at the IPR is 284 bar from LedaFlow and 291 bar from OLGA. Similarly in well 4 with a pressure from LedaFlow and OLGA of 225 bar and 232 bar, respectively. In well 7, the pressure at the IPR is 198 bar and 205 bar, respectively. Deviation for LedaFlow and OLGA is shown in Figure 49 for pipeline, well 1, 4 and 7.

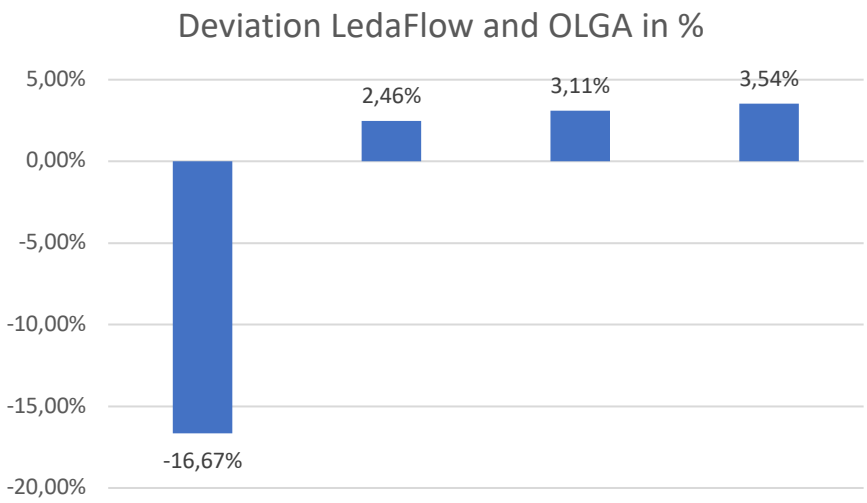

Figure 49: Deviation in pressure profiles for LedaFlow and OLGA

4.3.3 100 bar inlet, well injection rate

For this simulation run, additional data for the well injection rate was extracted. This is the mass flow injected into the reservoir from the well. Inflow gives a negative value and production gives a positive value. This data was plotted as a trendline mass flow vs time. Plots for well 1, 4 and 7 are shown in Figure 50 - 52.

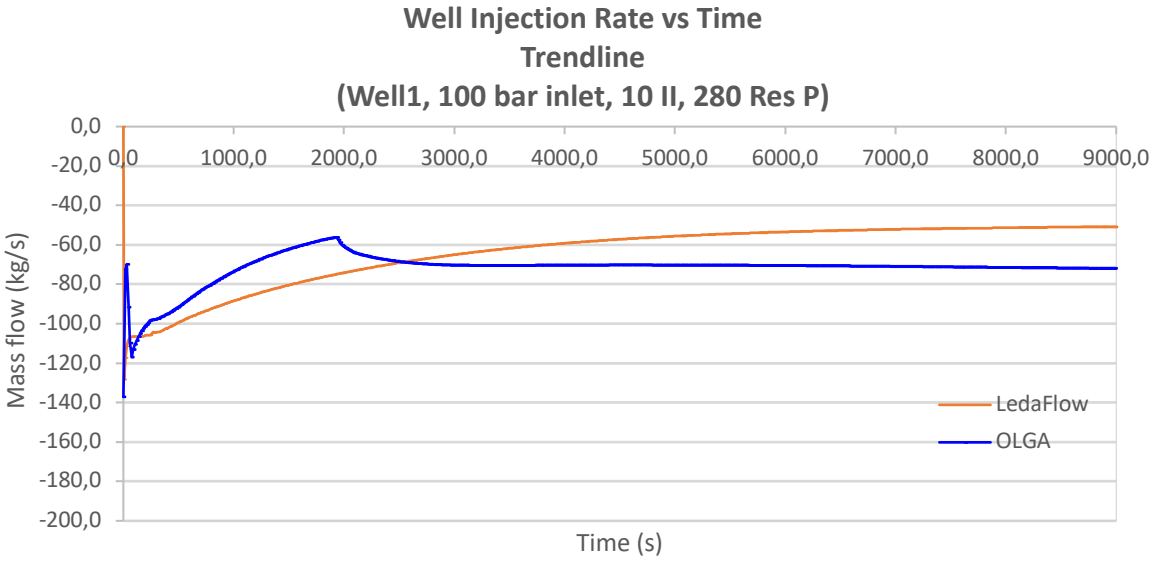

Figure 50: Well injection rate for 100 bar inlet at well 1

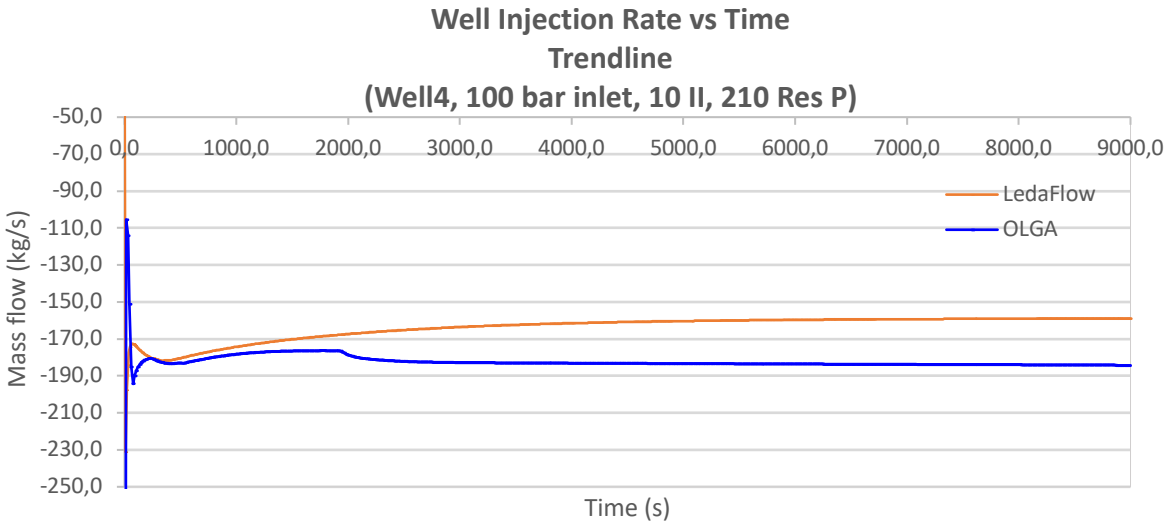

Figure 51: Well injection rate for 100 bar inlet at well 4

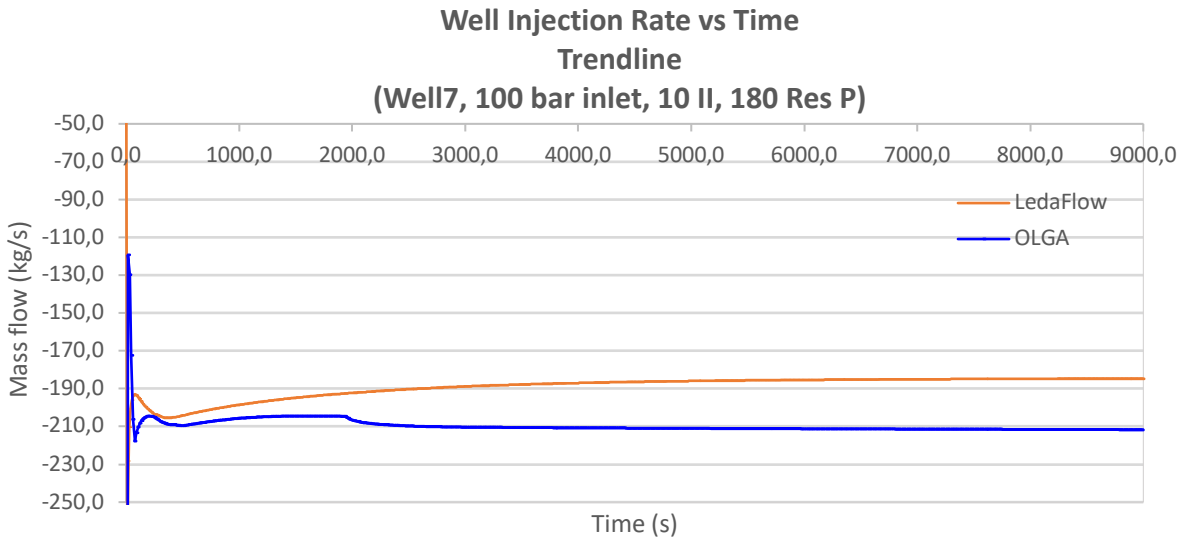

Figure 52: Well injection rate for 100 bar inlet at well 7

In Figure 50 the well injection rate after stabilization is given by LedaFlow and OLGA to be 51 kg/s and 72 kg/s, respectively. A higher injection rate is shown in Figure 51 for well 4, at 159 kg/s and 184 kg/s, respectively. And for well 7, the injection rate is 185 kg/s and 212 kg/s for LedaFlow and OLGA, respectively.

Deviation for LedaFlow and OLGA is shown in Figure 53 for well 1, 4 and 7, respectively.

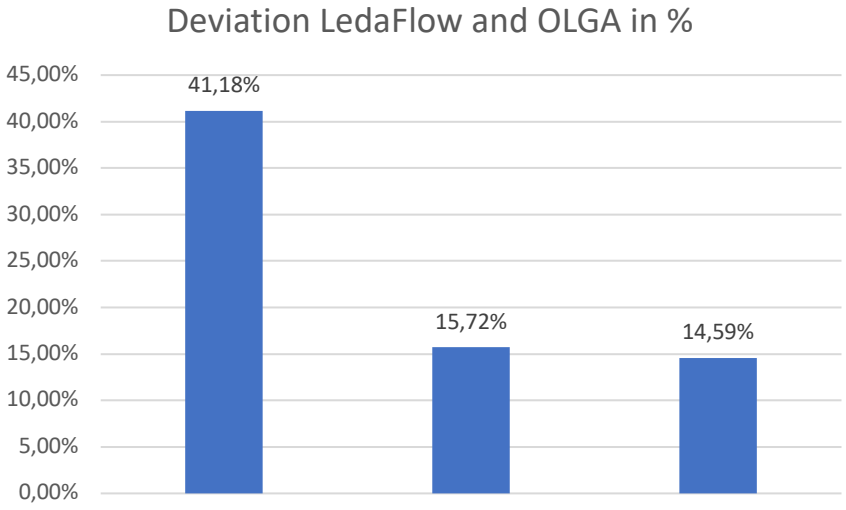

Figure 53: Deviation in well injection rate for LedaFlow and OLGA

4.4 Secondary case, 10 II

For these simulation runs, adjustments to the Snøhvit model were made. The pipeline was shortened and to compensate, the three flowlines was elongated. With a runtime of 9000 s and RKS and SW EOS used for LedaFlow and OLGA, respectively. The injectivity index for all wells were set to 10 kg/s-bar and every well had identical reservoir pressure at 250 bar. Additionally, reservoir temperature at 95°C and inlet fluid temperature at 6,85°C. In LedaFlow, the steady-state processor was used and for OLGA, the PH-formulation was used, thus needing user defined initial conditions. The parameters for the pipe system are shown in Table 6.

Table 6: Parameters for pipe system

	Length	**Diameter**	**Ambient temperature**	**Roughness**
Pipeline	110 km	860 mm	4°C	0,045 mm
Flowline 1	20 km	360 mm	4°C	0,045 mm
Flowline 2	10 km	360 mm	4°C	0,045 mm
Flowline 3	5 km	360 mm	4°C	0,045 mm
Well	3 km (depth)	180 mm	7-95°C (gradient)	0,045 mm

4.4.1 160 bar inlet, mass flow vs time

A simulation run with 160 bar inlet pressure was run. Data for mass flow vs time was extracted and plotted. Data for mass flow after stabilization is shown in Table 7.

Table 7: Mass flow for 160 bar inlet after stabilization

160 bar		**LedaFlow**	**OLGA**	
Flowline 1		386	440	kg/s
Flowline 2		470	536	kg/s
Flowline 3		539	613	kg/s

Additional plots for mass flow vs time are shown in Appendix A. Figure A21 shown mass flow for flowline 1 at 0 meters. A relative quick stabilization is observed with the mass flow for LedaFlow and OLGA at 386 kg/s and 440 kg/s, respectively. For flowline 2, shown in Figure A22, a slightly higher mass flow is observed, with 470 kg/s given by LedaFlow and 536 kg7S by OLGA. In Figure A23, for flowline 3, the measured mass flow after stabilization by LedaFlow and OLGA is given to be 539 kg/s and 613 kg/s, respectively.
The deviation in mass flow for LedaFlow and OLGA for flowline 1, 2 and 3, respectively, is shown in Figure 56.

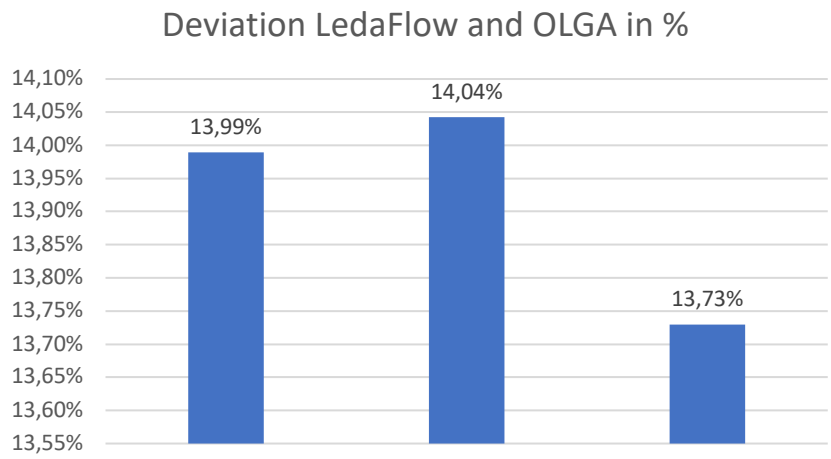

Figure 56: Deviation in mass flow for LedaFlow and OLGA

4.4.2 160 bar inlet, pressure profile

Data for pressure profiles was extracted from the same run and plotted as pressure vs length for the pipeline and flowline 1, 2 and 3. These plots are shown in Figure 57 - 60.

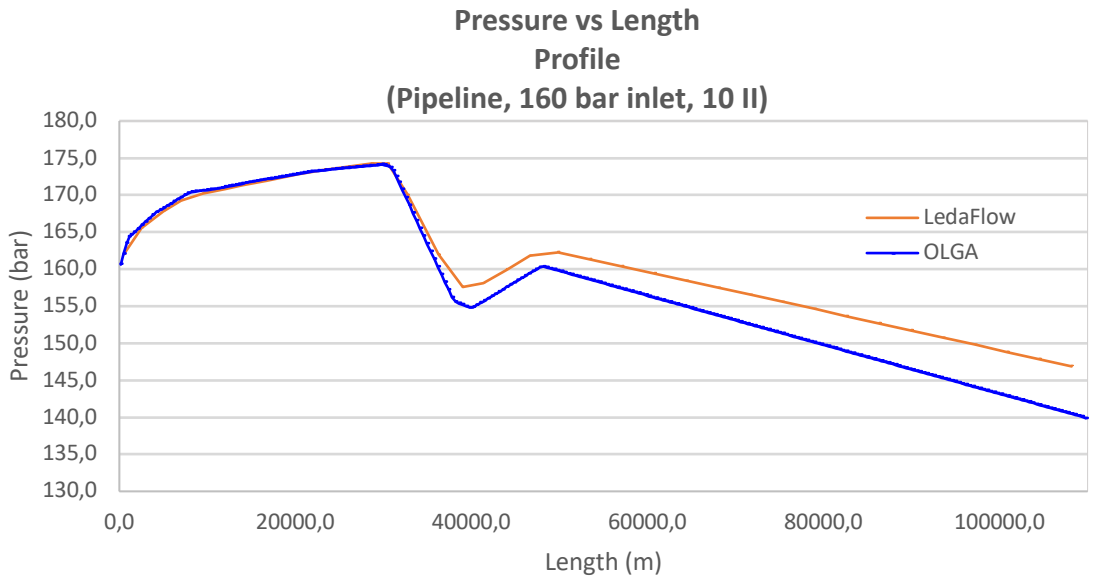

Figure 57: Pressure vs length for 160 bar inlet at inlet

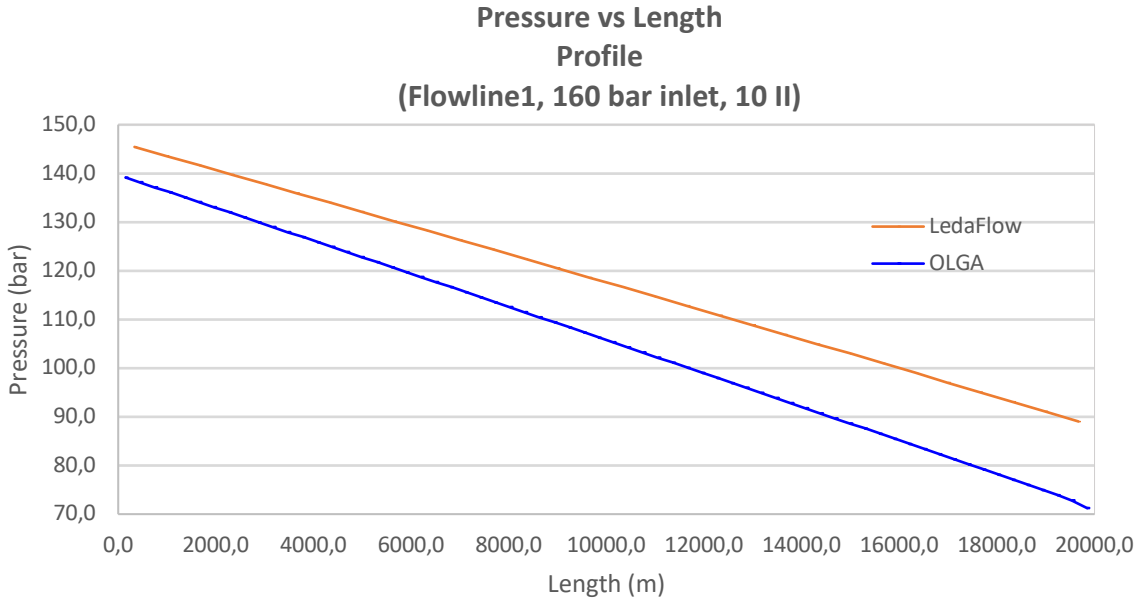

Figure 58: Pressure vs length for 160 bar inlet at flowline 1

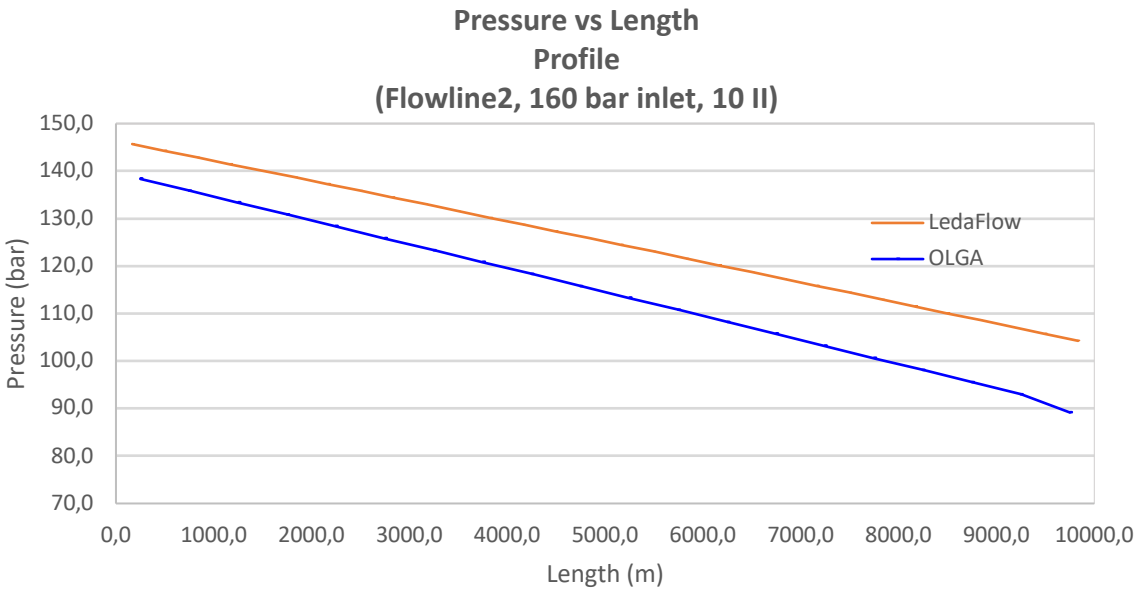

Figure 19: Pressure vs length for 160 bar inlet at flowline 2

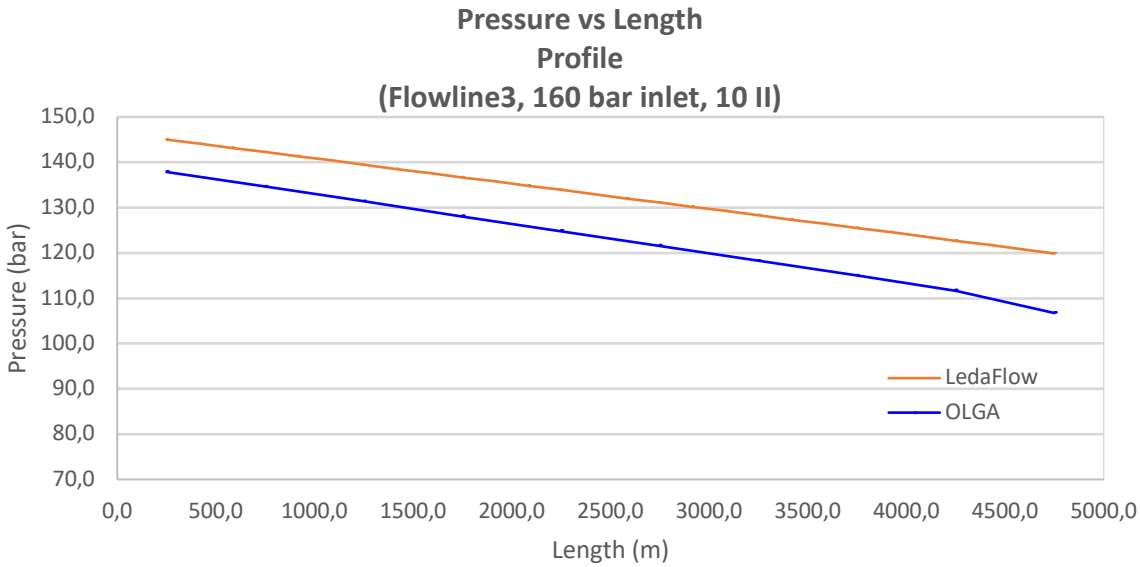

Figure 60: Pressure vs length for 160 bar inlet at flowline 3

In Figure 57, for the pipeline, a good coherence is observed for the first 30000 meters of the pipe, but a gradual deviation is observed beyond this point. At the outlet, LedaFlow and OLGA gave a pressure of 147 bar and 138 bar, respectively. For flowline 1,2 and 3 in Figure 58 - 60, the deviation between LedaFlow and OLGA are more or less constant along the pipe. At the outlet of flowline 1, 2 and 3, the pressure is 89 bar, 71 bar, and 104 bar, 89 bar, and 120 bar, 107 bar, given by LedaFlow and OLGA, respectively.

The deviation in pressure for LedaFlow and OLGA is shown in Figure 61 for pipeline and flowline 1, 2 and 3, respectively.

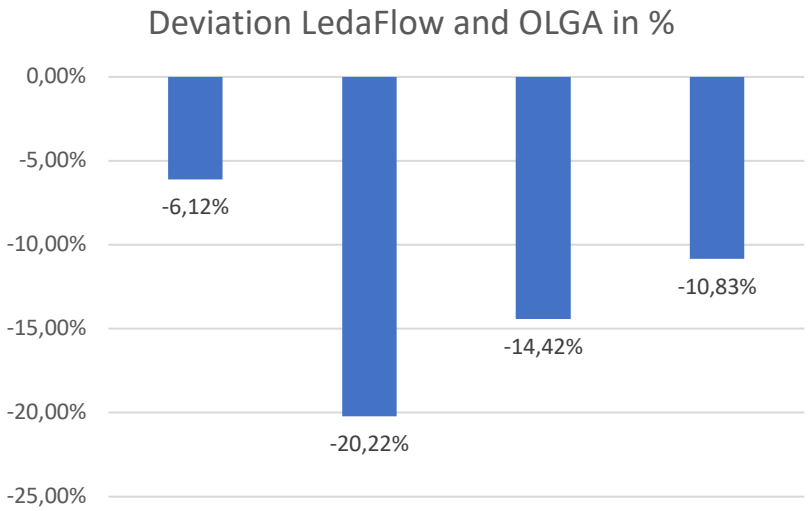

Figure 21: Deviation in pressure profile for LedaFlow and OLGA

4.4.3 160 bar inlet, well injection rate

Additionally for this simulation run, data for well injection rate was extracted and plotted. This data is presented as trendline plots. Plots for well 1, 4 and 7 are shown in Figure 62 - 64.

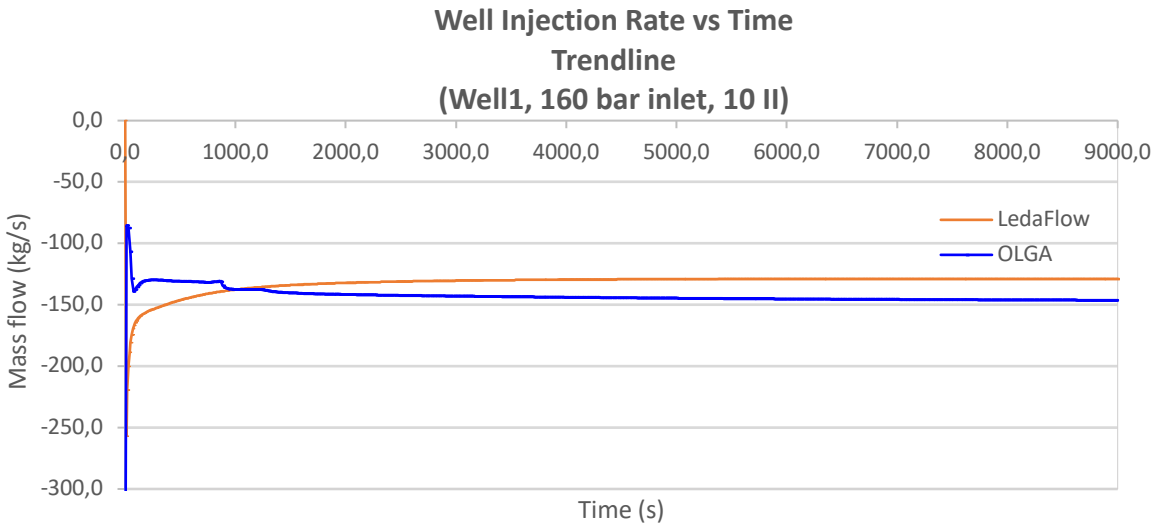

Figure 62: Well injection rate for 160 bar inlet at well 1

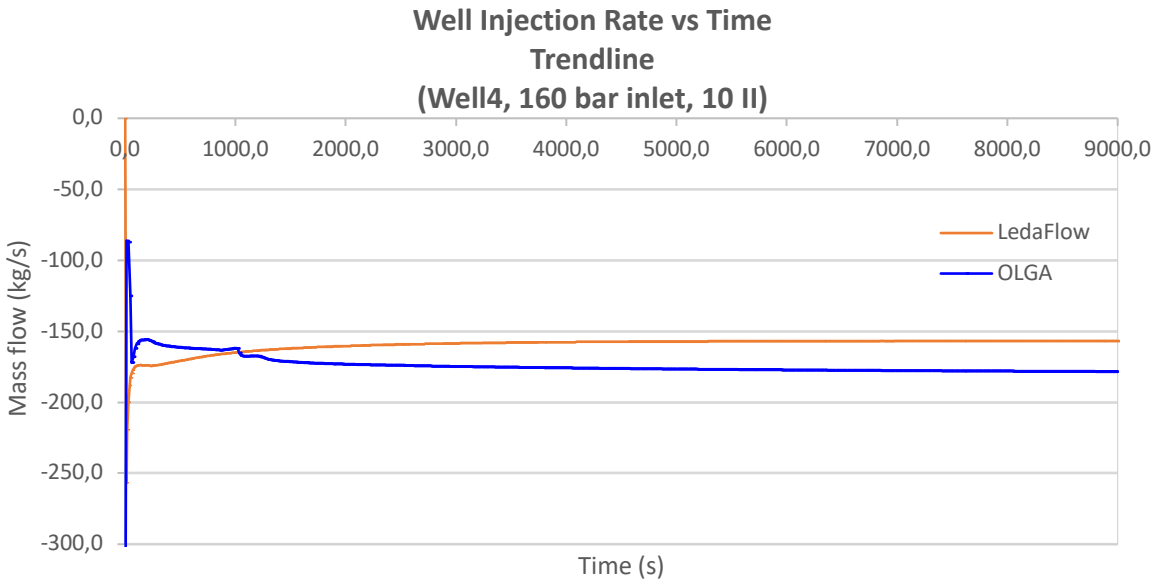

Figure 63: Well injection rate for 160 bar inlet at well 4

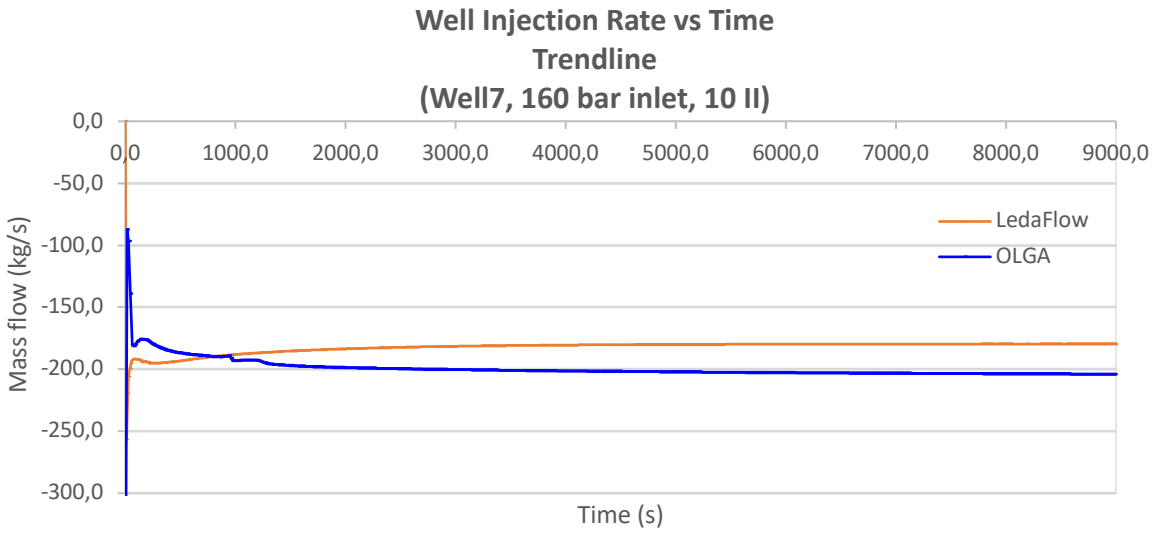

Figure 64: Well injection rate for 160 bar inlet at well 7

In Figure 62, for well 1, a quick stabilization is observed and a measured well injection rate of 129 kg/s and 146 kg/s by LedaFlow and OLGA, respectively. The same is to be said about the stabilization time for well 4 and 7, shown in Figure 63 and 64. The well injection rate given by LedaFlow and OLGA for well 4 is shown to be 157 kg/s and 178 kg/s, and 180 kg/s and 204 kg/s for well 7, respectively.

The deviation for LedaFlow and OLGA for well 1, 4 and 7, respectively, is shown in Figure 65.

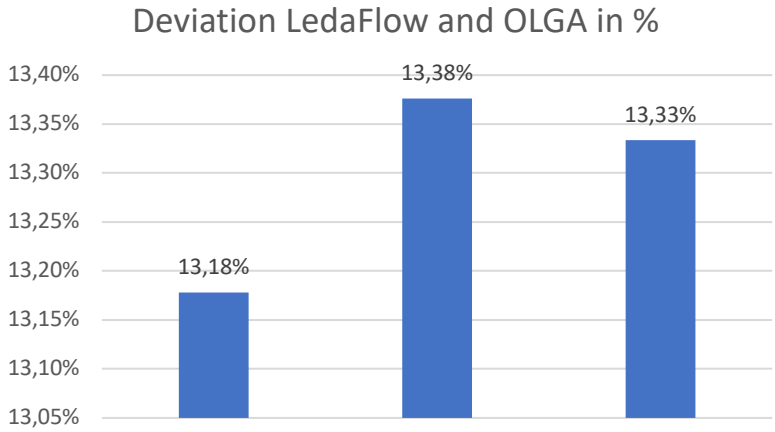

Figure 65: Deviation in well injection rate for LedaFlow and OLGA

4.5 Secondary case, 10 II, 230-250-260 bar reservoir pressure

For these simulation runs, the adjusted Snøhvit model was used. The pipeline was shortened and to compensate, the three flowlines was elongated. With a runtime of 9000 s and RKS and SW EOS used for LedaFlow and OLGA, respectively. The injectivity index for all wells were set to 10 kg/s-bar. The reservoir pressure for cluster 1, 2 and 3 was set to 230 bar, 250 bar and 260 bar, respectively. Additionally, reservoir temperature at 95°C and inlet fluid temperature at 6,85°C. In LedaFlow, the steady-state processor was used and for OLGA, the PH-formulation was used, thus needing user defined initial conditions. The parameters for the pipe system are shown in Table 6

4.5.1 160 bar inlet, mass flow vs time

After assembly of the model and simulation, data for mass flow vs time was extracted from LedaFlow and OLGA. Data for mass flow after stabilization is given in Table 8.

Table 8: Mass flow for 160 bar inlet after stabilization

160 bar		LedaFlow	OLGA	
Inlet		1399	1673	kg/s
Flowline 1		413	468	kg/s
Flowline 2		470	535	kg/s
Flowline 3		517	589	kg/s

The plots for this simulation are shown in Appendix A. In Figure A24, for inlet of the pipeline, some stability issues are observed in the LedaFlow simulation. At stabilization, LedaFlow and OLGA gave a mass flow of 1399 kg/s and 1673 kg/s, respectively. In flowline 1, 2 and 3, a relative quickly stabilization is observed by both LedaFlow and OLGA. The mass flow given after this point is 413 kg/s and 468 kg/s in flowline 1, 470 kg/s and 535 kg/s in flowline 2 and 517 kg/s and 589 kg/s in flowline 3, for LedaFlow and OLGA, respectively. The deviation in mass flow for LedaFlow and OLGA is shown in Figure 66 for pipeline and flowline 1, 2 and 3, respectively.

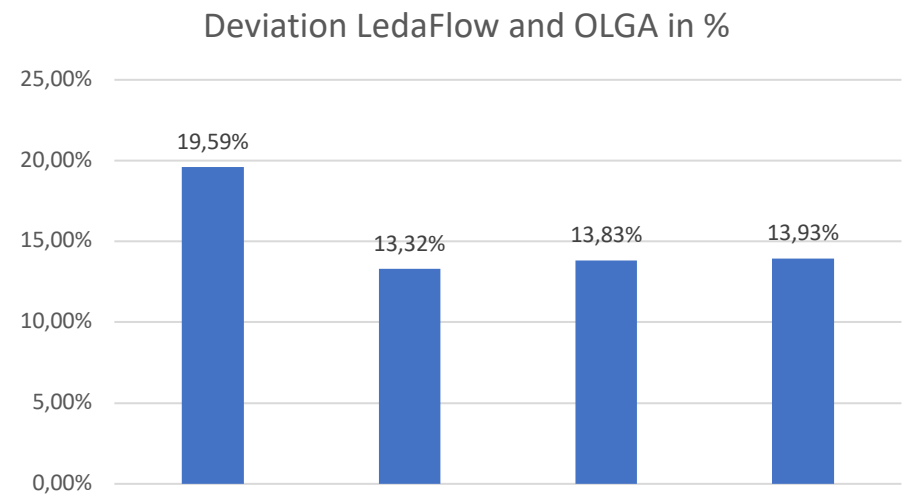

Figure 66: Deviation in mass flow for LedaFlow and OLGA

4.5.2 160 bar inlet, temperature profile

Data for fluid temperature was extracted from the same simulation. This data is presented as profile plots for the pipeline, well 1, 4 and 7, shown in Figure 67 - 70.

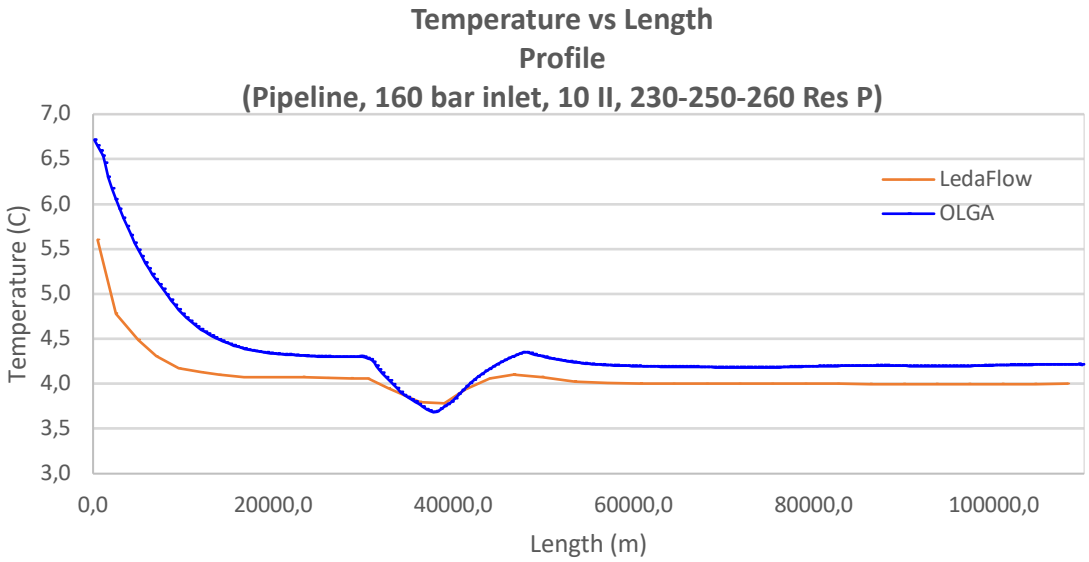

Figure 67: Temperature vs length for 160 bar inlet at inlet

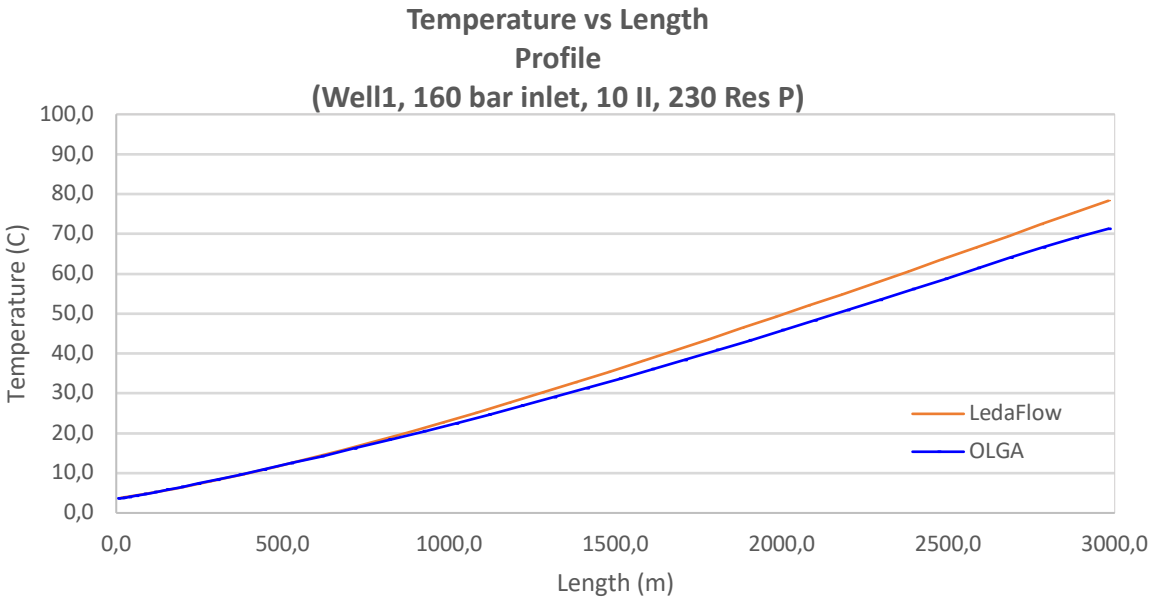

Figure 68: Temperature vs length for 160 bar inlet at well 1

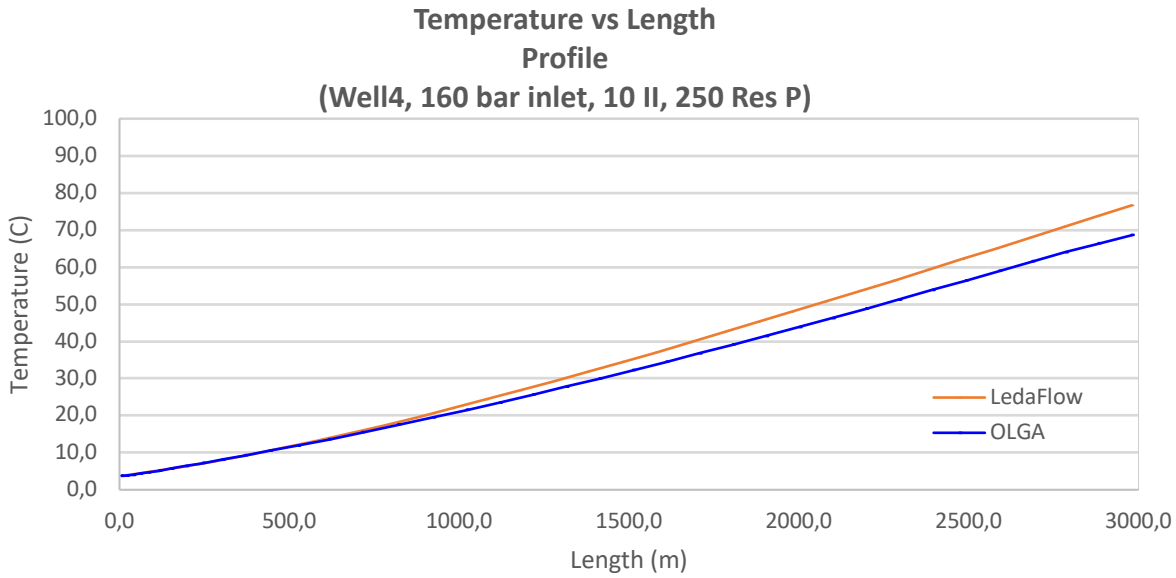

Figure 69: Temperature vs length for 160 bar inlet at well 4

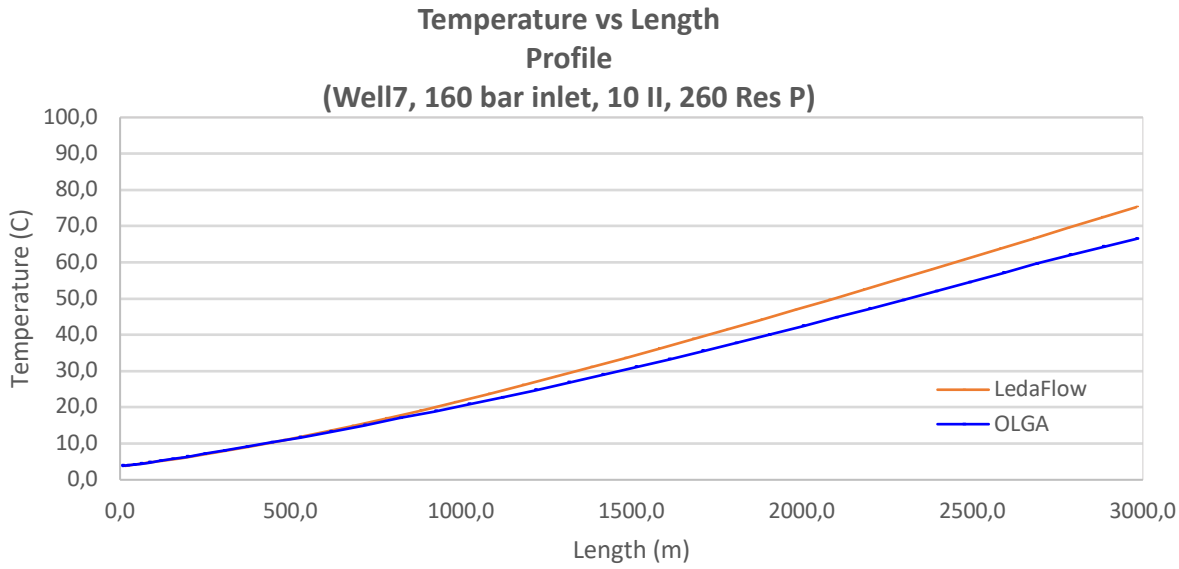

Figure 70: Temperature vs length for 160 bar inlet at well 7

In Figure 67, for the pipeline, the fluid temperature quickly settles to the ambient temperature. LedaFlow shown generally a lower temperature at 3,99°C versus OLGA at 4,2°C. For well 1, 4 and 7 shown in Figure 68 - 70, both LedaFlow and OLGA show a temperature of approximately 3,5°C at the inlet of the wells. At the IPR, OLGA show a lower temperature of 71,3°C, 68,6°C and 66,48°C for well 1, 4 and 7, respectively. Compared to LedaFlow at 78,3°C, 76,65°C and 75,2°C, respectively.

The deviation in fluid temperature for LedaFlow and OLGA is shown in Figure 71 for pipeline, well 1, 4 and 7, respectively.

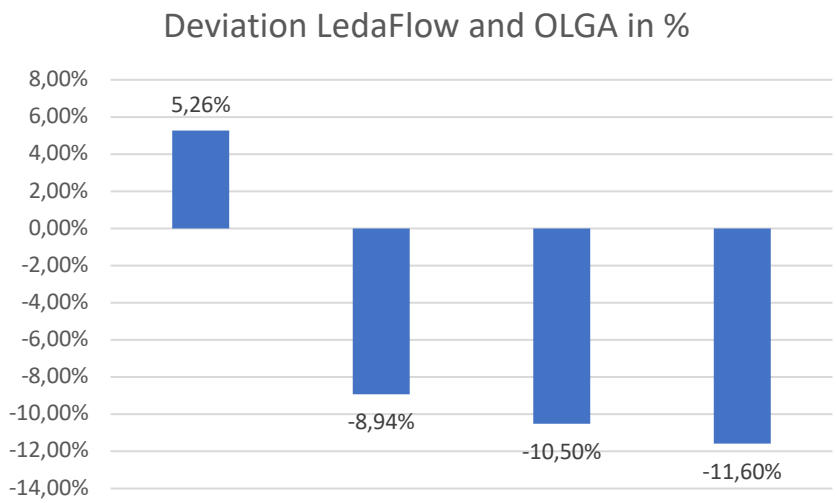

Figure 71: Deviation in fluid temperature for LedaFlow and OLGA

4.5.3 160 bar inlet, pressure profile

Data for pressure profile were extracted from LedaFlow and OLGA at some point after stabilization. Figure 72 - 74 show pressure profiles for well 1, 4 and 7, respectively.

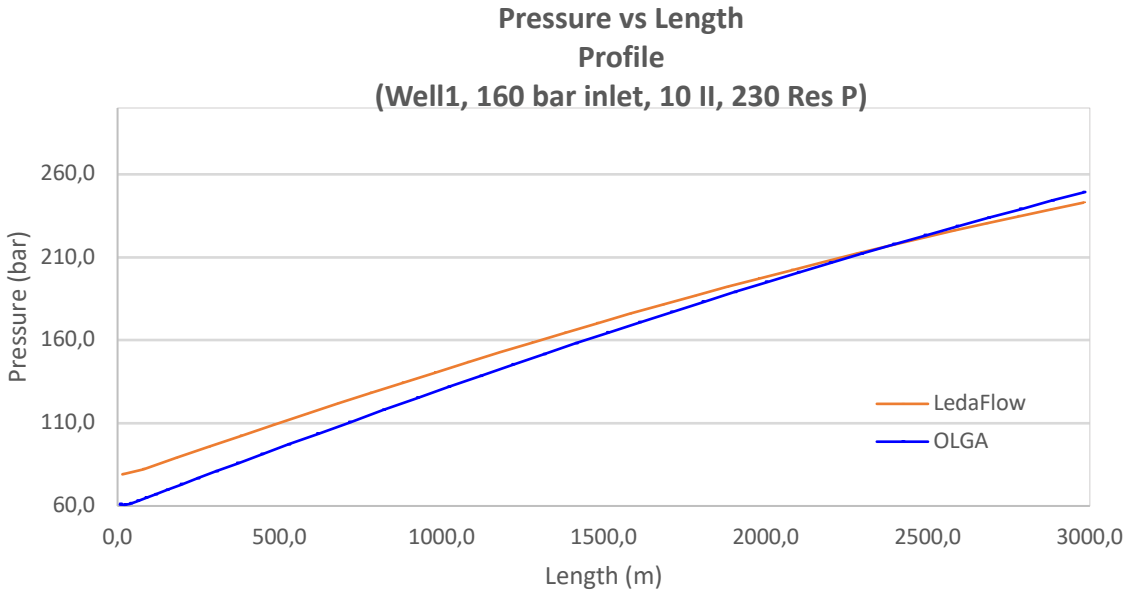

Figure 72: Pressure vs length for 160 bar inlet at well 1

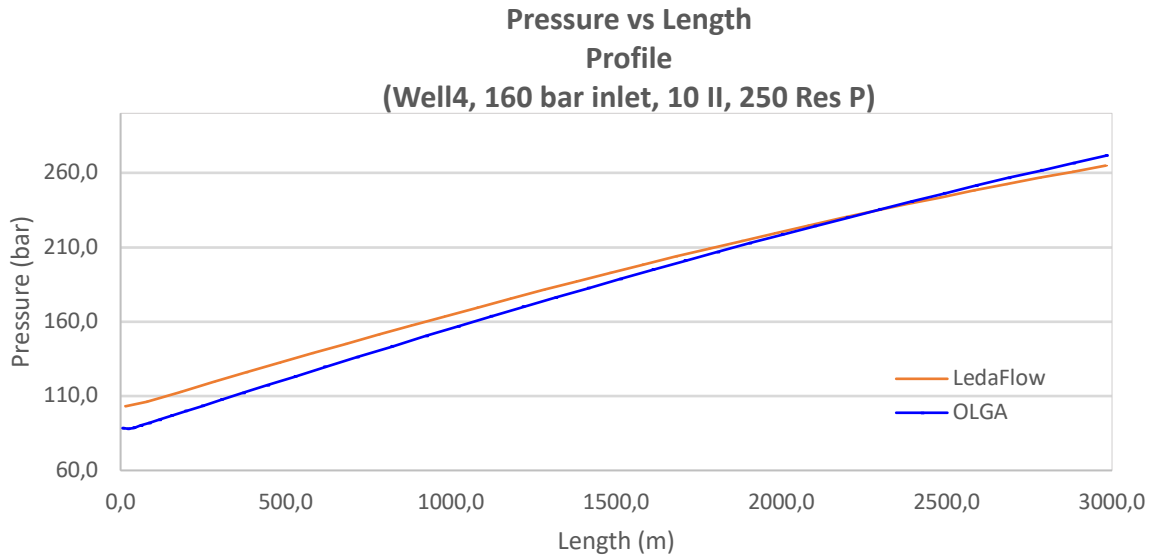

Figure 73: Pressure vs length or 160 bar inlet at well 4

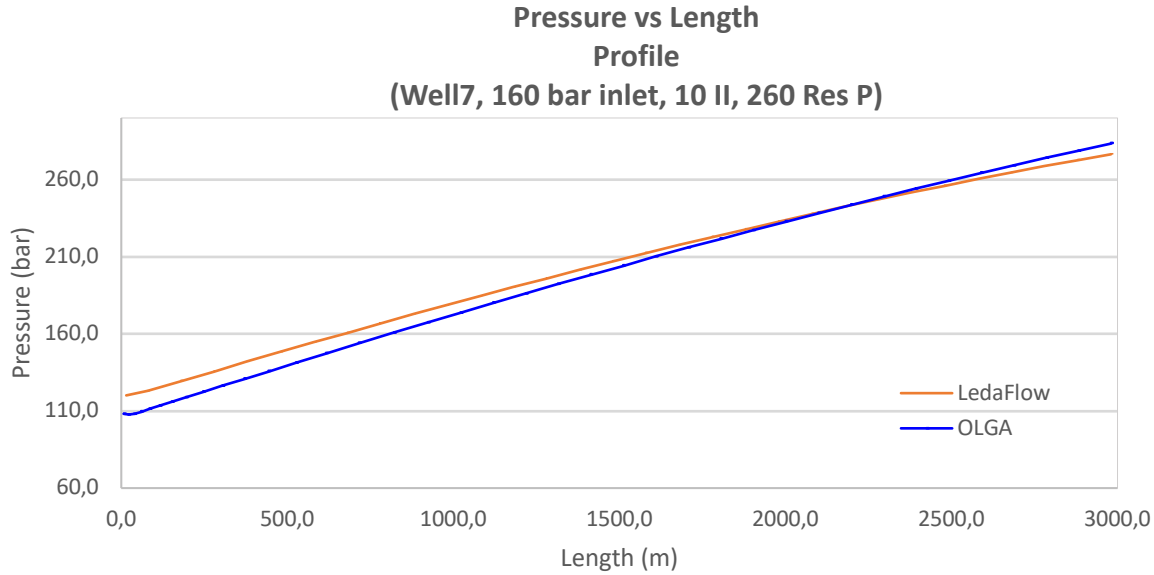

Figure 74: Pressure vs length for 160 bar inlet at well 7

Similar for all plots in Figure 72 - 74, is the higher inlet pressure given by LedaFlow, with OLGA eventually ending up with a higher pressure at the IPR. Pressure at the IPR in well 1 is 243 bar and 249 bar by LedaFlow and OLGA, respectively. For well 4, the pressure is 265 bar and 271 bar, and for well 7, the pressure is given to be 276 bar and 283 bar.

The deviation in pressure for LedaFlow and OLGA is shown in Figure 75 for well 1, 4 and 7, respectively.

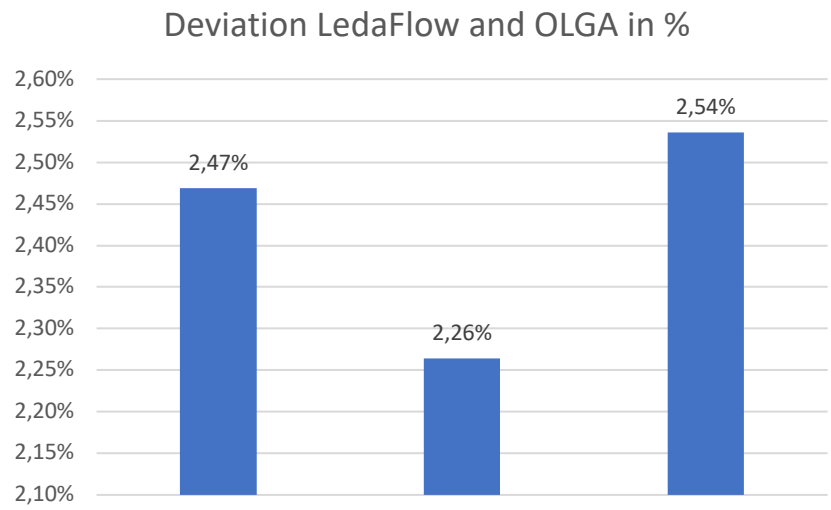

Figure 75: Deviation in pressure profiles for LedaFlow and OLGA

4.5.4 160 bar inlet, well injection rate

Data for well injection rate was extracted from the same simulation and plotted as mass flow vs time. Figure 76 - 78 show well injection rate for well 1, 4 and 7, respectively.

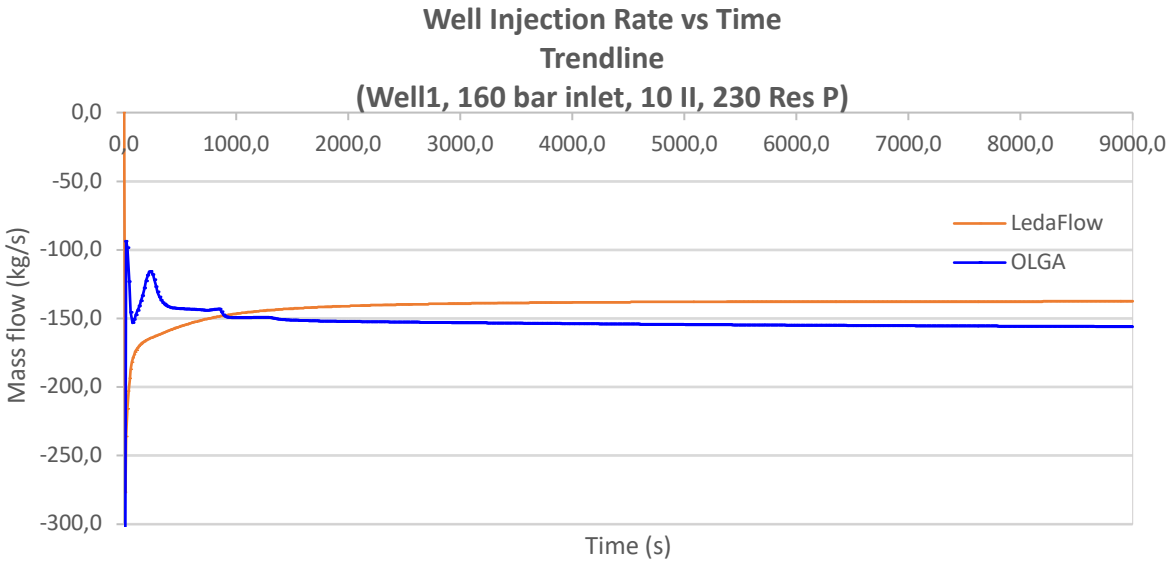

Figure 76: Well injection rate for 160 bar inlet at well 1

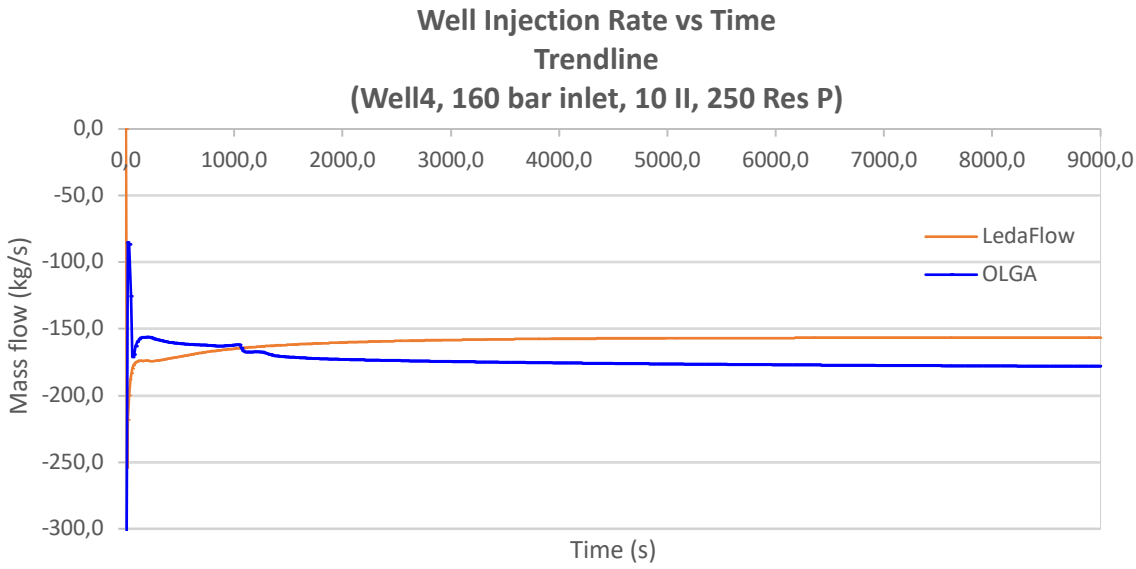

Figure 77: Well injection rate for 160 bar inlet at well 4

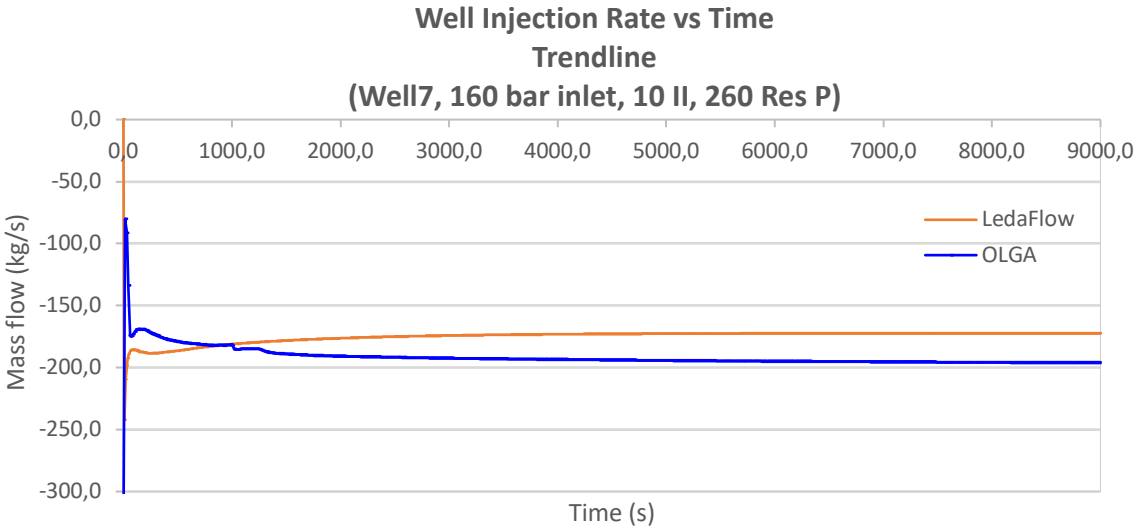

Figure 78: Well injection rate for 160 bar inlet at well 7

In Figure 76 for well 1, a quick stabilization is observed by both LedaFlow and OLGA, and after stabilization an injection rate of 138 kg/s and 156 kg/s was given by LedaFlow and OLGA, respectively. A similar stabilization time is shown for well 4 and 7 in Figure 77 and 78, and the given well injection rate to be 157 kg/s and 178 kg/s for well 4, and 172 kg/s and 196 kg/s for well 7.

The deviation in well injection rate for wall 1, 4 and 7 respectively, is shown in Figure 79.

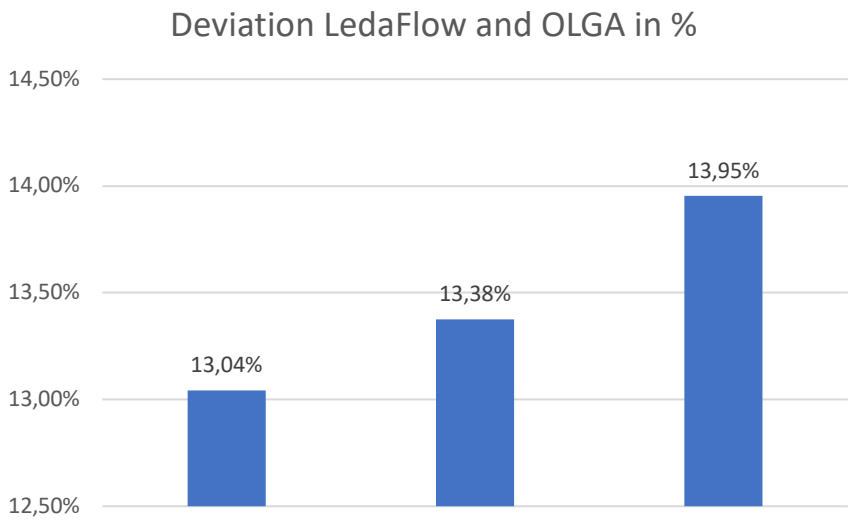

Figure 79: Deviation in well injection rate for LedaFlow and OLGA

5. Discussion

5.1 Base case, 10 II

When analyzing the plot for mass flow vs time in Figure A1, shown in Appendix A, some instability is present in the OLGA simulation for the first 1000 seconds. Due to the user defined initial conditions, some time is expected for the simulation to stabilize. Significantly more instability is present in the LedaFlow simulation, with large fluctuations in mass flow values for the first half of the simulation runtime. The same is observed for 100 bar inlet in Figure A4. This simulation gave a higher mass flow rate for both software programs due to the higher inlet pressure. The long time to reach steady state conditions may be due to flow regime transitions. These transitions may cause the mass flow rates to adjust to the changing flow patterns, and thus, such fluctuations are expected. When the simulations settle for a more dominant flow regime, stability will be reached. Additionally, numerical issues may be the cause of the instability. This can be convergence issues or a choice of less appropriate grid sizes, thus not capturing the dynamics of the system accurately.

For plots in Figures A2 and A3, a quicker time to stabilize is observed from LedaFlow, where a more gradual convergence is seen. Generally, for all 80 bar mass flow plots, OLGA gave a higher mass flow after stabilization, with OLGA predicting a mass flow of on average 11,7 % higher than LedaFlow for 80 bar inlet, and 9,9 % higher for 100 bar inlet.

Plots shown in Figure 22 and 23 show pressure profiles of 80 bar inlet at pipeline and well 1. The pressure profile at pipeline shows a good coherence up to approximately 40000 meters where OLGA experience a higher pressure drop compared to LedaFlow and eventually a lower pressure at the outlet of the pipe. When analyzing the pressure profile for well 1, LedaFlow experience a higher pressure drop and as much as 23 bar lower pressure than OLGA at the IPR.
For Figure 26 and 27, profile for the pipeline shows a more pronounced difference in pressure alone the pipe between the two software programs.
OLGA simulation displays a higher pressure drop immediately after inlet and a continuation of this pressure drop through the pipe. At outlet, the difference between the predicted pressure is as high as 16,67 %. For well 1, LedaFlow simulation enter the pipe at a higher pressure, however like the 80 bar run, experience a higher pressure drop along the well. Eventually crossing the line for OLGA.

Due to the similarity in geometry, pipe diameter, fluid, and roughness for the two a significant difference in pressure drop is not to be expected. Differences in flow regime may be the cause of the high pressure drop variations. As the flow regime changes from one type to another, and dependent on the flow being laminar or turbulent, changes in momentum transfer and fluid behavior can lead to pressure variations.

Figure 29 and 30, temperature profiles for pipeline and well is shown. The fluid temperature for the pipeline displays a rapid decrease as the fluid adjusts to the ambient temperature of 4°C. OLGA settles at a higher temperature than LedaFlow and remain constant for the rest of the pipeline. A clear correlation to the pipelines profile is shown in the sudden temperature drop at approximately 40000 meters. At this point a large pressure drop is also observed.
The temperature profile for well 1 displays a gradual increase in temperature further down the well. The ambient temperature is a linear gradient from 7 to 95°C. LedaFlow gave somewhat higher temperature at the IPR and OLGA a temperature 8,4 % lower that of LedaFlow.

5.2 Base case, 10-5-1 II

Figure A7 show the mass flow vs time at inlet at 100 bar. Compared to the 100 bar simulation in Base case, 10 II, a significantly larger deviation between the LedaFlow and OLGA results is observed at 28,8 %. As noted in previous simulation, LedaFlow show instabilities early in the simulation. Worth noting for this simulation, is the relatively longer duration used by OLGA to reach stability.

As for Figures A8 - A10 for flowline 1, 2 and 3, a relatively steady and coherent mass flow is recorded until stabilization. Due to the variation in injectivity index for each well cluster, the flow rate is affected accordingly. A higher injectivity index indicates a more favorable flow condition, thus allowing for a higher injectivity rate and therefor a higher flow rate in the flowlines leading up to the wells with the varying injectivity index. As flowline 1 is connected to the well cluster with the highest injectivity index, at 10 kg/s-bar, the higher flowrate of 425 kg/s and 503 kg/s for LedaFlow and OLGA respectively, is expected. Compared to 168 kg/s and 188 kg/s for LedaFlow and OLGA at flowline 3, connected to the 1 kg/s-bar cluster. Both LedaFlow and OLGA shows this trend of higher flow rate at higher injectivity index, but with some deviation present. For flowline 1, OLGA gave a flow rate of as much as 18,4 % higher

than that of LedaFlow. The deviation for flowline 2 and 3 is slightly lower at 17,6 % and 11,9 %, respectively.

Similar results are shown for well 1, 4 and 7 in Figures A11 - A13. Well 1, with 10 kg/s-bar injectivity index show the highest mass flow rate and well 7, the lowest. The same trend in deviation between LedaFlow and OLGA is also observed here, with a deviation in well 1 at 17,6 %, 17,3% in well 4 and 12,5 % in well 7.

When investigating the pressure profiles for well 1, 4 and 7 for this simulation run, shown in Figure 33 – 36, a higher bottom hole pressure is present at wells with lower injectivity indexes. As the injectivity index affects the pressure distribution within the reservoir and near the injection well, a higher injectivity index implies a lower pressure drop between the wellbore and the formation, thus a more uniform pressure distribution.
Similarly for previous simulation runs, LedaFlow enters the well at a higher pressure, but experiences a higher pressure drop along the well and eventually a lower bottom hole pressure. A relatively small deviation between LedaFlow and OLGA is observed here, with OLGA giving around 3 % higher bottom hole pressure.

Figure 38 – 40, show the temperature profile for well 1, 4 and 7 from the same run. For well 1 and 4, a gradual deviation between LedaFlow and OLGA is observed, where LedaFlow show a higher temperature. For well 7, a more parallel increase in fluid temperature is observed, and a close to identical temperature is shown.

Figure 42 and 43, show the flow regime along the length of pipeline and well 1. Some variation in the flow regime is detected by LedaFlow at the start of the pipeline. The flow transitions between slug flow, wavy and bubbly before settling for stratified smooth. OLGA show this flow regime the whole length of the pipeline.
For the flow regime shown in well 1. OLGA gave stratified smooth at the very start and end of the well and annular for the most part, where LedaFlow gave bubbly flow for the whole length of the well. Bubbly flow is characterized by dispersed bubbles. These bubbles cause significant friction, causing a relatively high pressure drop compared to annular flow. This may cause the higher pressure drop given by LedaFlow shown in Figure 33 – 36.

5.3 Base case, 10 II, 280-210-180 bar reservoir pressure

For this simulation run, different reservoir pressures for the three clusters were chosen to investigate LedaFlow and OLGA's ability to handle the varying reservoir pressures. Figure A14 show mass flow vs time for the pipeline. An interesting observation for this simulation is the instabilities given by LedaFlow. As seen in earlier runs, some instabilities is present early in the runtime, but for this run, some instabilities is present at the 7000 – 8000 s mark. Similar to previous runs, OLGA show significantly higher flow rates compared to OLGA, with mass flows at flowline 1 and well 1 being as much as 42,11 % and 41,18 % higher than LedaFlow, respectively.

Pressure profiles for well 1, 4 and 7 shown in Figure 45 – 48, show a larger pressure drop given by LedaFlow compared to OLGA. Additionally, a higher bottom hole pressure is detected for the wells where the reservoir pressures are higher. Both LedaFlow and OLGA seem to capture this phenomenon with a small deviation between the software programs of only 2,5%, 3,1 % and 3,5 % for well 1, 4 and 7 respectively.

Figure 50 – 52 show the well injection rate for well 1, 4 and 7 from this simulation. A clear correlation between the reservoir pressure and well injection is present. For the wells with a lower reservoir pressure, a higher differential pressure between the bottom hole and reservoir is in place, and thus a higher injection rate is achieved. Both LedaFlow and OLGA correctly predicts this fact, but to a different degree. As plots for pressure profiles show OLGA with a higher bottom hole pressure, the well injection rate will be higher in the OLGA simulation. For well 1, 4 and 7, OLGA gave a well injection rate of 41,2 %, 15,7 % and 15 % higher than that of LedaFlow.

5.4 Secondary case, 10 II

With the intent of gathering a wider selection of data for comparison purposes, adjustments were made to the network model. Due to the extension of the model, a higher inlet pressure was chosen. In Figures A21 - A23 for mass flow vs time for flowline 1, 2 and 3, a rapid stabilization is observed in both LedaFlow and OLGA. Like previous mass flow runs, some deviation between LedaFlow and OLGA is observed with OLGA giving around 14 % higher mass flow rates than LedaFlow.

Figure 58 – 60 show the pressure profile for flowline 1, 2 and 3. Due to a higher pressure drop by OLGA in the pipeline, the inlet pressure from OLGA is lower in the flowlines. The pressure drop in the flowlines from LedaFlow and OLGA are close to parallel, but for flowline 1, the longest flowline, clearly a higher pressure drop in the OLGA simulation is present. For this pipeline LedaFlow gave a pressure at the outlet of the flowline of 20,2 % higher than OLGA.

In Figure 62 – 64, well injection rate for well 1, 4 and 7 is shown. A rapid stabilization time is observed in all plots, from both LedaFlow and OLGA. Due to the higher pressure drop in the longer flowlines, a lower bottom hole pressure is present at these wells, thus giving a lower injection rate. This is clearly shown in both LedaFlow and OLGA, with a deviation of around 13 %.

5.5 Secondary case, 10 II, 230-250-260 bar reservoir pressure

By adjusting the reservoir pressure for the different clusters, to compensate for the differencing lengths of the flowlines, a more even well injection rate was aimed for. Figures A24 - A27 show the mass flow vs time to stabilize for inlet, flowline, 1, 2 and 3. A high mass flow at the inlet is present in both LedaFlow and OLGA, but as previously seen, OLGA gives a significantly higher mass flow that LedaFlow. In this case, 20 % higher. The mass flow for the flowlines show similar results to the previous simulation, but a more even mass flow between the flowlines. The deviation is similar, at around 14 %.

Figure 67 – 70 show the temperature profile for the pipeline and well 1, 4 and 7 respectively. The temperature profile for the pipeline show a quick adjustment to the ambient temperature. Some variations is observed as the profile changes around 40000 meters. A slightly higher temperature is shown by OLGA. The temperature profile for the wells are more or less identical. With a steady increase in fluid temperature as the ambient temperature increases down the depth of the well. At the IPR, LedaFlow show a temperature of about 10 % higher than OLGA.

In Figure 72 – 74 the pressure profile of well 1, 4 and 7 show tendencies previously encountered. A higher pressure drop down the well is detected by LedaFlow, causing a lower

bottom hole pressure. Additionally, a higher bottom hole pressure in general is observed by wells connected to the reservoir with a higher reservoir pressure.

This bottom hole pressure correlates directly to the well injection rate, shown in Figure 76 – 78. Well 7 show the highest injection rate, followed by well 4, then well 1, with the lowest injection rate. Due to the different bottom hole pressure given by LedaFlow and OLGA, a variation in well injection rate, as seen, is expected. Similar to previous simulation runs, the deviation between LedaFlow and OLGA is around 14 %.

5.6 Sources of error

When simulating in two vastly different software programs such as LedaFlow and OLGA, creating two identical models is challenging. Some minor difference in the assembly and verification of the two models, may lead to variations in the models, and thus cause imperfection in the comparison.

Another possible source of error is the use of P-T and P-H formulation by the programs. For pure CO2, OLGA uses the P-H formulation to calculate properties of the fluid. This incorporates both the internal energy and the flow work of the fluid. LedaFlow depends on the P-T formulation and is more equipped for calculations where the flow is predominantly single phase. The use of these two formulations in the two programs may lead to inaccuracies.

The use of different EOS by LedaFlow and OLGA can cause inaccuracies in the simulations. By default, OLGA uses SW for pure CO2, whereas LedaFlow depends on the Multiflash add-in. Due to some license issue, RKS was the chosen EOS for the LedaFlow simulation. Both EOS`s are expected to provide good accuracy in predictions of CO2 flow, SW is considered to be the more preferred EOS when using pure CO2.

6. Conclusion

This comparative analysis of the widely used transient multiphase flow simulators, LedaFlow and OLGA has provided valuable insight into their performance in simulating CO2 injection systems.

From multiple simulation scenarios, some initial instabilities was experienced by both LedaFlow and OLGA in the early stages of the simulation. However, it was observed that LedaFlow exhibited larger fluctuations compared to OLGA. After some amount of simulation time and the flow regime stabilized, both software programs demonstrated convergence towards more consistent measurements, suggesting the suitability of both tools for steady-state flow simulations.

In terms of mass flow predictions, a consistently higher mass flow rate was given my OLGA compared to LedaFlow. The average deviation between the two software programs was approximately 11,7 % for the 80 bar inlet scenarios and 9,9 % for the 100 bar inlet scenarios from the base case simulation. These variations in mass flow rates can be attributed to the differences in modeling assumptions or convergence issues.

Pressure profiles along the pipeline and within the wells revealed distinct differences between LedaFlow and OLGA. LedaFlow generally exhibit a higher pressure drop in wells, whereas OLGA show a higher pressure drop in the pipeline and flowlines.

Temperature profiles demonstrated relative similar trends between the two software programs, with slight differences observed. The consistent trends suggest that both LedaFlow and OLGA capture the thermal behavior of the injection system efficiently. However, further investigation and validation are necessary to fully understand the nuances and underlying causes of the temperature variations.

In the secondary case simulations, similar trends persisted. OLGA predicted higher mass flow rates, while LedaFlow tended to show a higher pressure drop in the wells, thus causing a lower bottom hole pressure. This directly correlates to the pressure difference between the well perforation and the reservoir, and thus to the slight deviation in well injection rates between LedaFlow and OLGA. Where the bottom hole pressure exhibit a deviation of on average 2,4 %, the deviation in well injection rate is 13,5 %.

This comparative analysis contributes to the development of more efficient CO2 injection systems for CCUS purposes. However, further research of simulation models and algorithms are necessary to validate the accuracy and reliability of these simulation tools in the simulation of CO2 injection systems.

6.1 Further work

The further work for this study should include a wider set of parameters, such as different pipe diameters, pipe profiles and reservoir depths. Additionally, simulations and subsequent comparisons of transient scenarios should be completed, preferably with the addition of start-up and shut-down cases. Due to the effect of impurities in CO2, additional simulations should include CO2 with impurities.

Bibliography

A. Jahanbani, S. S. (2009). Determination of Inflow Performance Relationship (IPR) by Well Testing. *Canadian International Petroleum Conference*.

Andrzej Witkowski, S. R. (2014). Anlaysis of pipeline transportation systems for carbon dioxide sequestration. *Archives of Thermodynamics*.

Bachu, S. (2003). *Screening and ranking of sedimentary basins for sequestration of CO2 in geological media in response to climate change.* Environmental geology.

Bhattacharyya, S. (2020). *Inverse Heat Conduction and Heat Exchangers.*

C.A. Rochelle, Y. M. (2002). *The solubility of supercritical CO2 in pure water and syntethic Utsira porewater.* British geological survey.

Cheng, E. (2006). *Multiphase flow handbook.* CRC press.

Christian Hermanruda, T. A. (2009). Storage of CO2 in saline aquifers – lessons learned from 10 years of injection into the Utsira Formation in the Sleipner area. *Energy Procedia*.

Dey, A. K. (2023). What is Slug Flow? Steps for Slug Flow Analysis. *What is piping*.

Equinor. (2020). *Årsrapport 2020 til Miljødirektoratet for Snøhvit, Albatross og Askeladd.*

Europeen Union. (2023, February). *climate.ec.europe.eu*.

Giljarhus, K. E. (2012). *Solution of the Span-Wagner equation of state using.* SINTEF Energy.

Global CCS Institute. (2013). ROAD project: Flow assurance and control philosophy. https://www.globalccsinstitute.com/publications/road-project-flow-assurance-and-control-philosophy.

Global CCS Institute. (2023, February). *Why CCS?* Retrieved from globalccsinstitute.com.

Hasan Muslemani, X. L. (2020). Business Models for Carbon Capture, Utilization and Storage Technologies in the Steel Sector: A Qualitative Multi-Method Study. *MDPI*.

Holland, F. (1995). *gas-liquid two-phase flow.* In Fluid Flow for Chemical Engineers.

Hongfang Lu, X. M. (2020). *Carbon dioxide transport via pipelines: A systematic review.* Journal of Cleaner Production.

IPCC. (2005). *IPCC Special Report on Carbon Dioxide Capture and Storage.*

James P. Brill, H. M. (1999). *Multiphase flow in wells.* Society of Petroleum Engineers.

J.P. Brill, H. M. (1999). Multiphase flow in wells. *Society of Petroleum Engineers*.

Jostein Pettersen, S. (2011). Snøhvit field development.

Kim, Y. (2007). Equation of State for Carbon Dioxide. *Journal of Mechanical Science and Technology*.

Kwong, O. R. (1949). *On the thermodynamics of solutions. v. an equation of state.* Chemical reviews.

LedaFlow. (2023). *ledaflow.com.* Retrieved from The history of LedaFlow.

M. Loizzo, B. L. (2010). Reusing O&G-Depleted Reservoirs for CO2 Storage: Pros and Cons. *SPE Projects Facilities & Construction.* .

Mohamed, M. A. (2022). Experimental study of CO2 injectivity impairment in sandstone due to salt precipitation and fines migration. *Journal of Petroleum Exploration and Production Technology*.

Mohammad Ahmad, S. G. (2014). Water Solubility in CO2 Mixtures: Experimental and Modelling Investigation . *Energy Procedia*.

Morten Langsholt, J. A. (2014). Simulating Flow of CO2 with Impurities in OLGA; Dealing with Narrow Phase-envelopes and the Critical Point. *Energy Procedia*.

National Petroleum Council. (2020). *Meeting the Dual Challenge: A Roadmap to At-Scale Deployment of Carbon Capture, Use, and Storage.* EEIA.

O. Izgec, B. D. (2005). COw Injection in Carbonates. *OnePetro*.

Oil & Gas iQ. (2023, February). *3 Key Challenges for CCUS.* Retrieved from oilandgasiq.com.

P.Aursand, M. S. (2013). *Pipeline transport of CO2 mixtures: Models for transient simulation.*

Pina, V. B. (n.d.). *Transient two-phase injection of CO2 in a wellbore.* UPC.

R. Belt, B. D. (2011). Comparison of commercial multiphase flow simulators with experimental and field databases. *ResearchGate*.

R.W. Lockhart, R. M. (1949). Proposed correlation of data for isothermal two-phase, two-component flow in pipes. *Chemical Engineering Progress*.

Regjeringen. (2023). *CO2-avgiften.* Retrieved from regjeringen.no.

Rutger Tromp, L. M. (2021). Multiphase Flow Regime Characterization and Liquid Flow Measurement Using Low-Field Magnetic Resonance Imaging. *ResearchGate*.

Soave, G. (1972). *Equilibrium constants from a modified redlich-kwong equation of state.* Chemical engineering science.

Statoil. (2010). *Technical Achievement 2010 Snøhvit CO2 Storage: Snøhvit CO2 Tubåen Fm. storage capacity and injection strategy study.* Statoil.

Tan, J. F.-Y. (2017). *A review of optimization and decision-making models for the planning of CO2 capture, utilization and storage (CCUS) systems.* Elsevier: Institution of Chemical Engineers.

V.E. Onyebuchi, A. K. (2018). *A systematic review of key challenges of CO2 transport via pipelines.* Renewable and Sustainable Energy Reviews.

Yong Bai, Q. B. (2019). *Subsea Engineering Handbook.* Elsevier.

Appendix A

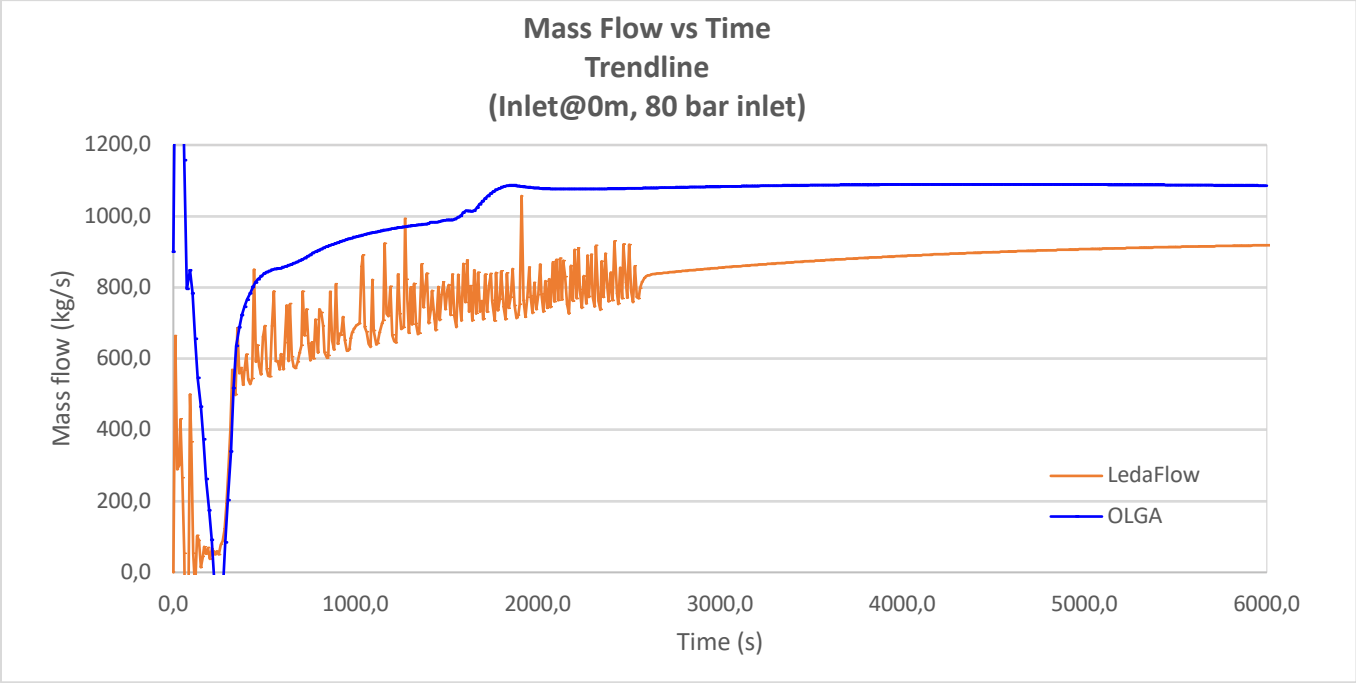

Figure A1: Mass flow vs time for 80 bar inlet at inlet

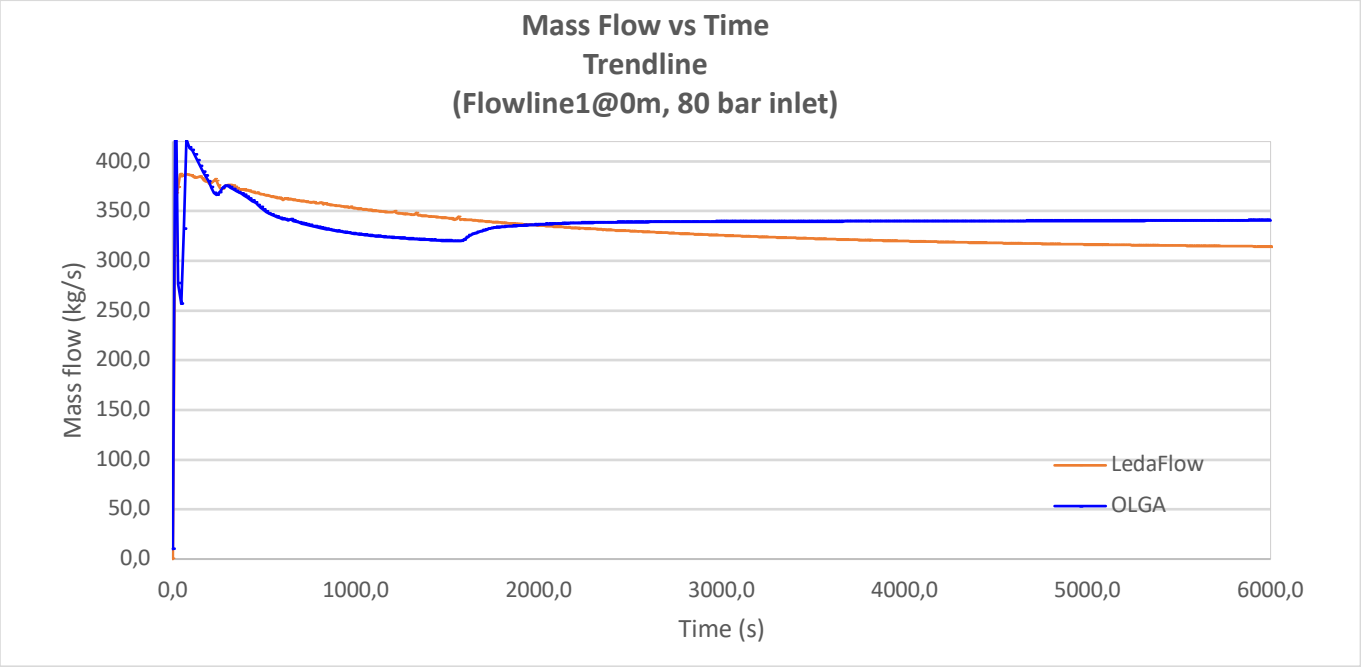

Figure A2: Mass flow vs time for 80 bar inlet at flowline 1

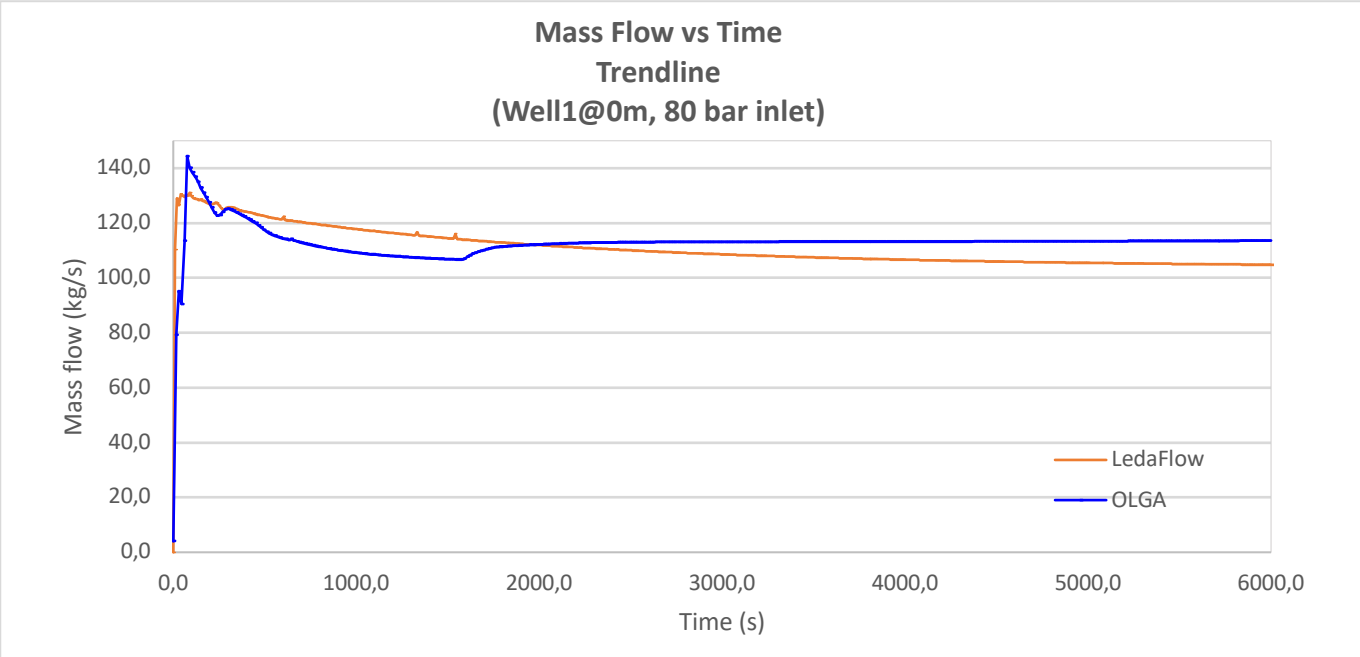

Figure A3: Mass flow vs time for 80 bar inlet at well 1

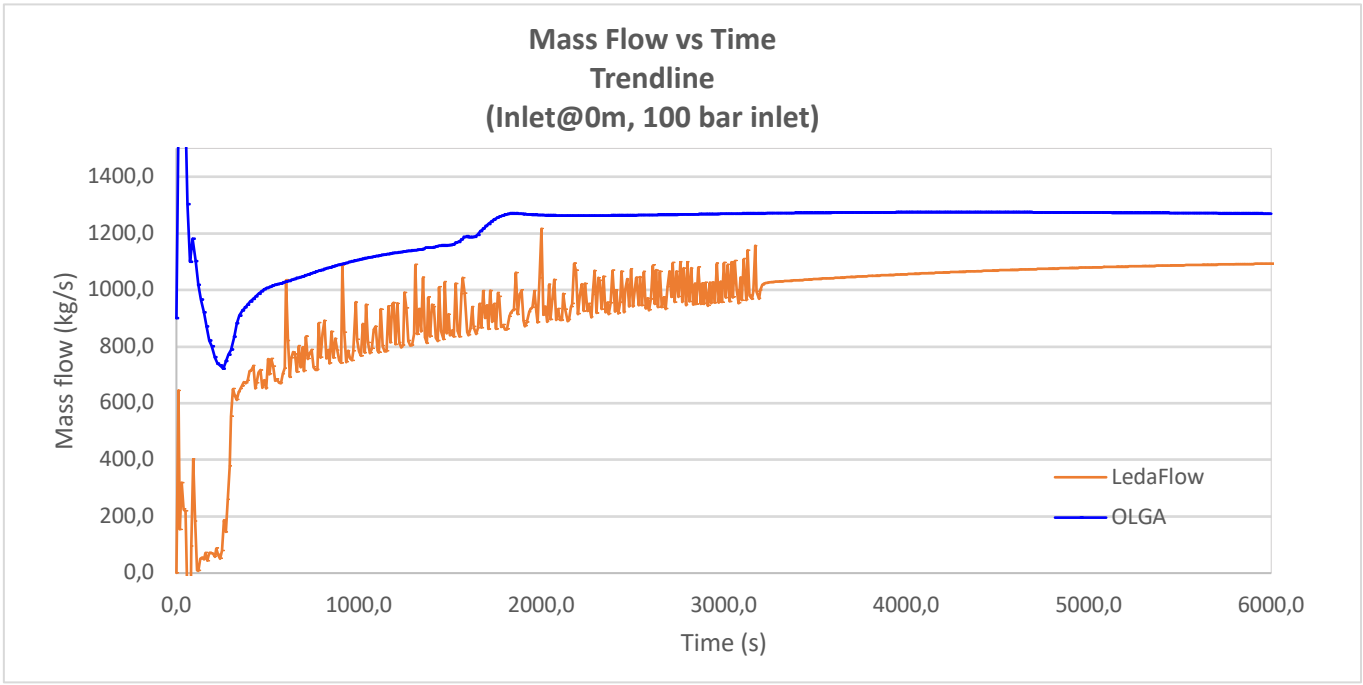

Figure A4: Mass flow vs time for 100 bar inlet at inlet

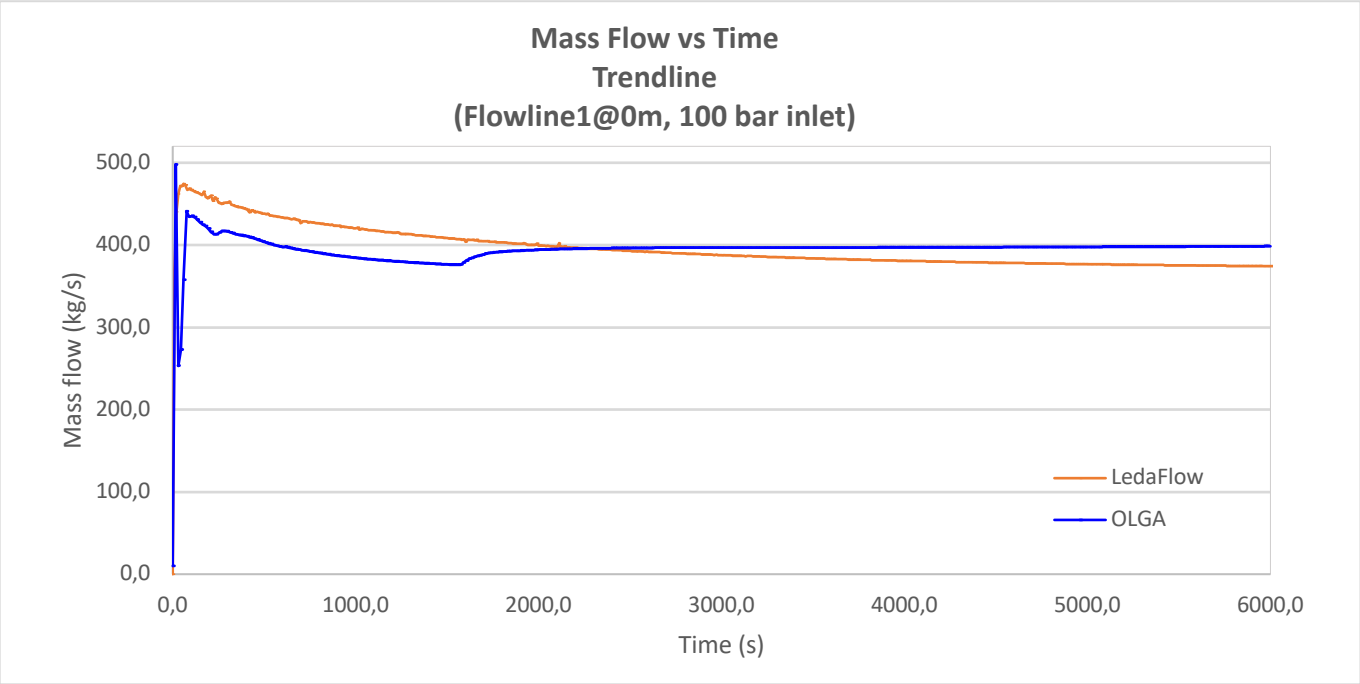

Figure A5: Mass flow vs time for 100 bar inlet at flowline 1

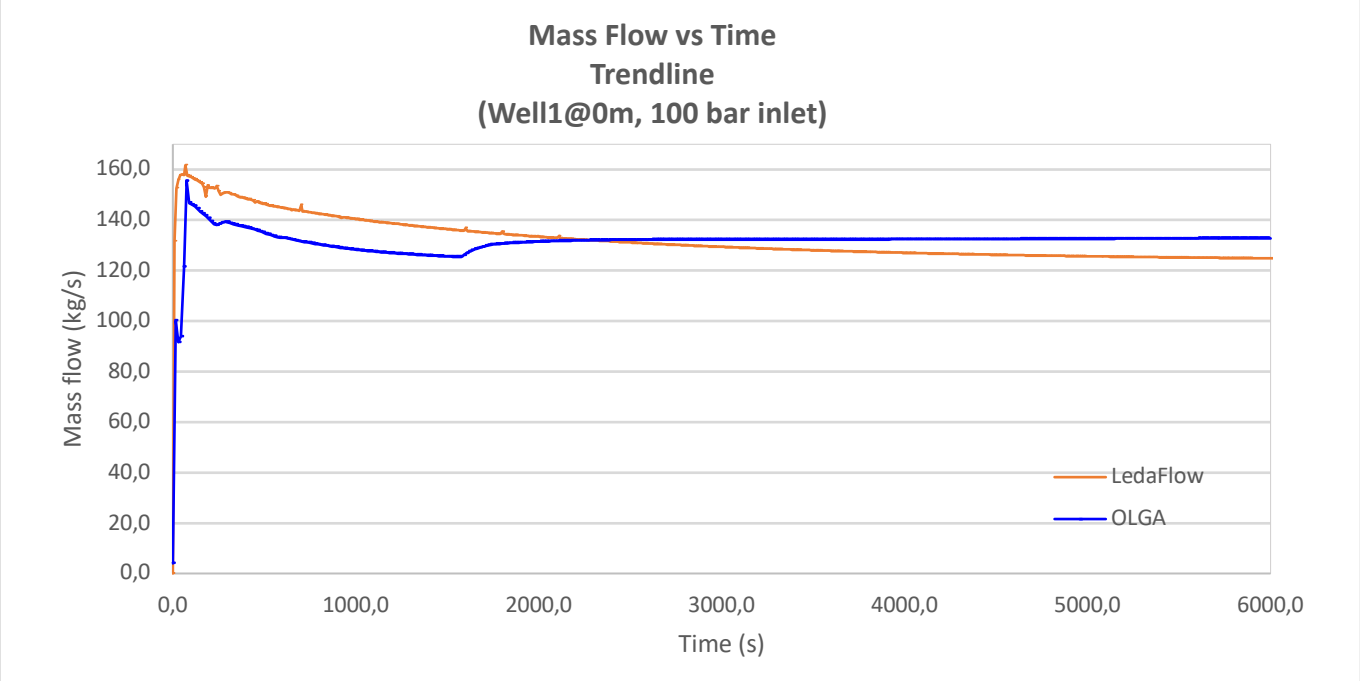

Figure A6: Mass flow vs time for 100 bar inlet at well 1

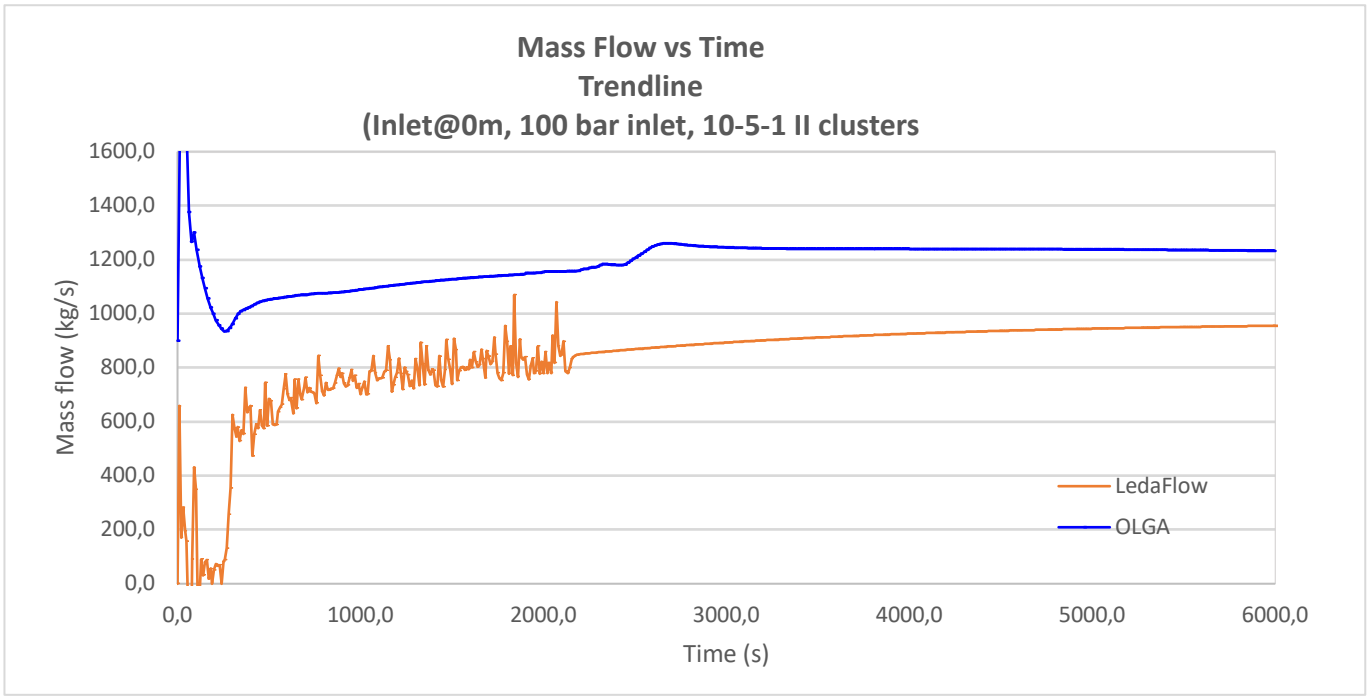

Figure A7: Mass flow vs time for 100 bar inlet at inlet

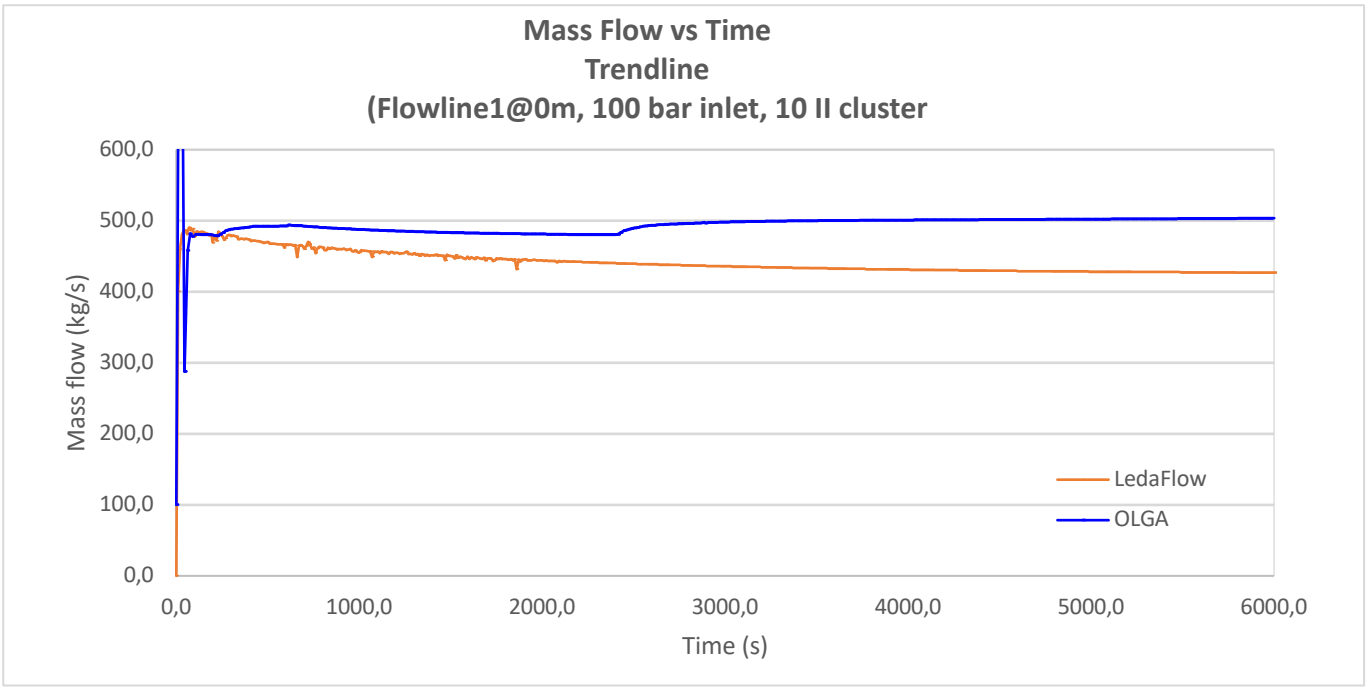

Figure A8: Mass flow vs time for 100 bar inlet at flowline 1

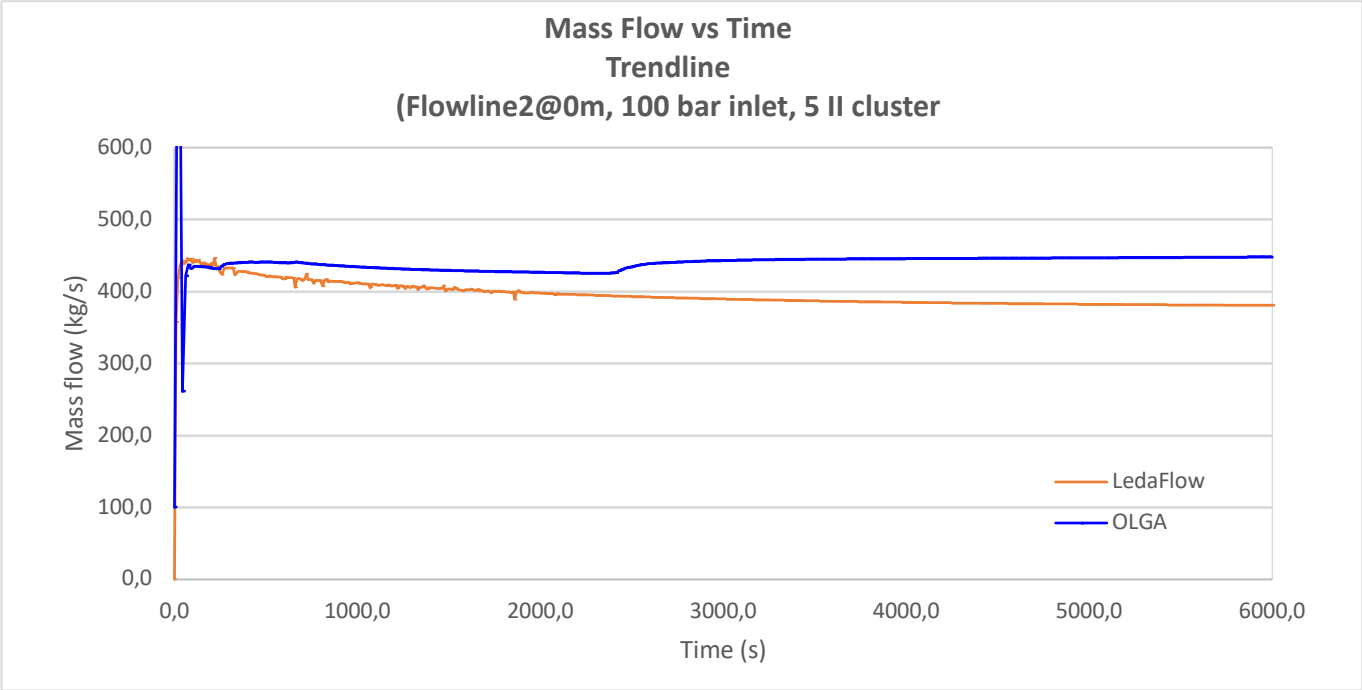

Figure A9: Mass flow vs time for 100 bar inlet at flowline 2

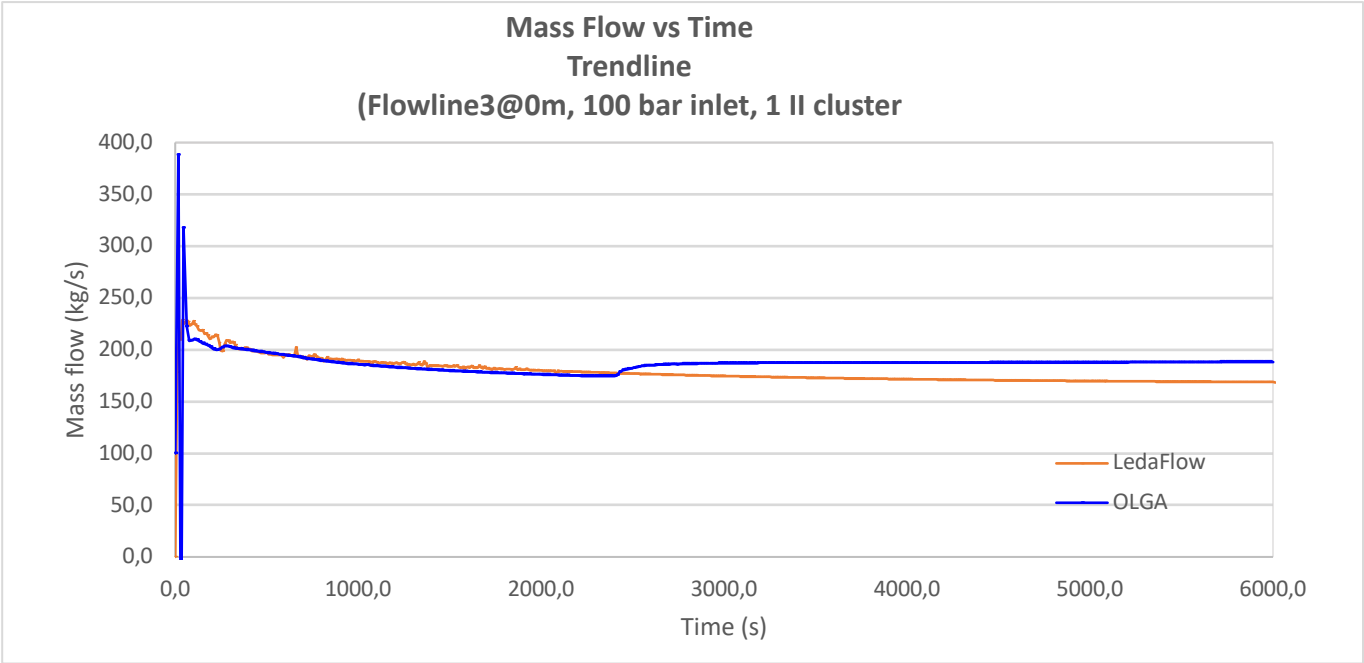

Figure A10: Mass flow vs time for 100 bar inlet at flowline 3

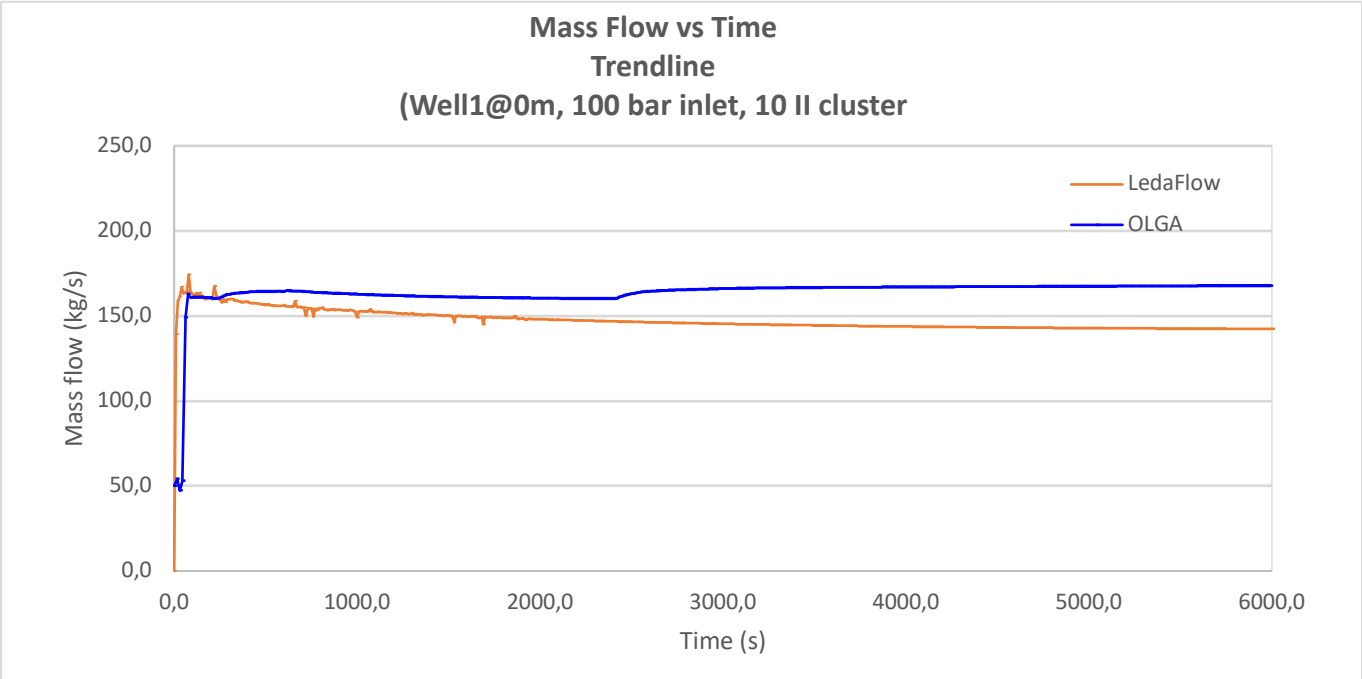

Figure A11: Mass flow vs time for 100 bar inlet at well 1

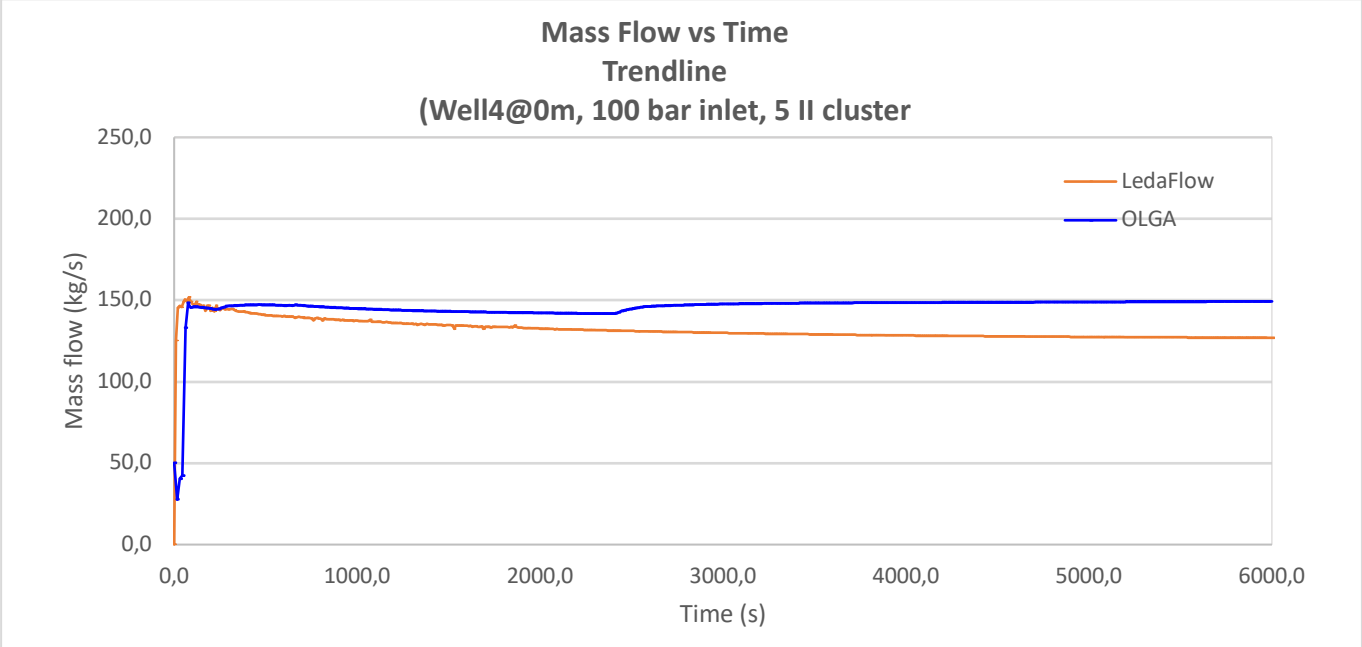

Figure A12: Mass flow vs time for 100 bar inlet at well 4

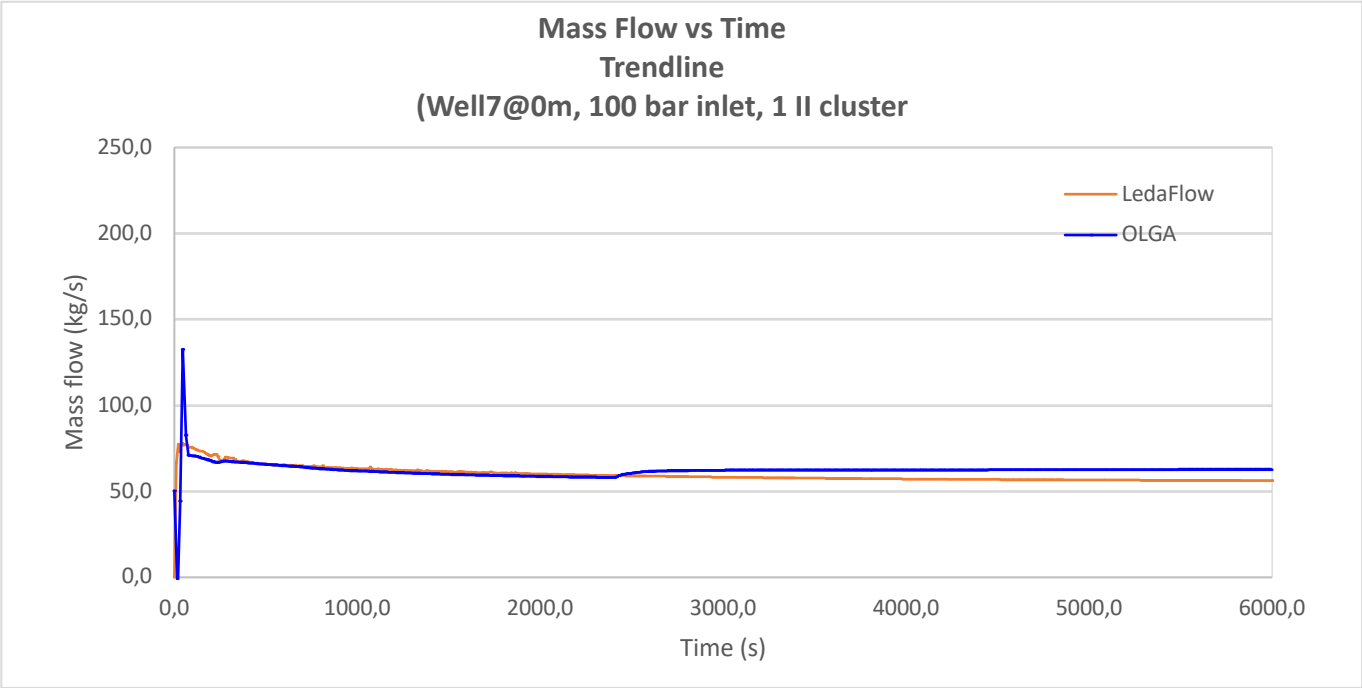

Figure A13: Mass flow vs time for 100 bar inlet at well 7

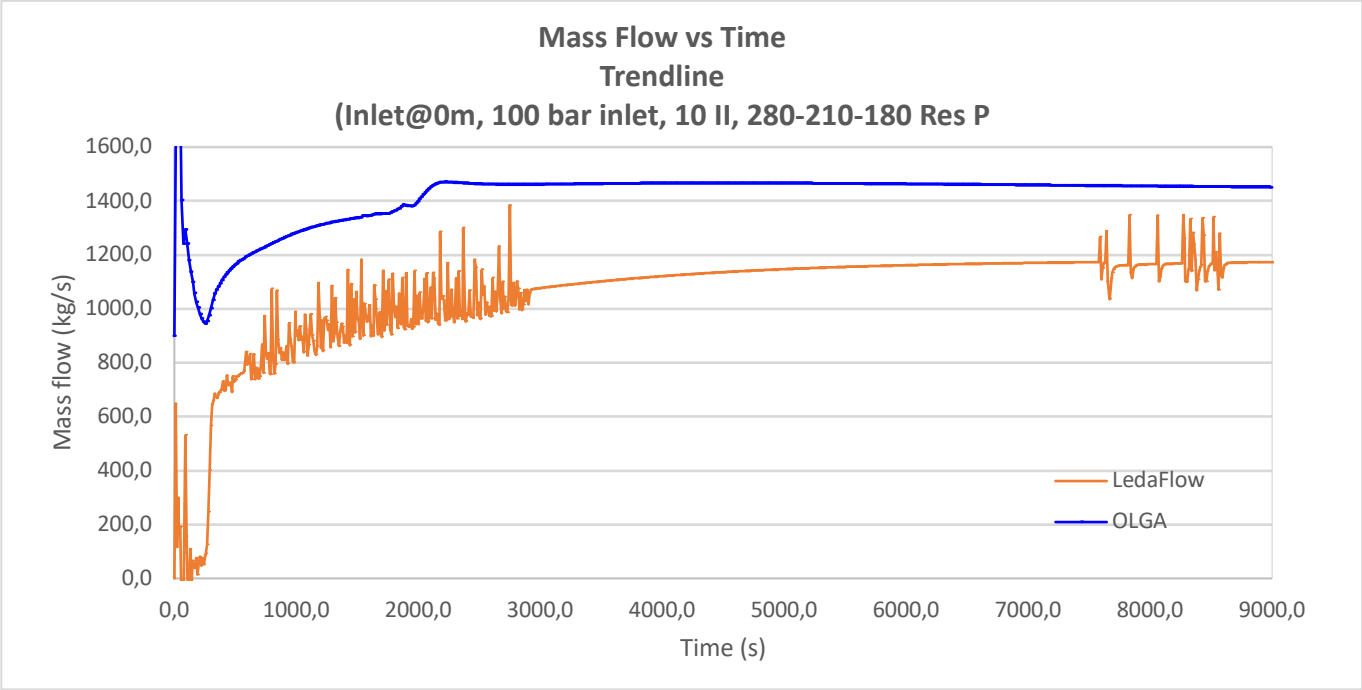

Figure A14: Mass flow vs time for 100 bar inlet at inlet

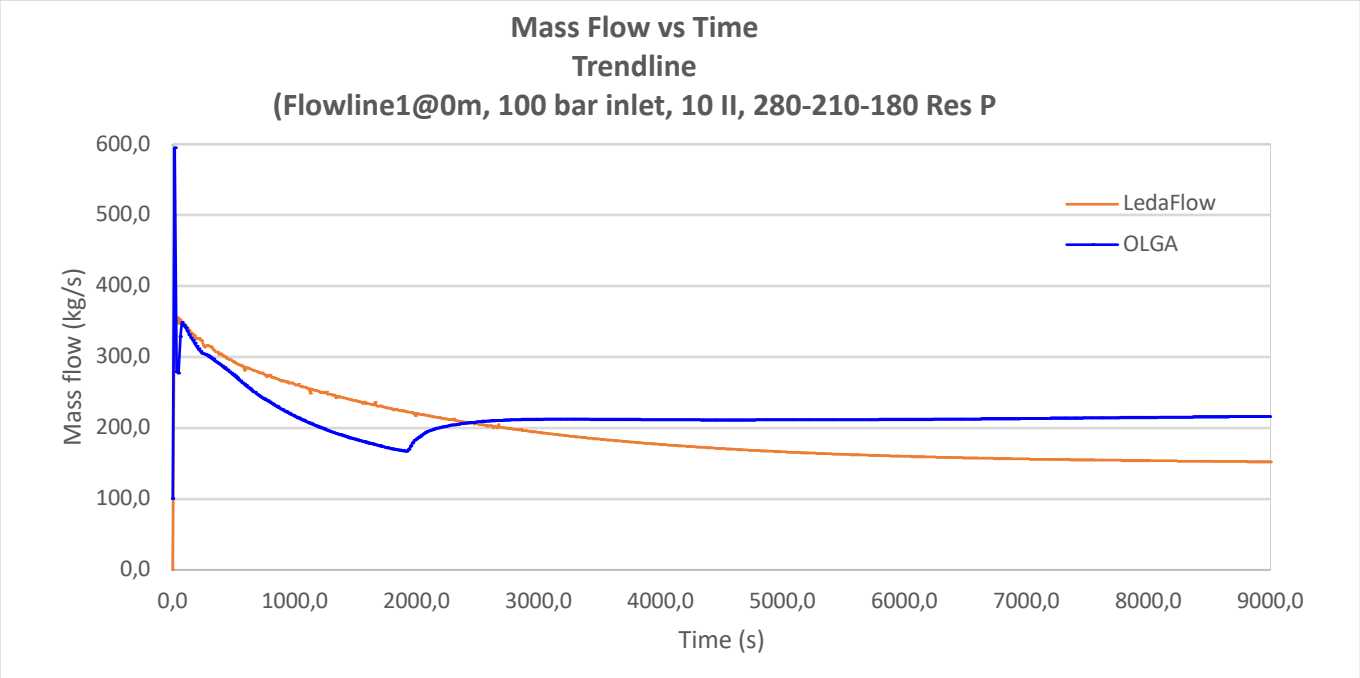

Figure A15: Mass flow vs time for 100 bar inlet at flowline 1

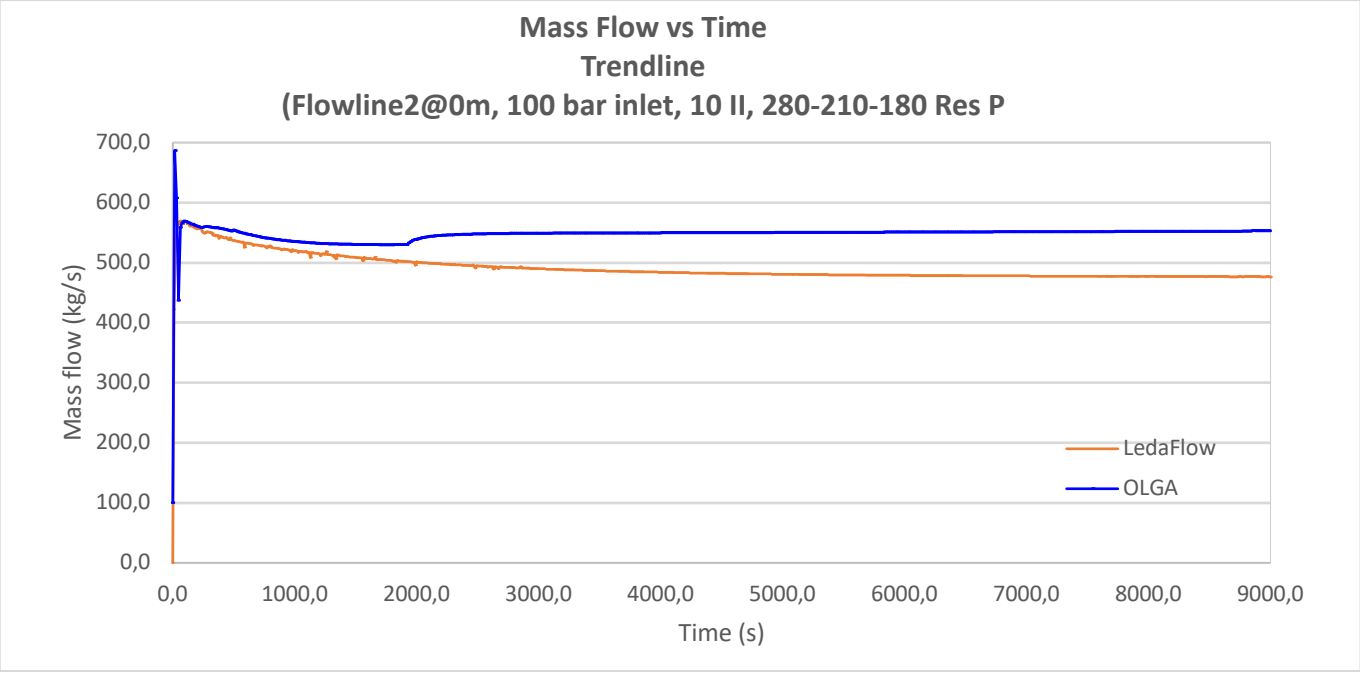

Figure A16: Mass flow vs time for 100 bar inlet at flowline 2

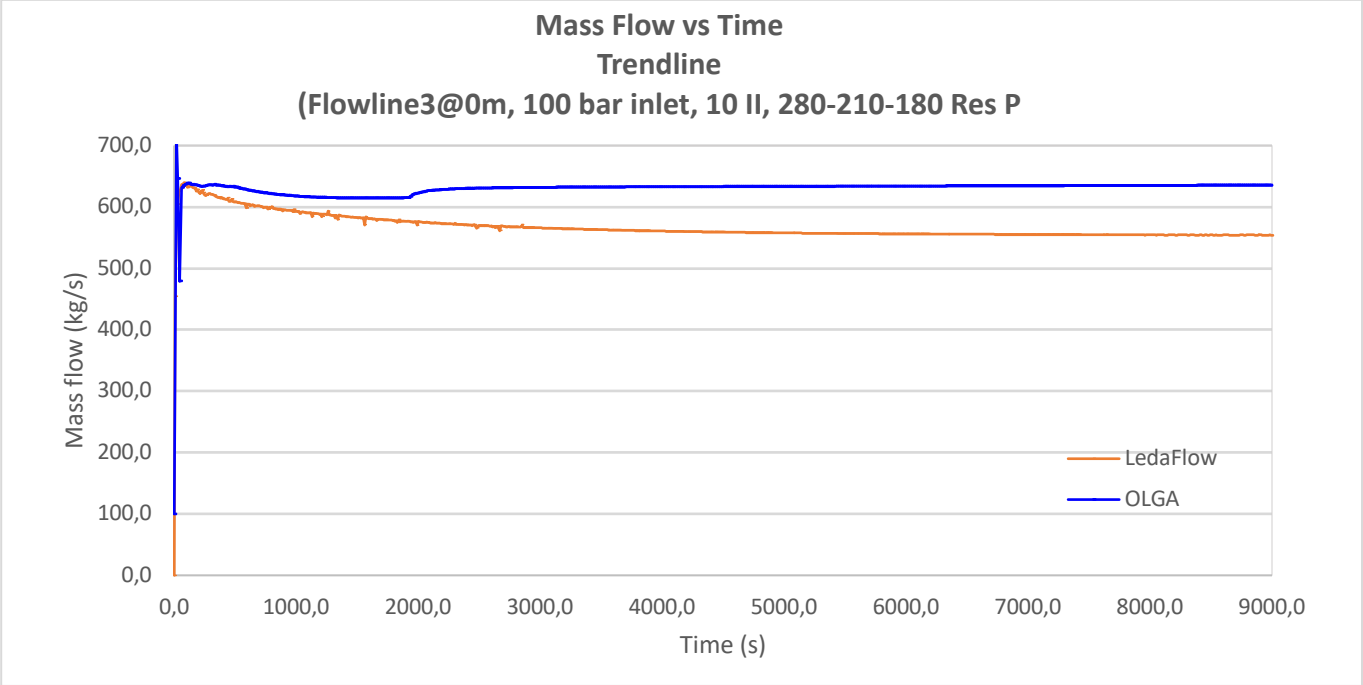

Figure A17: Mass flow vs time for 100 bar inlet at flowline 3

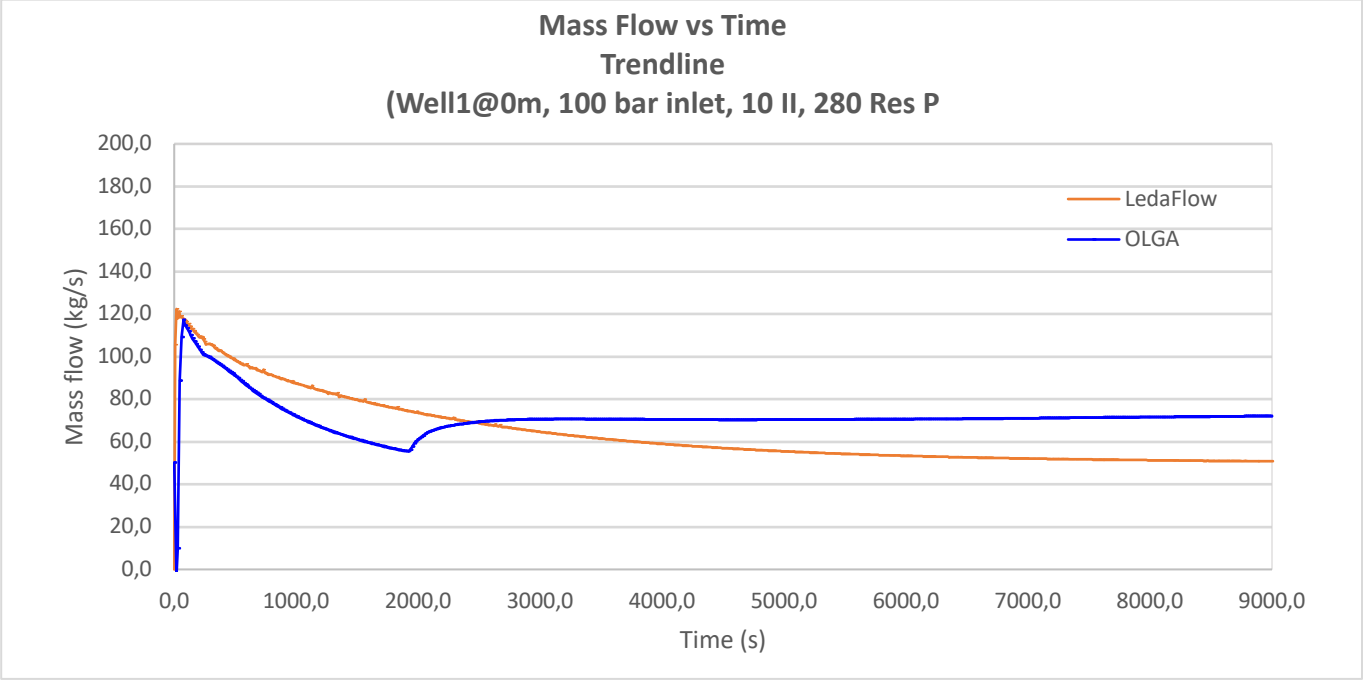

Figure A18: Mass flow vs time for 100 bar inlet at well 1

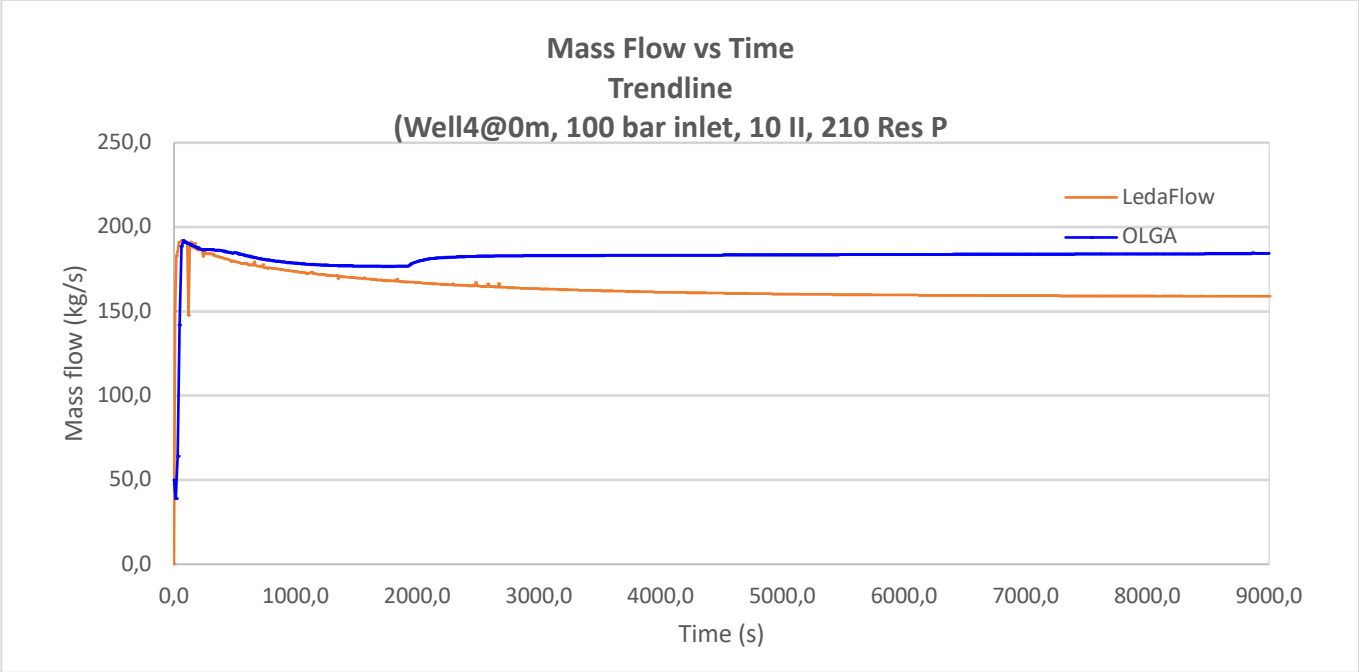

Figure A19: Mass flow vs time for 100 bar inlet at well 4

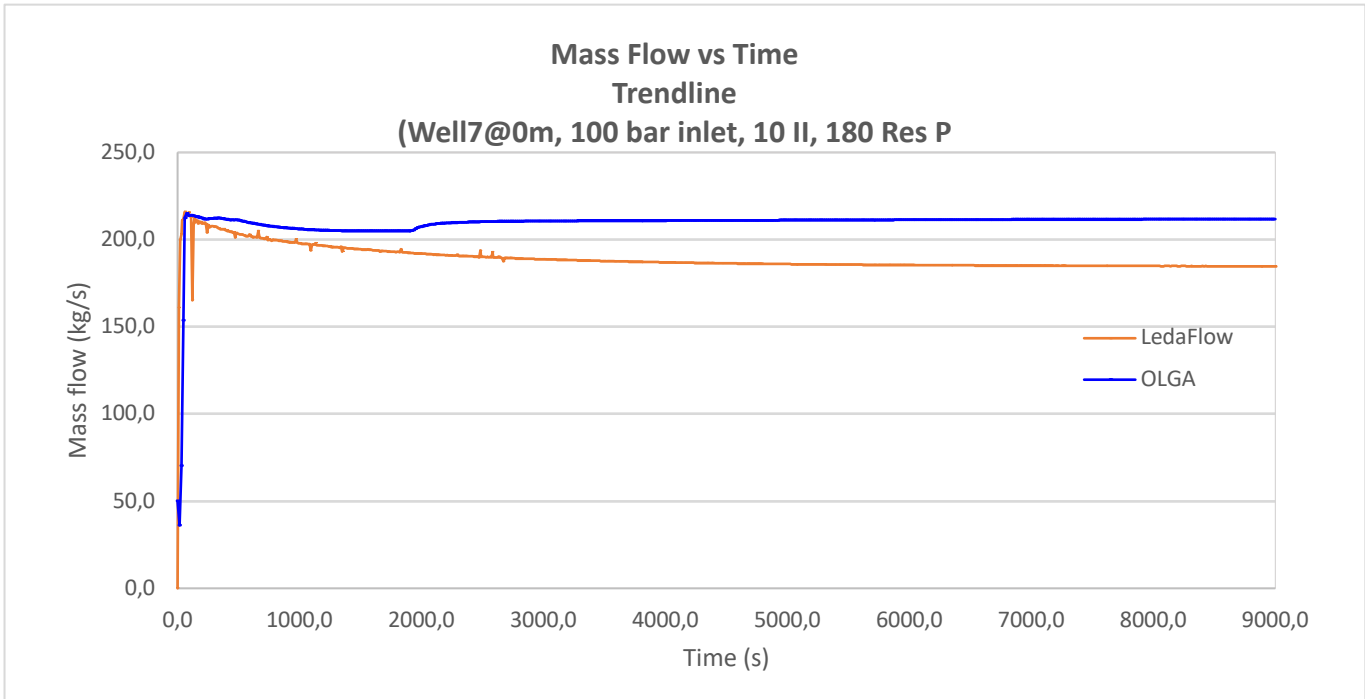

Figure A20: Mass flow vs time for 100 bar inlet at well 7

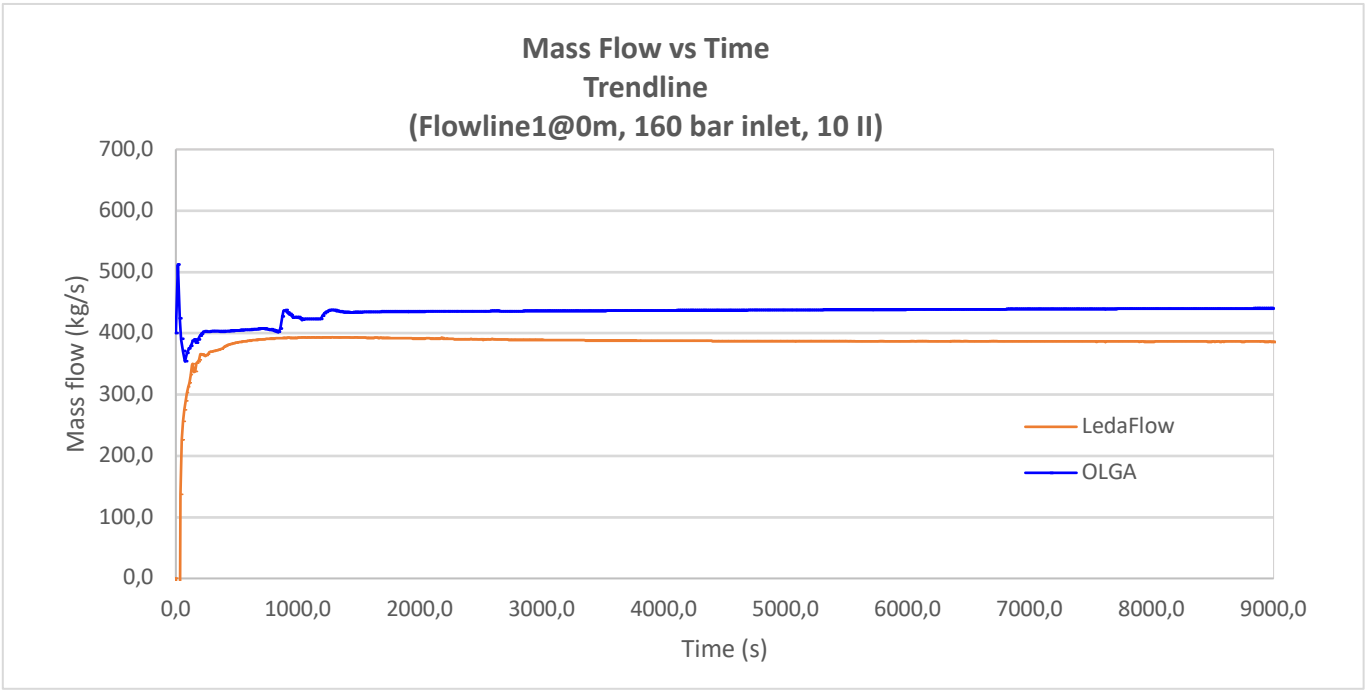

Figure A21: Mass flow vs time for 160 bar inlet at flowline 1

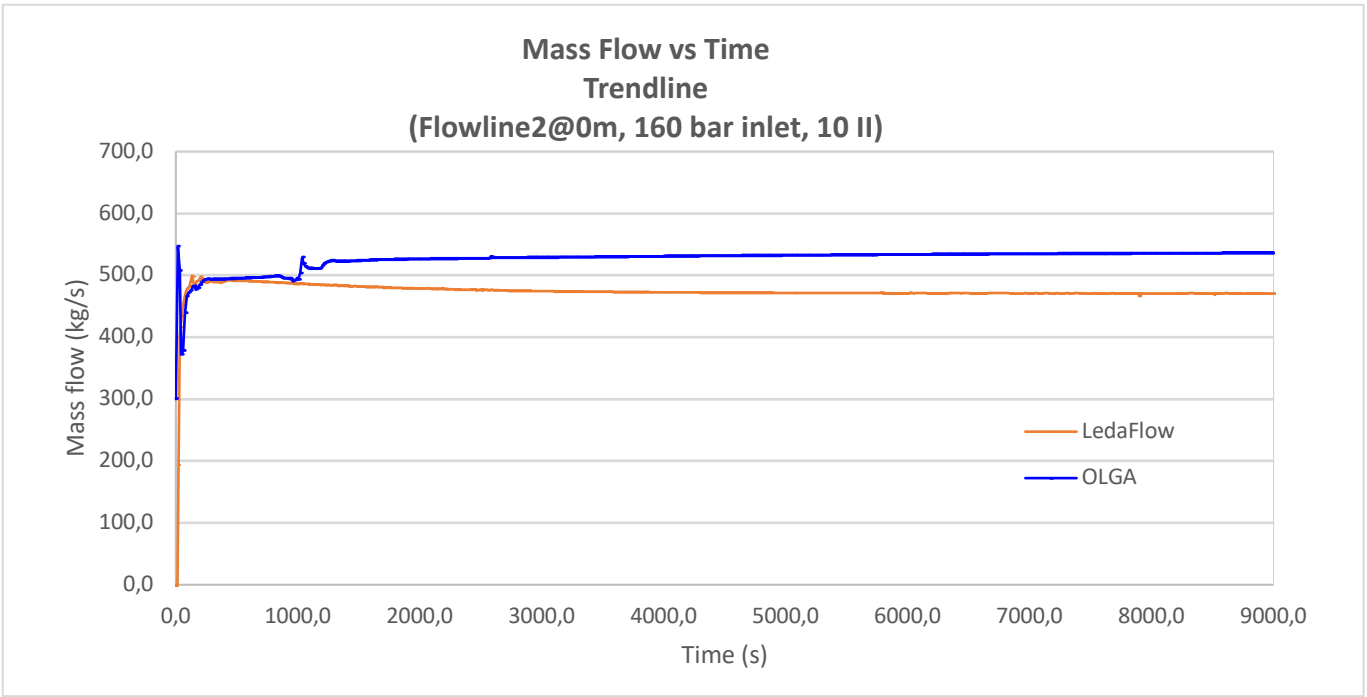

Figure A22: Mass flow vs time for 160 bar inlet at flowline 2

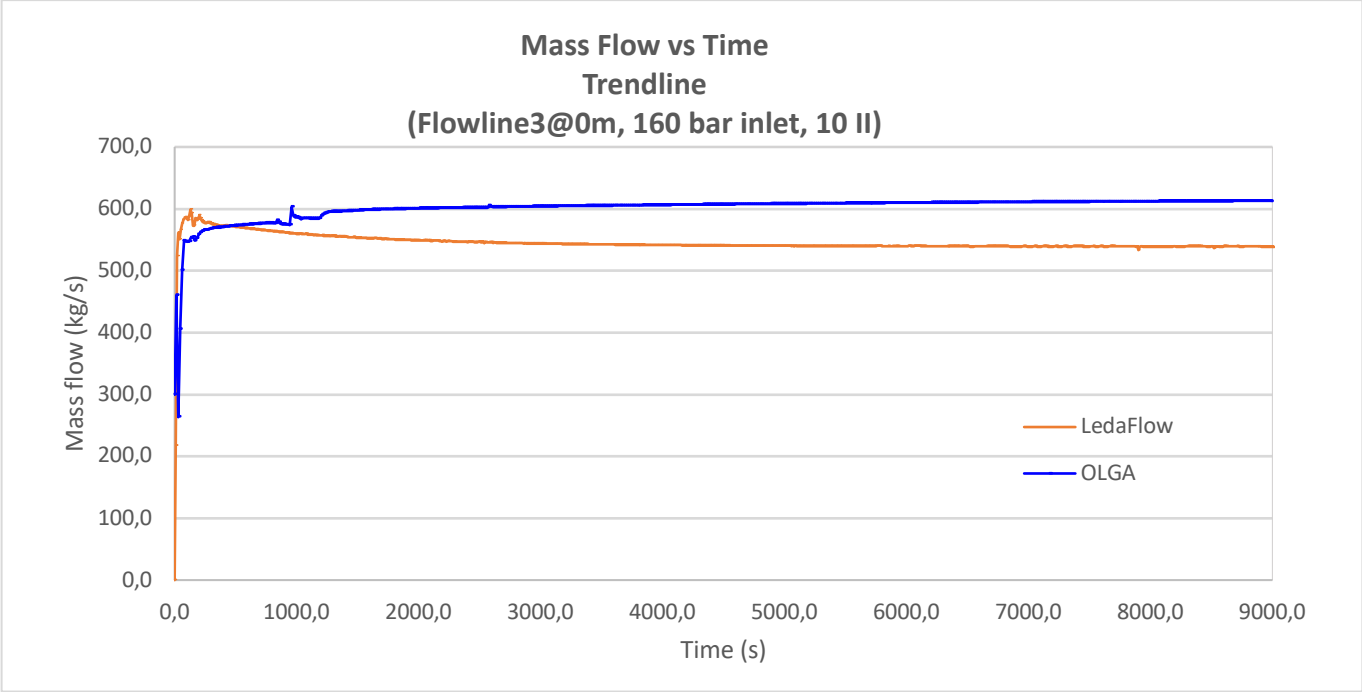

Figure A23: Mass flow vs time for 160 bar inlet at flowline 3

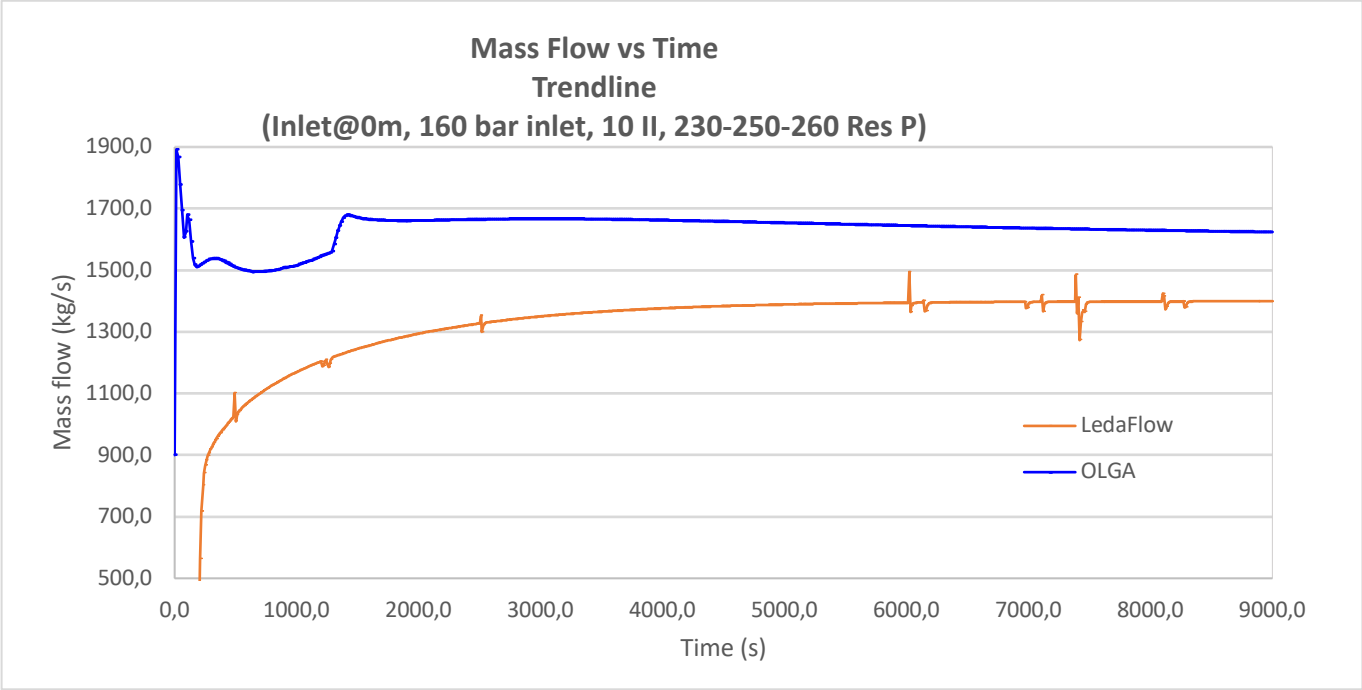

Figure A24: Mass flow vs time for 160 bar inlet at inlet

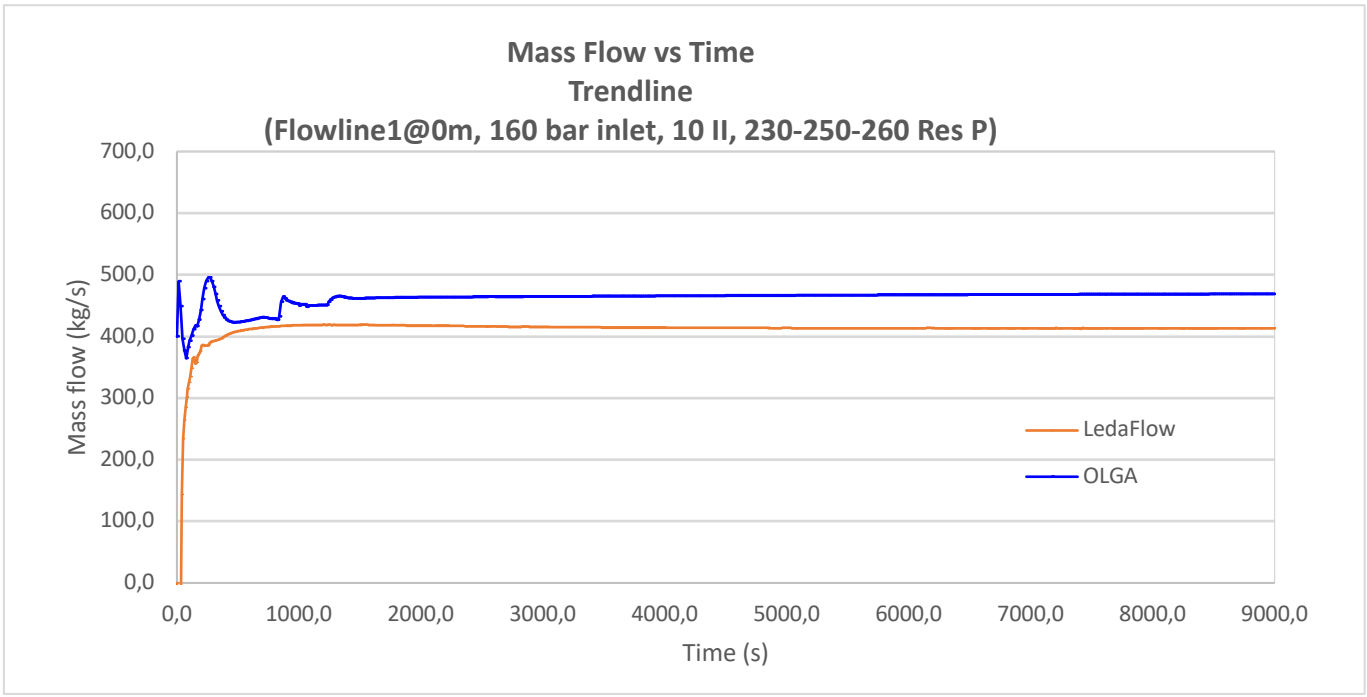

Figure A25: Mass flow vs time for 160 bar inlet at flowline 1

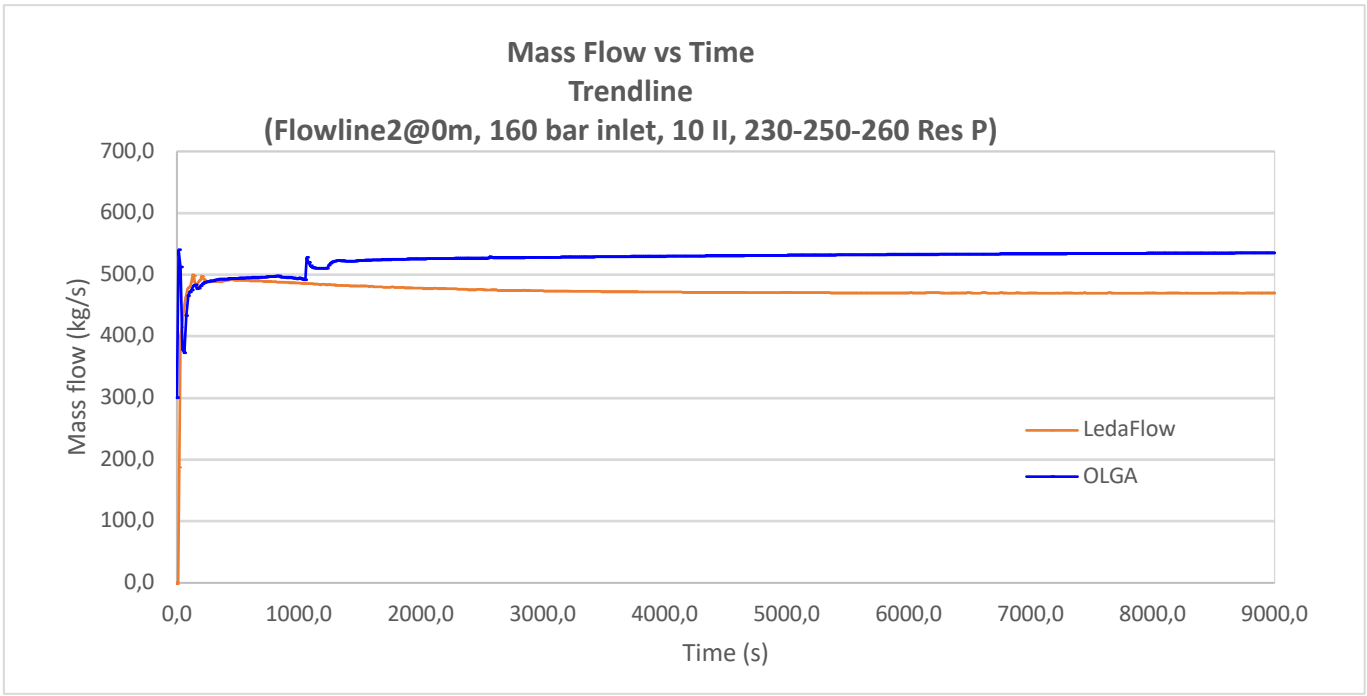

Figure A26: Mass flow vs time for 160 bar inlet at flowline 2

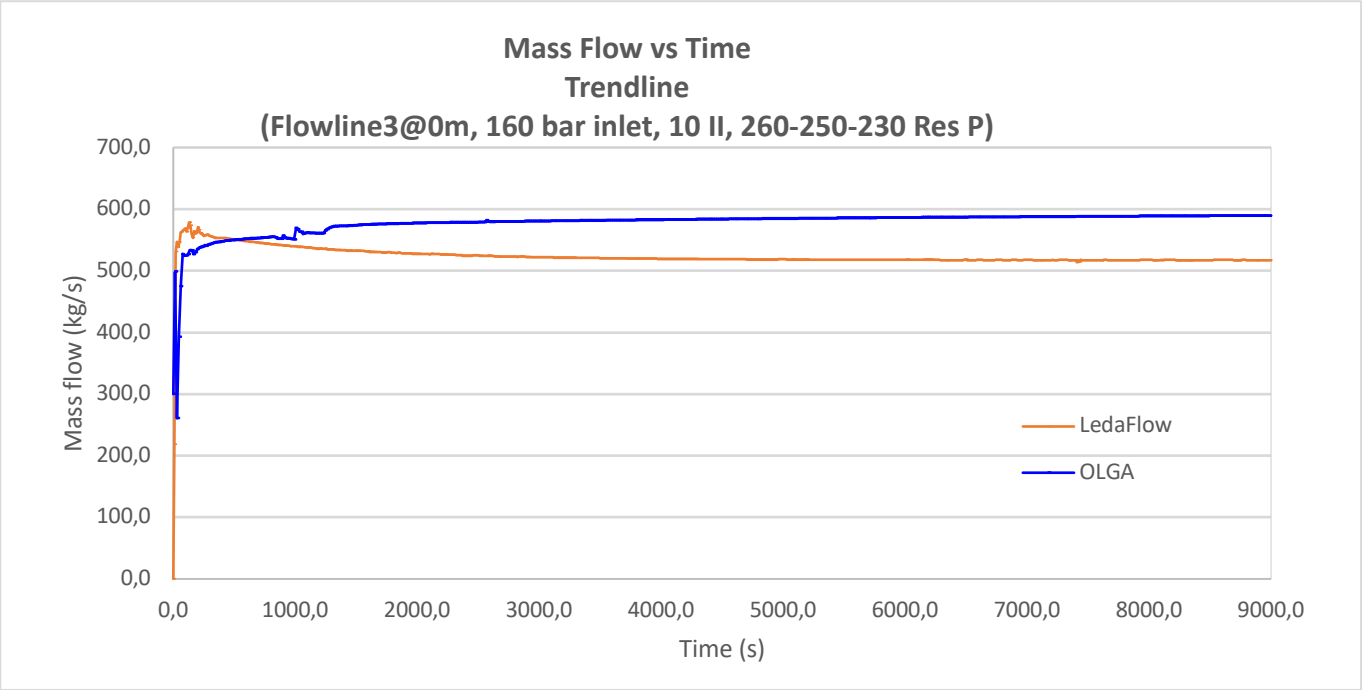

Figure A27: Mass flow vs time for 160 bar inlet at flowline 3

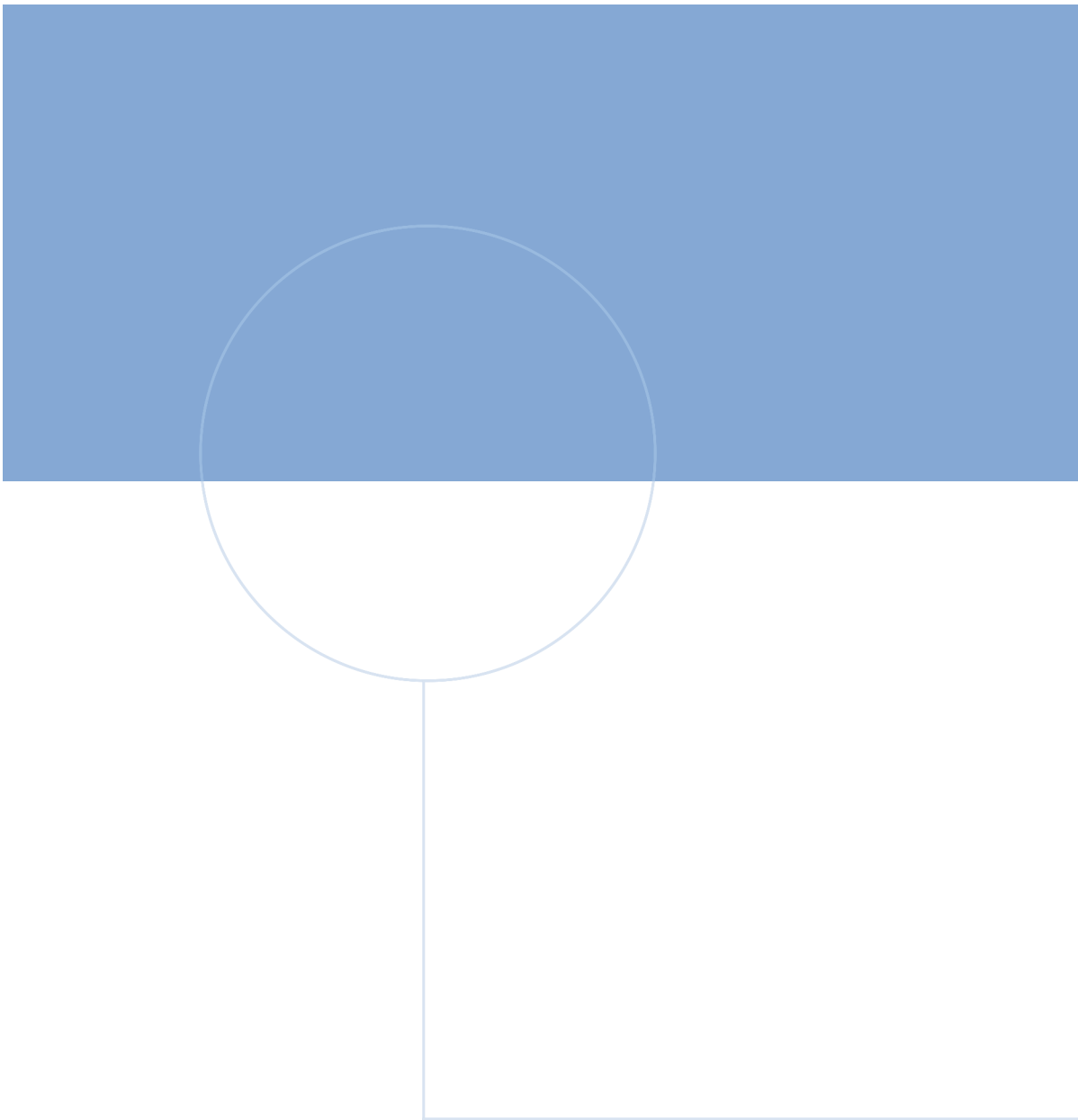

NTNU

Norwegian University of
Science and Technology